THESIS ON MECHANICAL ENGINEERING E111

Electroconductive Oxide Ceramics with Hybrid Graphenated Nanofibers

MARIA DROZDOVA

TTÜ PRESS

TALLINN UNIVERSITY OF TECHNOLOGY
SCHOOL OF ENGINEERING
Department of Mechanical and Industrial Engineering

This dissertation was accepted for the defence of the degree of Doctor of Philosophy in Engineering on November 3, 2017.

Supervisor: Prof. Irina Hussainova
School of Engineering, Department of Mechanical and Industrial Engineering, Tallinn University of Technology, Tallinn, Estonia

Opponents: RNDr. Pavol Hvizdoš
Director, Institute of Materials Research, Slovak Academy of Sciences, Košice, Slovak Republic

Dr. Ants Lõhmus
Senior Research Fellow, Faculty of Science and Technology, Institute of Physics, University of Tartu, Tartu, Estonia

Defence of the thesis: December 6, 2017, at 12:00, Tallinn University of Technology, room U05-215.

Declaration:
Hereby I declare that this doctoral thesis, my original investigation and achievement, submitted for the doctoral degree at Tallinn University of Technology has not been submitted for doctoral or equivalent academic degree.

ISSN 1406-4758
ISBN 978-9949-83-183-8 (publication)
ISBN 978-9949-83-184-5 (PDF)

MEHHANOTEHNIKA E111

Elektrijuhtiva oksiid-grafeenkiudkeraamika tehnoloogia ja püsivus

MARIA DROZDOVA

TTÜ KIRJASTUS

CONTENTS

LIST OF PUBLICATIONS

The present dissertation is based on the following papers, which are referred in the text by the Roman numerals I–III.

I. **Drozdova, M.**, Hussainova, I., Pérez-Coll, D., Aghayan, M., Ivanov, R., Rodríguez, M.A., Drozdova, M., Pérez-Coll, D., Aghayan, M., Ivanov, R., Rodríguez, M.A., A novel approach to electroconductive ceramics filled by graphene covered nanofibers. – *Materials and Design*, 2016, 90, 291–298. DOI:10.1016/j.matdes.2015.10.148.

II. Hussainova, I., Baronins, J., **Drozdova, M.**, Antonov, M., Wear performance of hierarchically structured alumina reinforced by hybrid graphene encapsulated alumina nanofibers. – *Wear*, 2016, 368–369, 287–295. DOI:10.1016/j.wear.2016.09.028.

III. Hussainova, I., **Drozdova, M.**, Pérez-Coll, D., Rubio-Marcos, F., Jasiuk, I., Soares, J.A.N.T., Rodríguez, M.A., Electroconductive composite of zirconia and hybrid graphene/alumina nanofibers. – *Journal of the European Ceramic Society*, 2017, 37 (12), 3713–3719. DOI:10.1016/j.jeurceramsoc.2016.12.033.

Contribution of the author:

I. Design of the experiments; Sintering and characterization of materials; Data analysis; Drafting of the publication

II. Design of the experiments; Mechanical, chemical and microstructural characterisation; Discussion of the results;

III. Design of the experiments; Sintering and characterization of materials; Data analysis; Drafting of the publication

Other related publications:

IV. Ivanov, R., Hussainova, I., Aghayan, M., **Drozdova, M.**, Pérez-Coll, D., Rodríguez, M.A., Rubio-Marcos, F., Graphene-encapsulated aluminium oxide nanofibers as a novel type of nanofillers for electroconductive ceramics. – *Journal of the European Ceramic Society*, 2015, 35 (14), 4017–4021. DOI:10.1016/j.jeurceramsoc.2015.06.011.

V. **Drozdova, M.**, Ivanov, R., Aghayan, M., Hussainova, I., Dong, M., Rodríguez, M.A., Fabrication of alumina nanocomposites reinforced by a novel type of alumina nanofiber and graphene coated alumina nanofiber. – *Proceedings of the 9th International Conference of DAAAM Baltic Industrial Engineering : 24-26st April 2014, Tallinn, Estonia*, 2014, 337–341.

VI. Hussainova, I., **Drozdova, M.**, Aghayan, M., Ivanov, R., Pérez-Coll, D., Graphene Covered Alumina Nanofibers as Toughening Agent in Alumina Ceramics. – *Advances in Science and Technology*, 2014, 88, 49–53. DOI:10.4028/www.scientific.net/AST.88.49.

VII. **Drozdova, M.**, Pérez-Coll, D., Aghayan, M., Ivanov, R., Rodríguez, M.A., Hussainova, I., Hybrid graphene/alumina nanofibers for electrodonductive zirconia. – *Key Engineering Materials*, 2016, 674, 15–20. DOI:10.4028/www.scientific.net/KEM.674.15.

VIII. Patent application: Authors: **Drozdova M.**, Ivanov R., Hussainova I.; A ceramic composite material with funcionally graded properties; Owner: Tallinna Tehnikaülikool; Priority number: P201700026; Priority date: 7.07.2017.

ABBREVIATIONS

ANF – Alumina Nanofibers
ANFC – Alumina Nanofibers covered with graphene
CNT – Carbon Nanotubes
COF – Coefficient of Friction
CVD – Chemical Vapor Deposition
DTA – Differential Thermal Analysis
DTG – Derivative Thermo-gravimetric
EDM – Electrical Discharge Machining
FE-SEM – Field-Emission Scanning Electron Microscopy
FSZ – Fully Stabilized Zirconia
FT-IR – Fourier-Transform Infrared Spectroscopy
GNP – Graphene Nanoplatelets
GNS – Graphene Nanosheets
GO – Graphene Oxide
HIP – Hot Isostatic Pressing
HP – Hot Pressing
HRTEM – High Resolution Transmission Electron Microscopy
HV – Vickers Hardness
IFT – Indentation Fracture Toughness
MWCNT – Multi-Walled Carbon Nanotube
NMP – N-Methyl-Pyrrolidone
PSZ – Partially Stabilized Zirconia
RGO – Reduced Graphene Oxide
RIB – Relative Index of Brittleness
SEM – Scanning Electron Microscopy
SEVNB – Single-Edge V-Notch Beam
SPS – Spark Plasma Sintering
SWCNT – Single-Walled Carbon Nanotubes
TEM – Transmission Electron Microscopy
TG (TGA) – Thermo-Gravimetric Analysis
TZP – Tetragonal Zirconia Polycrystals
XRD – X-ray Diffraction
wt.% – weight percentage
vol.% – volume percentage

INTRODUCTION

At the present stage in material science, the great advancements have been achieved in materials development, production and new areas of applications. A large proportion of this progress falls on composite materials – a combination of two or more materials with different physical or chemical properties aimed at specific final cumulative characteristics that are not achievable by any of the individual component. Among all composites, the ceramic matrix composites exhibit a combination of highly demanded physical and mechanical properties, including high hardness, high refractoriness, high wear and corrosion resistance, lightweight and high chemical stability.

Development of nanotechnology even more widely opens the door to the new composites with outstanding properties. Among advanced materials, the special and growing attention is paid to the recently discovered carbon allotropes: fullerenes, carbon nanotubes, and graphene. Graphene, which is a single one-atom-thick layer of graphite, is the basic structural element of many allotropes. It exhibits extraordinary strength, unique electrical properties and efficient heat conductivity. Such exceptional properties make it a subject of a large number of studies, including usage as additives/reinforcements in composite materials.

Significant improvements in mechanical and electrical properties of ceramics reinforced with carbon nanotubes (CNT) or graphene nanoplatelets (GNP) are continuously reported. It was shown that initially insulating oxide-ceramic can be turned into conductive state by adding conductive graphene-based particles in amount that exceeds a percolation point. The electro-conductive ceramics represent a huge potential for structural and functional applications, such as electronic devices, thermoelectric devices, heaters, electrodes or conductors for water processing or dialysis, additionally, they are able to withstand aggressive environmental conditions. However, amount needed to guarantee sufficiently high electrical conductivity (about 2-3 vol.% and more) of additives leads to deterioration of hardness of the material and appearance of high amount of defect-like areas in the matrix. Main reason for this is difficulty to avoid their tangling or agglomeration, which hampers dispersion of the fillers in a ceramic matrix. These problems associated with degradation of some mechanical properties could be minimized by reducing the amount of graphene-based fillers to the lowest possible portion while keeping conductivity considerably high by providing good dispersion of the fillers. This requirement can be met by an increase in an aspect ratio (length-to-diameter) of the fillers and possibility of their homogeneous dispersion throughout the matrix.

Another concept on the verge of nanomaterial science, which expands the possibilities for the production of advanced materials, is the concept of hierarchically structured materials. Inspired by the nature, hierarchically structured composites contain structural elements that themselves have own structure. Such approach allows to design wide variety of new complex

characteristics in materials, managing the composition or structure of substructures at one or more levels of hierarchical architecture. Approach of designing hierarchical structure of the graphene-based fillers is helpful to decrease percolation threshold of the carbon needed for electricity to run through the material. Very high aspect ratio ceramic nanofibers can perform as substrate for very few graphene layers and provide stiffness of the fillers, which would make them less prone to tangle and easier to disperse into a matrix. At the same time low amount of graphene layers on the fiber warrants the absence of thick graphitic stockings, which are considered as the defect points in a sintered material.

The focus of this study is the design, production and characterisation of metal oxide ceramic-based composites doped by hierarchically structured hybrid nanofibers. Combining remarkable properties of both ceramic matrix and graphenated fillers, and implying concept of hierarchical structure in materials, new approach to production of electroconductive oxide ceramic composites without deterioration of the hardness and with improvement in toughness and wear performance is proposed.

1. REVIEW OF THE LITERATURE

1.1. Ceramics

Historically, term «ceramics» had been used for materials and items that were made of clays and their mixtures [1]. With the growth of knowledge about materials the term has expanded to the broader meaning, covering also materials comprising pure oxides, nitrides, carbides and others. Further, with the emergence of industries and advance of technical progress a new class of advanced ceramics has appeared, being complementary to the prior "traditional" ceramic materials that were used for tableware, pottery, sanitary ware, tiles, bricks and similar. The new advanced materials are primarily produced by powder metallurgy methods, which allows production of materials with a relative density of 99% and above. Modern ceramic materials, having such useful properties as low density, high strength, chemical resistance, abrasion resistance, high temperatures resistance, and, with possibility to tailor some properties in very complex ways, are now able to fill a niche that cannot be filled by metals, glasses or polymers in such progressive applications as aerospace engineering, electronics, mechanical engineering, automotive engineering, bioengineering and others. Properties of ceramics are determined by composition, bonding type, microstructure and presence of defects. Usually ceramic materials possess mixed ionic and covalent bonds, both being of very strong nature. High strength of the bonds is responsible for the high hardness of materials, and their stability with regard to chemical and thermal attacks. However, brittleness along with other flaws of ceramics, such as large scatter of strengths due to defects and subcritical crack growth are still restricting the use of ceramics in many applications. Efforts to overcome their intrinsic brittleness and lack of reliability while maintaining all other advantages are made by many researcher groups all over the world. Another great interest for scientific community and industry is multi-functionality of ceramics, including electrical conductivity. Electrically conductive materials are in high demand in present technological age. Besides, the electrical conductivity of ceramics allows the better machining capabilities such as Electrical Discharge Machining (EDM) that can be used to produce near net shape parts of hard and brittle materials independently of their mechanical properties. The following sections give a brief overview of ceramics being under consideration at the present work.

1.2. Oxide ceramics

By chemical composition, technical ceramics can be divided into two large groups of oxide ceramics and non-oxide ceramics. Oxide ceramics, by definition, are compounds of oxygen with non-organic elements. The most beneficial properties of oxide ceramics are wear resistance, heat insulation, low density, resistance to corrosion, electrical insulation, high temperature strength and biocompatibility, which are utilized in many important areas of industry. Even though oxides are falling behind of the metal carbides with respect to hardness and melting point, they are less brittle and are easier to sinter [2]. Moreover, since oxides represent the highest oxidation state of the metal, these ceramics are very

stable, not prone to oxidising any further or having other chemical reactions. Some of the most important oxides are: Al_2O_3, SiO_2, ZrO_2, MgO, CaO, BeO, ThO_2, TiO_2, UO_2, ZnO, CeO_2 and a number of mixed oxides [3,4].

1.2.1. Alumina

Alumina (Aluminium oxide, Al_2O_3) is one of the most frequently used technical ceramics due to its relatively high strength, thermal conductivity, maximum service temperature, high chemical inertness, high dielectric properties and low cost relative to other technical ceramics [5]. Alumina has one thermodynamically stable form α-Al_2O_3 (corundum) and several metastable polymorphs (also called «transition» polymorphs), including γ-Al_2O_3 (cubic spinel), δ-Al_2O_3 (either tetragonal or orthorhombic), etc. [6]. Common processing routs to obtain different metastable alumina polymorphs and subsequent phase transformation toward the stable α-Al_2O_3 phase are summarized in **Figure 1.1**.

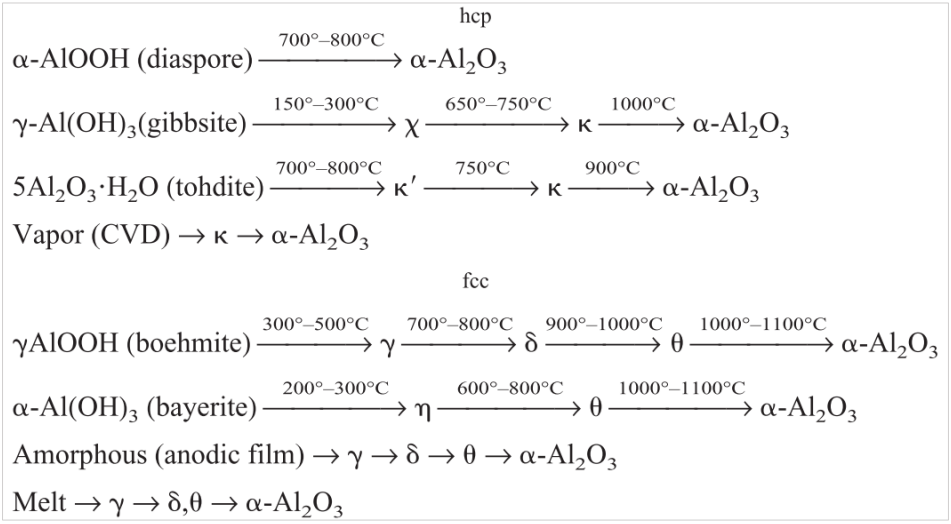

Figure 1.1 *Common processing routs for obtaining different Al_2O_3 phase [6].*

The transitional alumina structures are irreversible transformed to the α-Al_2O_3 when heated up to the temperatures above 1200 °C. Being thermodynamically stable, α-Al_2O_3 is the most suitable for technical and structural applications. It can be used for producing sealing disks, printed circuit boards, cutting tools, sandblast nozzles, protective tubes for thermocouples, spark plugs, bearings, valves, thread guides for textile machines, pump elements, slip rings, implants for human medicine, burner nozzles, crucibles, rotating spindles, etc. [7]. Crystal structure of α-Al_2O_3 is hexagonal and has a close-packed arrangement of oxygen ions. The mechanical, thermal and electrical properties of the widely used grade of α-Al_2O_3 are listed in Table 1. However, it should be taken into account that the properties of alumina, as well as those of other ceramics, are heavily dependent on the properties of raw powder such as its purity, dispersity, activity, etc., and the technology used to consolidate the material.

Table 1 *Dense Al_2O_3 properties*

Al_2O_3 (99.9%)			
Mechanical properties [8]		***Conditions***	***Values***
Density, ($g \cdot cm^{-3}$)		Room temperature	>3.97
Strength (MPa)	Tensile		250-300
	Compressive		2000-3000 (4000)
	Flexural		300-500
Fracture toughness, K_{IC} ($MPa \cdot m^{1/2}$)			4-5
Fracture threshold, K_{IO} ($MPa \cdot m^{1/2}$)			2.0-2.5
Elastic modulus (GPa)			400-450
Hardness (Vickers) (GPa)			14-16

Thermal properties [9]	***Conditions***	***Values***
Max. working temperature (°C)	-	1700
Thermal expansion coefficient ($10^{-6}K^{-1}$)	25 – 300 °C	7.8
Thermal conductivity ($W \cdot m^{-1} \cdot K^{-1}$)	20 °C	28
Shock resistance (ΔT°C)		180-200

Electrical properties [9]	***Conditions***	***Values***
Dielectric strength (ac-kv/mm)	2.5mm tk	10
Dielectric constant	1 MHz	9.7
Volume resistivity, Ω·cm	20 °C	$>10^{14}$
	300 °C	10^{10}
	1000 °C	10^{6}
Loss Factor	1 MHz	0.009
Dissipation Factor	1 MHz	0.0001

1.2.2. Zirconia

Zirconia (ZrO_2, zirconium dioxide) is one of the toughest structural ceramics. For their toughness zirconia-based materials have especially extensive application in medicine, particularly in dentistry.

Zirconia exists in several crystallographic modifications (**Figure 1.2**). At the room temperature and atmospheric pressure, pure zirconia exists in monoclinic phase (**Figure 1.2**, a). Increasing temperature to approximately 1170 °C results in transformation to the tetragonal form (**Figure 1.2**, b). Above 2370 °C zirconia converts to cubic phase (**Figure 1.2**, a). Both transformations are of the martensitic nature, i.e. diffusionless change in a crystal structure [10,11]. On cooling, the expansion in volume of unconstrained crystals of zirconia is about 2.5 % in the c → t, and 4-5% in the t → m phase transition [12,13]. This transformation can be also induced by external stress loading under isothermal conditions [14]. This characteristic of martensitic transformation makes a significant contribution to zirconia's very high (for ceramic materials) toughness.

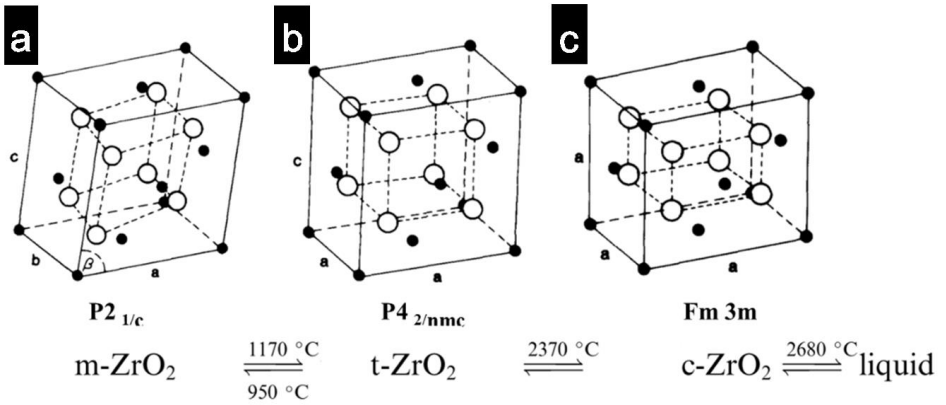

Figure 1.2 *Schematic of three zirconia polymorphs (a – monoclinic, b – tetragonal, c – cubic) and their phase transitions (adopted from* [14] *and* [12]*)*

Generally, zirconia is used in its high-temperature phases – tetragonal or cubic, which can be stabilized or partially stabilized for use at room temperature by adding oxide dopants such as MgO, Y_2O_3, La_2O_3, CaO, CeO [15]. Fully stabilized zirconia (FSZ) is the zirconia totally consisting of the stabilized cubic phase. Partially stabilized zirconia (PSZ) is a mixture of cubic and tetragonal and/or monoclinic phases. The low concentration of the stabilizing oxides is not enough to provide full stabilization of the cubic phase in PSZ, so it constitutes a matrix of a large-grained cubic zirconia with dispersion of metastable tetragonal zirconia intra-granular precipitates [15]. A composition of these phases is responsible for intrinsic mechanism of transformation toughening due to transformation of metastable t-ZrO_2 to m-ZrO_2 induced by the stress field around a propagating crack. Due to outstanding mechanical properties of PSZ, it is of the greatest interest for engineering applications. MgO or CaO are most commonly used as PSZ stabilizers. Tetragonal zirconia polycrystals (TZP), usually stabilized by Y_2O_3 or CeO_2, consist of nearly 100% t-ZrO_2 material. Mechanical, thermal and electrical properties of 3mol% Y_2O_3-stabilized TZP and 8mol% MgO-stabilized PSZ ceramics are listed in Table 2.

Table 2 *Dense partially stabilised zirconia properties* [8,16]

Composition			**3Y-TZP**	**Mg-PSZ**
Mechanical properties		***Conditions***	***Values***	***Values***
Density, ($g \cdot cm^{-3}$)		Room temperature	6.05	5.75
Strength (MPa)	Tensile		800	300-400
	Compressive		3000–4000	2000-3000
	Flexural		1000–1500	600–700
Fracture toughness, K_{IC} ($MPa \cdot m^{1/2}$)			6-12	6-10
Fracture threshold, K_{IO} ($MPa \cdot m^{1/2}$)			3.0–3.5	
Elastic modulus (GPa)			200-250	200-250
Hardness (Vickers) (GPa)			12-14	10-12

Table 2 continued *Dense partially stabilised zirconia properties* [8,16]

Composition		**3Y-TZP**	**Mg-PSZ**
Thermal properties	***Conditions***	***Values***	***Values***
Max. working temperature (°C)	air/inert	1200/2200	1000
Thermal expansion coefficient ($10^{-6}K^{-1}$)	25 – 1000 °C	11	7-8
Thermal conductivity ($W \cdot m^{-1} \cdot K^{-1}$)	20 °C	2-2.8	2
Shock resistance (ΔT°C)		300-400	260

Electrical properties	***Conditions***	***Values***	***Values***
Dielectric Strength (ac-kv/mm)	50 Hz	30-40	
Dielectric Constant	1 MHz	16-18	
Volume resistivity, Ω·cm	20 °C	10^{10}	10^{10}
	400 °C	10^{4}	10^{2}-10^{3}
	1000 °C	10^{3}	30-10^{2}
Loss Factor	1 MHz	0.001	0.001

1.3. Electroconductive ceramic composites

The vast majority of ceramics are good electrical insulators. The most common among them are alumina (Al_2O_3), mullite ($3Al_2O_3 \cdot 2SiO_2$), forsterite ($2MgO \cdot SiO_2$), and aluminum nitride (AlN) [17]. Insulating ceramics can be widely found in our everyday life – integrated circuit supports and packages, spark plug insulators and power line insulators, mobile phones, cars, etc. [18]. In terms of electrical properties, existing conductive ceramics are widely used in resistors and as an electrode material in fuel cells, sensors and displays [19]. In semiconductor industry ceramics are widely utilized as rectifiers, thermistors, thermal switches, solar cells, varistors, sensors, heating elements or electrodes. Altogether, ceramic materials cover the entire spectrum from complete insulators to superconductors.

1.3.1. Percolation

Often specific applications require specific properties, and the cost of material is also playing a significant role. The intrinsic electroconductive ceramics are expensive and may lack important characteristics and be difficult to handle. Cost-effective electrically conductive ceramic composites can be developed by distributing conductive second phases throughout the insulating matrix to obtain the desirable electrical and mechanical properties. It is important to take into account that a large amount of additives strongly affects the mechanical properties of ceramics, which can be either advantage or disadvantage considered the application. A certain threshold value for the volume fraction of conductive second phase has to be exceeded before the composite becomes electrically conductive. This amount is commonly called percolation threshold and varies depending on the microstructure, the sizes and shape of the conductive additives, their aspect ratio and the quality of distribution. Spherical particles in a continuous matrix require about 20–30 vol.% to form a percolating network [20], while particles with a large aspect ratios, like flakes or fibers, require significantly smaller amounts of fillers [21]. Even lower percolation threshold became possible due to the development of graphene and graphene-derived

nanostructures, such as carbon nanotubes (CNT), graphene nanoplatelets (GNP), graphene ribbons and reduced graphene oxide (RGO). The high aspect ratio and small dimensions allow the conductive percolation network to form with a very small portion of the fillers of only a few volume percent [22–24].

From experimental data it is clear that the factors like more homogenous distribution of the fillers and their high aspect ratio are decreasing the amount of conductive phase needed to obtain a reliable electroconductive oxide ceramic. A new approach to incorporate graphene into the ceramic matrix in non-agglomerated state is needed in order to improve mechanical and electrical properties by adding a very small amounts of fillers.

1.3.2. Ceramic/CNT and ceramic/graphene composites

Since carbon nanotubes (CNT, Figure 1.1 a) have been discovered by Iijima [25], a study on carbon allotropes became of great interest among the scientific community. CNTs have become a promising additive material for different types of composites due to the outstanding mechanical [26,27], electrical [28], and thermal [27] properties. In the context of ceramic matrix composites, the main emphasis has been put on CNTs as a reinforcement media to enhance the toughness and strength of monolithic ceramics. Great number of reports on improved fracture toughness by CNTs have been published [29–32]. In the recent years, the ceramic/CNT composites have started to draw more attention in terms of their functional properties such as electrical and thermal conductivity as the demand in industry for such advanced materials is growing. The addition of CNTs to the insulating matrix such as alumina or zirconia can convert them to highly electrically conductive materials [33]. Evidently, high quality single-walled CNTs (SWCNT) are the most advantageous for producing highly electrically conductive materials due to their perfect structure.

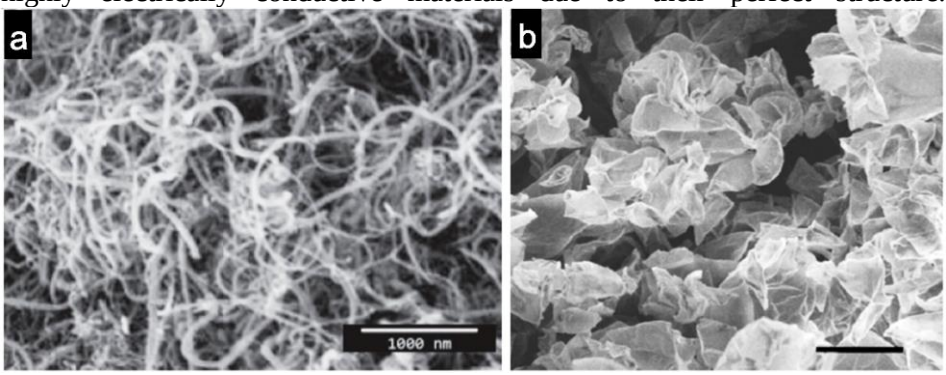

Figure 1.1 *a – Carbon nanotubes (CNT) and b – graphene nanoplatelets (GPL)*[34]

A value of the electrical conductivity of 3345 $S \cdot m^{-1}$ has been reported by Zhan et al. [35,36] for the 15 vol.%SWCNT in alumina produced by spark plasma sintering (SPS). However, a high cost of such SWCNTs is a limiting factor for the large scale applications. While the addition of multi-walled CNTs (MWCNT) also results in effective drop in electrical resistivity; however, the

hardness is usually compromised due to the drop in density. For example, Kumari et al. [37] in their work have reached electrical conductivity of 3336 $S \cdot m^{-1}$ with mixing 33.1 vol.% of MWCNT into Al_2O_3 matrix, but the density of SPS-ed sample dropped down to about 60% of theoretical density. While high amount of carbon additives is enhancing electrical properties, it is responsible for the loss of other substantial properties of the raw material at the same time. Nevertheless, in order to turn insulating ceramics into conductive, there is no need to add such excessive amount of CNTs. Michálek et al.[38] in their work have reported an increase of electrical conductivity in Al_2O_3/CNT composite from 10^{-12} to $2.2 \cdot 10^{-3}$ $S \cdot m^{-1}$ and $2.8 \cdot 10^{-5}$ $S \cdot m^{-1}$ with addition of 0.5 vol% of MWNTs to alumina and ZTA matrices, which places the percolation point for these composites to be less than 0.5 vol.%. For zirconia/CNT composites a percolation point below 0.38 vol.% of SWCNTs has been reported by Shin et al. [32]. However, even with such amount of CNTs, a deterioration of hardness has been observed. Mechanical properties strongly depend on the homogeneity of distribution of the CNTs in the ceramic matrix, as well as amount of residual porosity. For now, a proper de-agglomeration of CNTs and full densification of the composites remains a costly and time- and labour-consuming process. Similar challenges are faced when CNFs (carbonaceous fibers with dimensions far exceeding those of CNTs) are used as fillers [39–41].

In the recent years, graphene has become a sensational discovery and overtook the leading place of CNTs in the role of nanofiller for the tough and electrically conductive composites. Graphene has a larger specific surface area, and its dispersion throughout the composite materials is noticeably better compared to CNTs. However, the large scale production of a single layer high quality graphene is not viable due to the high cost. Thus, in case of the bulk engineering composites the term “graphene” is usually referring to the carbon nanomaterials consisting of several layers of graphene, including graphene nanoplatelets (GNP, Figure 1.1 b), graphene nanosheets (GNS) and reduced graphene oxide (RGO) platelets [42]. The main drawback is a lack of the real control over the thickness of the graphene platelets. Moreover, surface structural damage is introduced in case of oxidation and reduction of GO, which is worsening the properties of the final composite [42,43]. Outstanding results on producing alumina matrix composite containing 15 vol.% of GNS have been reported by Fan et al. [33]. More than 97% relative density and electrical conductivity of 5709 $S \cdot m^{-1}$ have been obtained. The percolation threshold for the prepared composites has been found around 3 vol.%. In another study Fan et al.[44] have reported the percolation threshold of Al_2O_3/graphene composite, produced with the help of colloidal processing and direct reduction of GO during SPS, to be only 0.38 vol.%. The electrical conductivity values have been found increased from 1 $S \cdot m^{-1}$ for 0.42 vol.% of graphene content up to 1038.15 $S \cdot m^{-1}$ for 2.35 vol.%. Even lower percolation threshold has been achieved by Centeno et al. [45] by adding 0.22 wt.% of GNP, leading to an increase in conductivity of alumina up to 6.7 $S \cdot m^{-1}$. Similar to CNTs, quality of graphene and its dispersion in the composites is significantly affecting properties of the final material. In order to reach further improvement

in electrical conductivity and mechanical properties of ceramic/graphene composites at low contents of additives, cost-effective and efficient dispersing techniques, which can provide avoided damage of the graphene and its agglomeration during processing, should be invented.

1.3.3.Electrical Discharge Machining (EDM)

It is very difficult to machine hard and brittle ceramics. It is a great challenge to produce a near net shape by the means of conventional sintering processes, so diamond tools are commonly required to machine ceramic components. However, for the electrically conductive materials, an alternative machining approach, namely Electrical Discharge Machining (EDM), can be applied. EDM allows complex forms and shapes and it is very helpful when high precision of the products is required. According to König et al.[46], requirement for the materials to be processed by EDM is a value of electrical conductivity not less than of the order of 0.01 $S \cdot cm^{-1}$ (100 $\Omega \cdot cm$). Other study [47] has demonstrated that with applying appropriately selected machining parameters, the ZnO/Al_2O_3 ceramic with the electrical resistivity of 3410 $\Omega \cdot cm$ could be effectively machined by EDM with the copper electrodes. However, this requirement of electrical conductivity is a large limitation in a case of insulating ceramics. To overcome this restriction, electrical conductivity of such ceramic can be enhanced. It has been shown that by introducing electrically conductive secondary phases, even otherwise insulating materials with a high electrical resistivity can be machined by EDM [48–50]. However, a too high concentration (about 40 vol.%) of most second phase additives such as TiB_2, TiN, TiC, WC, TiCN is needed for the material to be properly machined by EDM, which leads to completely changing the properties of the base material. Nevertheless, in a recent work of Singh et al. [51] it has been shown that machining ability of Al_2O_3/MWCNT composites is satisfactory when only 7.5 vol.% (or more) MWCNTs is added. Even 2.5 vol.% of MWCNT addition allowed EDM; however, too many defects have been introduced during the process due to the low electrical conductivity of the composites.

Improving electrical conductivity to such extent that use of EDM becomes possible for shaping hard ceramic materials while keeping amount of conductive additives to minimum can open new application fields for initially insulating ceramics of a high hardness. Graphene and other carbon-derived nanofillers are good candidates for such composites, as a very low content is needed to boost the electrical conductivity of the composite.

1.4. Processing of ceramic/graphene composites

The main challenge in production of ceramic/graphene composites is to disperse graphene homogenously throughout the ceramic powders, as it tends to agglomerate due to van der Waals forces. The other problem is to retain high quality of graphene during processing. In this section the most common techniques employed to obtain ceramic/graphene composites reported in the literature are described.

1.4.1. Processing routes

The two most common processing routes for ceramic/graphene composites are (i) powder processing, and (ii) colloidal processing.

1.4.1.1. Powder processing

Powder processing routes are the easiest, cost-effective and, therefore, most common routes to produce ceramic/graphene composites. In this approach, ceramic powders are mixed with graphene by conventional ball milling or high energy ball milling after possible prior de-agglomeration of graphene using ultrasonication, ball milling or stirring. A different media such as ethanol, isopropanol, acetone, N-methyl-pyrrolidone (NMP), water (in case of GO) and others are commonly used as dispersant. However, the ball milling can damage graphene introducing multiple defects or undesirable impurities.

1.4.1.2. Colloidal processing

Colloidal processing is a more complicated technique for producing ceramic powder and graphene suspensions. Stable suspensions are slowly mixed together, usually using magnetic stirring or ultrasonication to ensure uniform dispersion of graphene. In order to have uniform dispersing medium during mixing, the same solvent is preferred for both ceramic and graphene suspensions. Surfaces of components are modified to ensure a control over interparticle forces. The method provides a more homogenous distribution of the graphene and provides highly regular particle packing in the sintered material. However, a colloidal processing route still needs more consideration and tuning in order to make it cost-effective and scalable for the extensive productions of the composites.

1.4.2.Consolidation techniques

Conventionally, to consolidate ceramic composites, high temperatures and long processing times are required. However, when working with graphene, high temperature and long holding times can cause its degradation due to the low thermal stability of graphene at the temperatures above 600 °C. Shorter sintering times and lower temperatures are preferable to avoid the degradation. However, the densification of ceramic powders at lower temperatures is rather impossible, unless some external pressure or other mechanisms contributing to densification are involved. For example, with pressure assisted consolidation methods, including Hot Pressing (HP), Hot Isostatic Pressing (HIP) and Spark Plasma Sintering (SPS), the consolidation temperatures can be lowered, but the first two densification techniques still require hours of processing to produce fully dense materials.

1.4.2.1. Hot Isostatic Pressing

Hot isostatic pressing (HIP) is a process of consolidation that involves high temperature and high pressure of the gas applied to the workpiece. The main advantage of the technique is complete isotropy of the sintered materials, as the pressure is applied isostatically from all sides of the sample. However, the cycle of heating and dwelling is significantly longer than that of spark plasma sintering. Moreover, according to the literature [39,52,53], when the two methods

are compared, the ceramic/graphene composites processed by HIP tend to have more difficulties to densify and end up with theoretical densities and mechanical properties lower than those made by SPS.

1.4.2.2. Spark Plasma Sintering (SPS)

Spark plasma sintering (SPS), also called Field Assisted Sintering Technique (FAST) or Pulsed Electric Current Sintering (PECS), is a promising technology based on mechanical pressure and produced by the electric current Joule heating of the pressing tool and a sample (Figure 1.2).

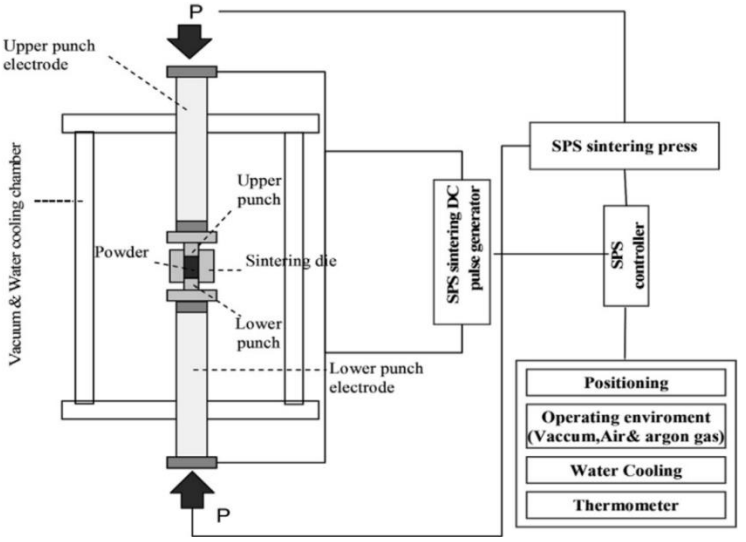

Figure 1.2 *SPS system scheme* [54]

The process can take place under vacuum or in a protective atmosphere. Heating rates can be set to up to 1000 $^{o}C \cdot min^{-1}$. The main superiority of this technique over the conventional sintering as well as other pressure assisted sintering methods such as Hot Pressing (HP) and Hot Isostatic Pressing (HIP) are short sintering times and relatively low temperatures needed to consolidate the material to a high density. These conditions allowed by the SPS can minimize the degradation of graphene, making it the most promising consolidating technique for ceramic/graphene composites. Among the drawbacks of SPS complicity and high cost of the equipment, inability to produce large scale and net-shape batches can be named. However, already now there are suggested new technological concepts of SPS furnaces with simultaneously produced batches of samples and tools for near net shape processing [55].

1.5. Objectives of the study

The present study is motivated by the urgent need for a well-developed procedure ensuring reliability of the multifunctional electroconductive oxide ceramic-based composites.

The *overall objective* of the PhD work is to design, produce and comprehensively analyse a novel grade of alumina and zirconia-based composites added by graphenated alumina nanofibers, which were recently developed in TUT.

The *main task* of the study is to design and prototype the alumina and zirconia nanocomposites with optimized nano-geometry of the fillers and high electrical conductivity combined with enhanced fracture toughness without deterioration of hardness.

The *activities* related to the objectives are as following:

(i) design of a novel approach to electroconductive oxide ceramic-based composites added by graphenated nano-fillers;

(ii) development of a procedure for homogeneous dispersion of graphene-coated nano-fillers throughout ceramic matrix;

(iii) design, sintering and optimization of the SPS processing route for production of the flaw-less electroconductive alumina and zirconia;

(iv) structural, chemical, mechanical, and tribological characterisation of the sintered materials;

(v) testing electrical properties of the composites.

2. MATERIALS AND EXPERIMENTAL METHODS

2.1. Precursors

A novel type of graphene/alumina hybrid fillers were introduced into a ceramic matrix to develop hierarchically structured composites. Produced by controlled liquid phase oxidation, the bundled gamma-alumina nanofibers (ANF) with an average single fiber diameter of 7±3 nm, length of 4-6 cm and a specific surface area of 155-160 $m^2 \cdot g^{-1}$ (estimated by BET method), shown in Figure 2.1 and described in details in [56], were used as substrates for deposition of a few layers of graphene by the means of catalyst-less one-step chemical vapor deposition (CVD), as shown in Figure 2.2 and described in [Paper IV].

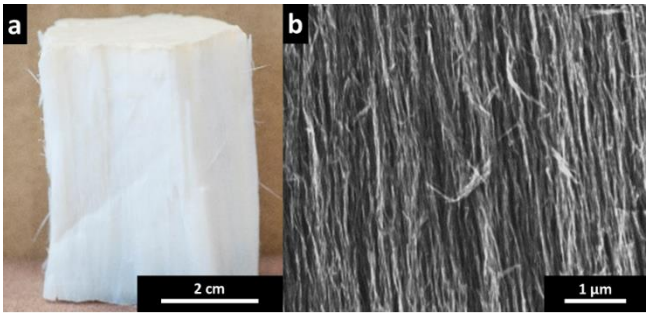

Figure 2.1 *Alumina nanofibers (ANF) a – photograph, b – SEM image – side view.*

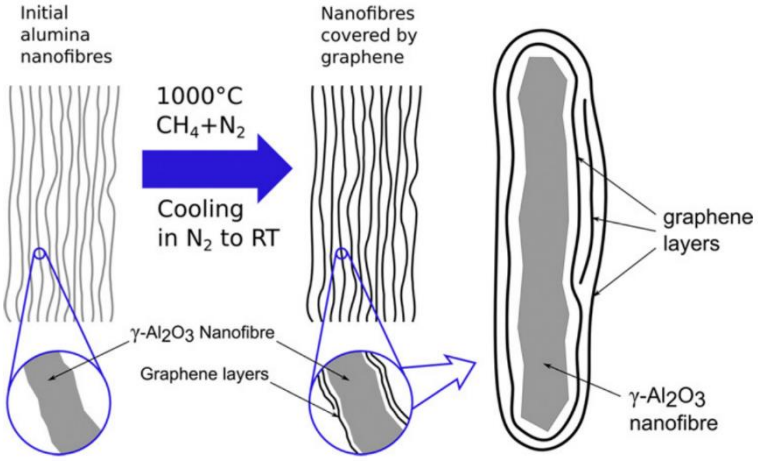

Figure 2.2 *Scheme of catalyst-free CVD growth of graphene layers onto the Al_2O_3 nano fibers. [Paper IV]*

Commercially available alumina and zirconia were selected as the matrix materials to study the effects of hybrid nanofibers addition on the properties of ceramic composites. The ultra-fine α-alumina (purity >99.99%, TM-DAR, Taimei Chemicals Co, Ltd, Japan) with an average particle size of 100 nm and PSZ powder stabilized with 3 mol% yttria (TZ-3Y-E, Tosoh, Japan) with an average particle size of 40 nm were used in this study.

2.2. Processing of composites

2.2.1. Powder compositions

The research was conducted in two stages. First step was work on alumina-based composites which was an outset to determine best compositions and optimise other powder processing conditions. Composites of Al_2O_3 powder with 1 vol.% (A1), 3 vol.% (A3), 5 vol.% (A5), 10 vol.% (A10) and 15 vol.% (A15) graphene-augmented alumina nanofibers (ANFC) were produced. The second stage of thesis focused on zirconia-based composites, where compositions were narrowed to 3 optimal fractions: 1 vol.% (Z1), 3 vol.% (Z3) and 5 vol.% (Z5) of hybrid fibers.

2.2.2. Ultrasound and attrition milling

After the CVD procedure, graphene-augmented alumina nanofibers keep the tight bundle form with fibers aligned in one direction. Fibers need to be ground and separated from each other in order to prepare uniform and well dispersed nanocomposites. First, the bundles were ground to a powder state in a mortar by hand to facilitate and reduce the duration of the subsequent procedures of ultrasonification and attrition milling. The grounded ANFCs were sonicated in ethanol by stick ultrasound (Hielscher UP400S) at the full cycle with amplitude 80% for 1 hour at 400 watt and 24 kHz, with additional cooling by a container with ice. Further, fibers were treated in an attrition mill with zirconia balls of 3 mm in diameter for 1 hour. During attrition milling the shear forces improve de-agglomeration of fibers to the level that cannot be achieved with ultrasonication alone. Subsequently appropriate amounts of ceramic powders were added to the milling vessel and the resulting content was milled further for 1 hour to ensure a homogenous distribution of hybrid fibers through the powder. Obtained mixtures were further dried at 65 °C for 24 hours, then sieved by 100 μm sieve.

2.2.3. SPS

Composites were sintered by Spark Plasma Sintering (SPS) technique in SPS-510CE furnace (Dr. Sinter, Japan). Appropriate amount of powder mixtures were loaded into a graphite die using a sheet of graphitic paper between the punch and die, and the powder for easier withdrawal of the sample after sintering. More details such as sintering temperatures and dwelling times can be found in [Paper I] for alumina systems and [Paper III] for zirconia systems.

2.3. Characterization methods

2.3.1. Microstructural analysis

The ANFCs and precursor powders were studied by a JEOL 2100F transmission electron microscope (TEM/HRTEM) operating at 200 KV and equipped with a field emission electron gun providing a point resolution of 0.19 nm. The powder mixtures and microstructure of the sintered ceramics were evaluated using Field Emission Scanning Electron Microscopes, FE-SEM HITACHI S-4700 and Zeiss HR FE-SEM Ultra 55 equipped with a Bruker EDS system ESPRIT 1.8.

2.3.2. Phase characterisation

To identify phases in the sintered samples by X-ray diffraction a Bruker diffractometer (D8) with CuKα radiation was used.

Raman spectroscopy is an important tool for characterizing carbon allotropes. It helps to learn about structure, defects, edges and others characteristics of carbon nanostructures based on the vibrational modes of their molecules. Raman spectroscopy with a Horiba Jobin Yvon LabRAM 300 spectrometer equipped with a 633 nm laser wavelength excitation was used to determine the degree of structural perfection of sp^2 carbon and the presence of the graphene in the sintered product.

2.3.3. Thermal analysis

The thermal behaviour of the ANFC was studied using two setups. Differential thermal and thermo-gravimetric analyses (DTA/TG) in air was carried out by SETARAM, SETSYS 16/18 system. Evolved gas analysis(EGA) and gas flow Fourier-transform infrared spectroscopy (FT-IR) coupled with thermo-gravimetric analyses (TG) were carried out by a and a Nicolet 6700 combined with TG from TA Instruments SDT (Q600 model).

DTA/TG were carried out in order to study the thermal behaviour of the sintered samples and determine the amount and form of carbon in them. The thermal analyses were performed on a Netzsch STA 449 F3 Jupiter Simultaneous Thermal Analyzer (TG–DSC/DTA Apparatus) coupled with a Netzsch QMS 403D Aeolos (mass 1–300 amu). The samples, ground to powder, were analysed in Pt/Rh crucibles with a lid and a removable liner composed of thin-walled Al_2O_3.

2.3.4. Density and mechanical properties

The density of the sintered samples was measured both by a conventional geometric method and Archimedes method using distilled water as the immersion medium. The theoretical densities of the composites were calculated according to the rule of mixtures. Hardness was measured with a help of the Indentec 5030 SKV Vickers hardness tester. The indentation was performed on the polished surfaces with a standard Vickers tip and the load of 49 N with a 10 s hold. Microhardness was measured by microhardness tester (Buehler Micromet 2001, USA) under the load of 4.9 N and with a holding duration of 10 s. The generated indents were observed under an optical microscope Zeiss Axiovert 25 equipped with a camera Canon EOS 350D. Data reported from indentation procedures were taken from an average of at least 10 indents. The indentation fracture toughness (IFT) values were determined using the direct crack measurement method of HV5 indentations. The developed crack system was determined as Palmqvist crack system by polishing the indented surface and studying the cracks in the SEM. The Palmqvist crack model equation suggested by Niihara [57] was used to compute the fracture toughness (K_{IC}). The Young's modulus values used for calculations of IFT for alumina and zirconia ceramics were determined by the impulse excitation technique (IET) according to ASTM-E1876 to be 380 GPa and 210 GPa, respectively. Same values of Young’s modulus were used to determine

toughness of the composite materials with density higher than 99%. For the less dense materials the dependence $E \approx E_0 \times e^{-bP}$ was assumed, where E_0 is the modulus of material with no porosity, P is the volume fraction of porosity, and b is a characteristic number, which is equal to 3 in case of spherical pores [58]. It should be noted that the single-edge V-notch beam (SEVNB) method of measuring fracture toughness is considered more reliable for ceramic composites with CNTs and graphene as compared to the indentation fracture toughness. However, the IFT can give the comparison values for the composites within the same system to determine tendency in improvement or worsening. The IFT method was chosen over the SEVNB in this work due to difficulties in the sample preparation for SEVNB method.

2.3.5. Tribological properties

Wear experiments were carried out with a Universal Micro Materials Tester (UMT-2) from CETR (now Bruker) in a reciprocating mode with a stationary ball located above specimen (wear debris were remaining in wear scar). Specimens were fixed to a reciprocating table. Grade 10 alumina ceramic balls (manufactured by Red-Hill Balls, Czech Republic) with a hardness HV10 ≈ 1450 and roughness R_a = 0.02 μm were used as counter-bodies. Wear tests were repeated at least 3 times. Prior to the wear test, surfaces of samples were polished down to 0.5 μm; the surface of the sample was cleaned step by step with acetone, ethylene alcohol and then dried. The main conditions of the testing are in detail described in [Paper II].

2.3.6. Electrical properties

Samples that showed a high enough electrical conductivity were subjected to a study of the room temperature electrical properties by a dc-four probe method. Autolab potentiostat/galvanostat (Autolab PGSTAT 302N) was used to supply the current through the external electrodes and to record the voltage drop between the inner electrodes. Silver paint was used to attach fine wire silver electrodes, as shown in Figure 2.3. The electrical conductivity was calculated from the experimental resistances obtained by the slope of the V-I curves in the range 10-100 mA.

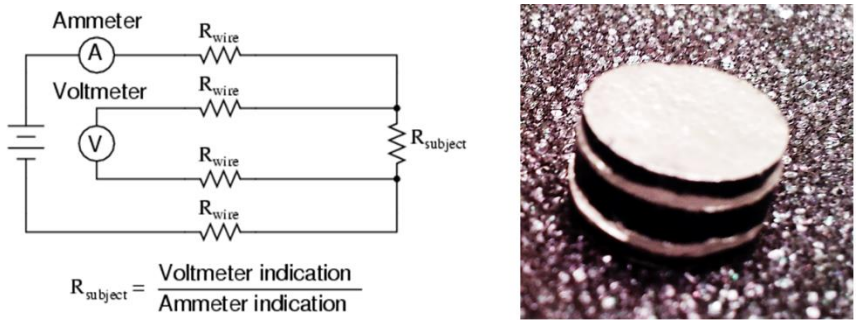

Figure 2.3 *Schematic illustration of the electrical circuit arrangement* [59] *and the sample prepared for electrical measurement.*

3. RESULTS AND DISCUSSION

In this chapter results of a study on effect of addition of hybrid graphene coated alumina nanofibers (ANFC) into the ceramic oxide matrix composites are reported. These results have been published in Paper I and Paper II.

3.1. Characterization of hybrid fibers used as fillers

The ANFC were prepared by depositing graphene on the alumina nanofibers using CVD procedure under the conditions of synthesis presented in [Paper IV]. These conditions were chosen as they provide a mass gain of about 10%, which was calculated to correspond to approximately 1-2 layers of graphene coating on 7-10 nm in diameter alumina fibers. It is desirable for the fillers to have minimal thickness of graphene coating (in order to minimize total carbon proportion in the composites), while still having the whole fiber surface completely covered (to maximize the positive impact of graphene).

3.1.1. Structure and quality of graphene layers

SEM, TEM and Raman analyses were performed in order to study the quality of graphene layers and overall structure of the obtained fibers.

The SEM and HR-TEM images of the hybrid fibers covered with graphene are shown in Figure 3.1. TEM analysis (Figure 3.1 b,c) confirmed that 1-3 layers of graphene are developed on the surface of Al_2O_3 nanofibers as a result of 10% mass augmentation during CVD procedure. The graphene layers form a "shell" around the ceramic support, rolling around the fibers along a longitudinal axis.

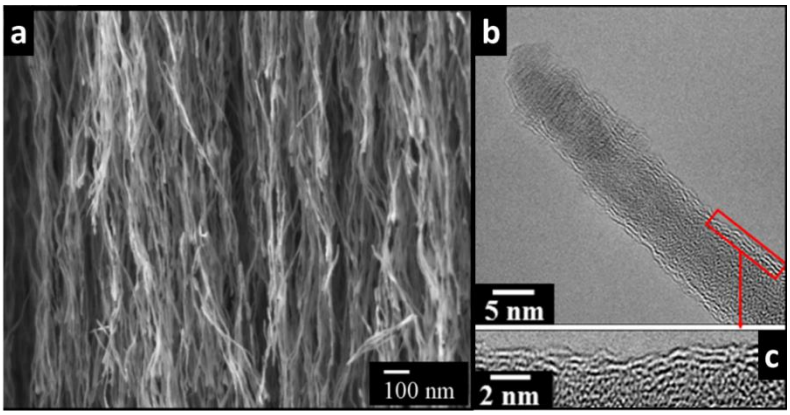

Figure 3.1 *a – SEM micrograph of the nanofibers; b – TEM image of the ANFC; c – HR-TEM image of the graphene layers.*

The interspace between the layers is measured to be about 0.3–0.4 nm. A number of edges were found with a help of HR-TEM (Figure 3.1, c) confirming the growing of discontinued structure of graphene flakes during CVD.

Raman spectra obtained from the hybrid fillers is presented in Figure 3.2. The typical 5 peaks, which usually feature "damaged" graphene [60] and also

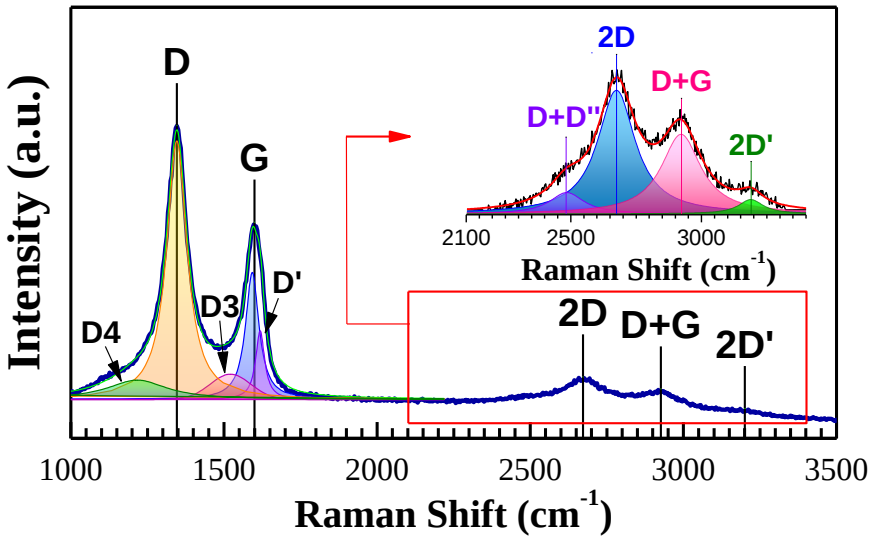

Figure 3.2 Raman spectra of the ANFC

observed for GPLs and MWCNTs [61], can be observed in the Raman spectra. Raman bands include the two signature peaks of sp^2 bonds representative to all graphitic carbon allotropes: the G band, located at 1597 cm^{-1}, which is related to the C–C bond stretching of all pairs of sp^2 atoms in both rings and chains [62] and the G′ band (also labelled 2D) at 2676 cm^{-1}, which is the second-order sp^2 Raman signature [60]. At 1346 cm^{-1} the defect-derived D band was observed, which is an indicator of disorder in the structure as it is activated due to presence of asymmetry. It has been reported to arise due to the discontinuity of graphite planes on the edges of graphene layers [63]. To quantify the "quality" of graphene by the amount of structural disorder or open edges, the intensity of D band was normalized by the intensity of G band. Calculated I_D/I_G ratio for the graphene shell deposited on the fibers was estimated to be about 1.6, which indicates presence of large amounts of defective structures. Probably these are edge defects in this case, as detected by TEM. The D', D3 and D4 peaks, not apparent in the observed spectrum, but presence of which is established by the need to fit the curve [61,64] are also marked in the Figure 3.2. The D' and D4 bands are, similarly to the D band, characteristic for disorder in the structure: D' is connected with carbon atoms vibration at the surface of a graphitic crystal (not sandwiched between two other graphene layers) and D4 is related to the disordered graphitic lattice [64]. The D3 band can be regarded as a sign of some amount of amorphous carbon [61,64]. In the second-order spectra bands D+D" and D+G are also activated by defects and indicating the disordered structure [65].

Raman and TEM analyses results allow concluding that the deposited carbon is in the form of highly defected graphene.

3.1.2. Thermal analysis

Study of thermal behaviour of the hybrid graphenated fibers gives us idea about their thermal stability and the processes taking place with the temperature rise. The thermogravimetric (TG) curve and its derivative (DTG) curve, differential thermal analysis (DTA) curve and evolved gas analysis (EGA) curve of ANFCs (a), and coupled with gas flow FT-IR spectra (b) are shown in Figure 3.3. From the EGA curve around point (1) (~ 110 °C) a sharp increase in gas flow can be observed, which is attributed to the intensive water evaporation, detected in the FT-IR spectra. The largest exothermic peak in the DTA curve and major weight loss (~7.5%) was observed between 400 and 600°C, which indicates the combustion of graphene layers. The FT-IR spectra taken at point (3), at 560 °C confirms this with highest absorbance peaks for CO_2 gas at 670 and 2300 cm^{-1}. Some mass loss (about 1.6 % or about 10% of the total mass loss) and vague exothermic peak in DTA, as well as CO_2 absorbance showing in the range between ~200 °C and ~400 °C can be attributed to the combustion of amorphous carbon. The behaviour is similar to the oxidation of MWCNTs in air where both amorphous carbon and graphene layers oxidize simultaneously [66]. Above 600 °C, a slight endothermic effect can be seen on the DTA curve, which is

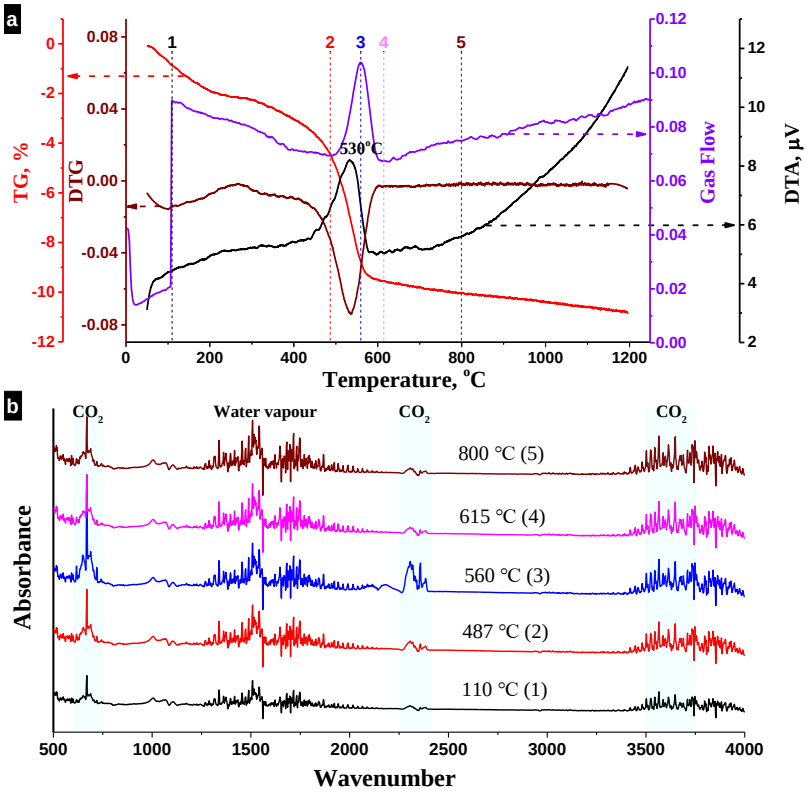

Figure 3.3 *TG, DTG and DTA curves of ANFCs combined with gas flow curve recorded during FT-IR analysis of the gases emitted by ANFCs heating (a); IR absorption spectra at selected temperatures (b).*

accompanied by an insignificant weight loss. However, the bands corresponding to CO_2 exhibit less intensity while bands corresponding to water are still well recognizable at 800 °C, point (5). It is presumed that the chemisorbed water (some kind of hydroxyls) evolves at the temperatures above 600 °C.

Thermal analysis of the fibers showed that the graphene layers of the ANFC show similar behaviour to MWCNT, which is expected, as ANFC can be seen as carbon nanotubes wrapped around the alumina fibers.

3.2. Characterization of powder mixtures

One of the important parts in understanding the properties of composite is related with a preparation process. Al_2O_3 and ZrO_2 powders were mixed with ANFCs in different ratios as described in Section 2.2. Figure 3.4 demonstrates FESEM images of alumina powder mixtures with 1 vol.%, 3 vol.%, 5 vol.% and 15 vol.% of ANFC. Although, the homogeneous distribution of the ANFC throughout ceramic matrix is confirmed, the existence of overlapped fibers and

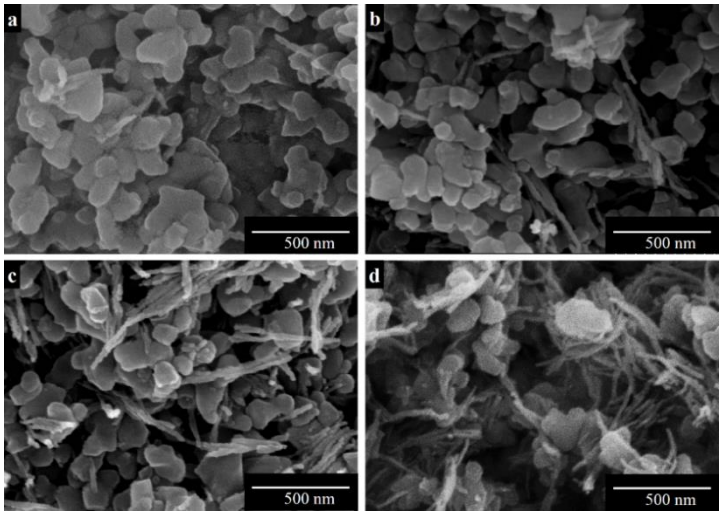

Figure 3.4 *SEM images of the powder mixtures of Al_2O_3 powder with a – 1 vol.%ANFC, b – 3 vol.%ANFC, c – 5 vol.%ANFC and d – 15 vol.%ANFC [Paper I].*

some bundles is also obvious, which indicates the moderate agglomeration of ANFC, especially in case of high concentration of the fiber additives. It can be seen that the length of the fibers is less than 1 μm after the processing, so the aspect ratio decreased to 10^2. The schematic representation of the different types of fibers that are possible to be found in the dried powder mixture is shown in Figure 3.5, depicting how block of ANFC is dismantled into bundles and single ANFC mono fibers, as well as some loose graphene flakes. Graphene flakes are forming additionally to dismantling process, when a crushing of fibers by impacts takes place, leading to formation of different size fibers with possibly a damaged (partly covered) graphene coatings, releasing some graphene flakes with a rounded structure. HR-TEM images of the final powder are demonstrated in Figure 3.6, showing that ultrasound processing and/or attrition milling in general

did not cause significant damage to the graphene. Unaffected 2–3 nm thick graphene layers can be well distinguished in Figure 3.6, b-c.

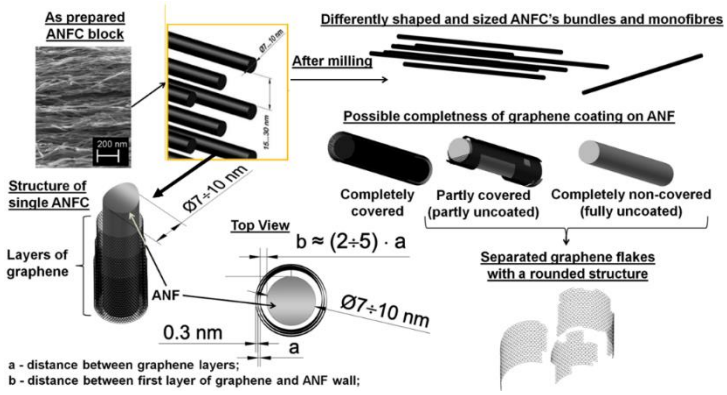

Figure 3.5 *Schematic of ANFC as prepared and after milling [Paper II]*

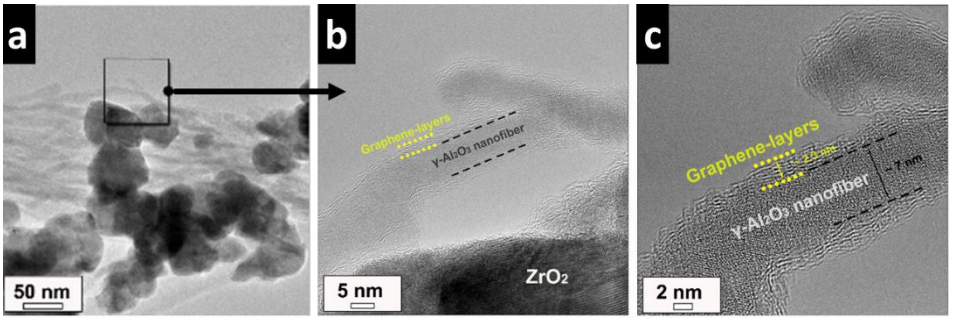

Figure 3.6 *HRTEM images of the processed PSZ-ANFC green powder: a – the general micrograph of the powder, b – HRTEM image of the area specified in (a) at a higher magnification, c – HRTEM image of the single fiber in the mixture.*

3.3. Synthesis and characterization of alumina-based composites

In this section the synthesis of alumina-based composites reinforced by the alumina-graphene hybrid fibers is reported. The goal of this work was to produce electroconductive alumina without deterioration of the mechanical properties.

3.3.1. Parameters of densification

To find out the optimal sintering temperature for alumina-ANFC nanocomposites, a set of tests were carried out. To roughly estimate sintering temperatures for the SPS experiments, a dilatometric study of alumina powders (Figure 3.7) was performed in pressureless conditions in air under conditions of the rate of temperature raise of 5 °C·min^{-1} from the ambient to 1550 °C. It was found that the shrinkage begins at about 940 °C and ends at about 1400 °C. The total contraction of the sample is ~14%. The maximum of densification rate, which is determined by the minimum point of derivative of the dilatometric curve,

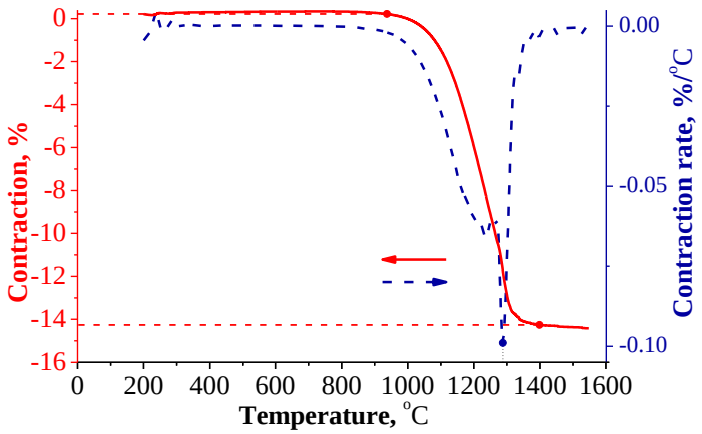

Figure 3.7 *Dilatometry of the alumina powder [Paper I]*

is reached at the temperature of 1290 °C. Series of SPS experiments were performed with the ranging in peak temperatures between 1350 °C and 1400 °C.

A reference alumina sample and composites with lower fractions of graphenated fillers (up to 5 vol.%) were consolidated to almost full density (>99 of theoretical density) when the temperature was 1380 °C and above, while the specimens prepared at lower temperatures had higher porosity. The difference in the relative density between samples processed at 1380 °C with low content of hybrid reinforcement up to 5 vol.% is ineffectual as shown in Table 3. Thus, it can be concluded that up to this amount the additives did not considerably affect the

Table 3 *Series of SPS experiments to determine optimal sintering temperature.*

ID	Temperature (°C)	ANFC (vol.%)	Density (g/cm^3)	TD (%)
	1350	**0**	3.92	98.9
	1350	**15**	3.71	94.4
A0	**1380**	**0**	3.94	99.4
A15	**1380**	**15**	3.77	95.8
A10	**1380**	**10**	3.84	97.4
	1400	**15**	3.76	95.5
	1400	**10**	3.82	96.9
	1350	**5**	3.90	98.7
A5	**1380**	**5**	3.95	100.0
A3	**1380**	**3**	3.95	99.8
A1	**1380**	**1**	3.96	99.9

densification behaviour of the composites. However, the composites added by 10 and 15 vol.% of the fillers possess a residual porosity at any temperatures tested, which can be attributed to the high concentration of agglomerated fibers in the precursor mixture, that is hindering the sintering process. Based on these results, an optimal sintering temperature for the further study of alumina-based composites was considered 1380 °C, and a preferable portion of additives to obtain the full density determined to be up to 5 vol.%.

3.3.2. Composition and structural integrity of graphene

The X-ray diffraction pattern obtained for the specimen with the highest amount of ANFC (15 vol.%, which corresponds to 1.5 wt.% of graphene) detects only α-Al_2O_3 peaks with no other compounds as presented in

Figure 3.8. It confirms insignificant or no reactions between graphene and alumina during the SPS processing.

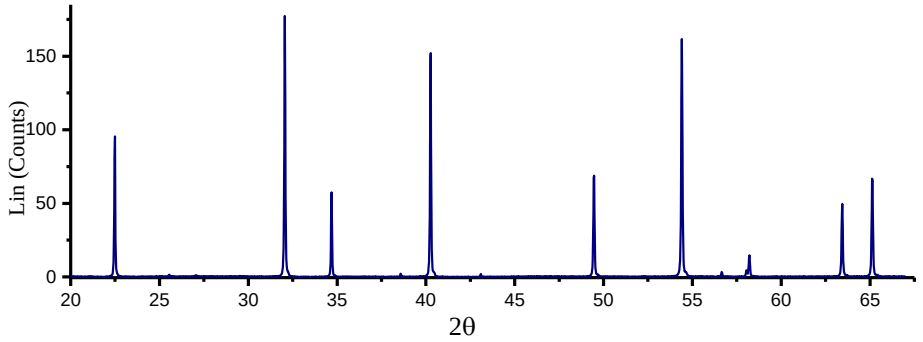

Figure 3.8 *XRD pattern of A15 (15 vol.% ANFC); all peaks correspond to α-Al_2O_3.*

To determine the amount of carbon in the sintered bulk composites, the DTA/TG analysis in air was conducted. TG and DTA curves of the A10 specimen were chosen to demonstrate composite specimens' performance (Figure 3.9). The

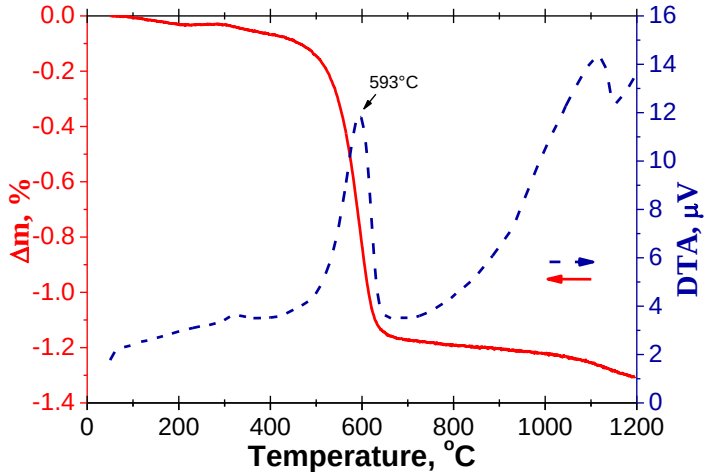

Figure 3.9 *DTA/TG curves for A10 (10 vol.% of ANFC)*

sharp decrease in weight (about 1% of the remained mass) was observed between 420 and 620 °C, which is accompanied by the exothermic effect. This mass loss effect is caused by the oxidation of the so-called "graphitized carbon", similarly to one found in the thermal behaviour of the pristine hybrid fibers described in Section 3.1. Thus, the amount of carbon in the sintered composite added by 10 vol.% of fibers is around 1 wt.%, which means each 1 vol.% of graphene covered nanofibers adds approximately 0.1 wt.% of carbon to the composites. This result is in agreement with previously estimated percentage of carbon deposited onto the fibers by CVD being about 10 wt.%.

The structural integrity of graphene in the composites after sintering were confirmed by Raman spectroscopy analysis as shown in Figure 3.10. The Raman spectrum of the sintered A10 specimen is shown together with one of the pristine fibers. The defect-derived D-band (~1350 cm^{-1}), the structure derived G-band (~1600 cm^{-1}) and the 2D band at ~2700 cm^{-1} can be clearly observed for the sintered specimen added by 10 vol.% fibers. Intensity of the D band normalized by the intensity of the G band was compared with the one of the untreated ANFC. The similar values of the I_D/I_G ratio for the fibers and the sintered composite sample indicates that the nanostructure of graphene remained undamaged during processing.

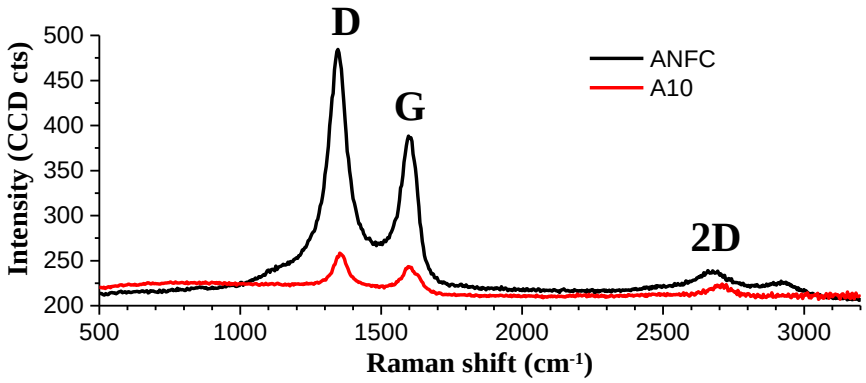

Figure 3.10 *Raman spectrum of pristine ANFC and A10 sample (10 vol.% ANFC)*

3.3.3. Microstructure of the composites

The microstructure and grain morphology of the composites was studied with the help of SEM imaging of the fractured surfaces as shown in Figure 3.11. The microstructure of pure alumina, presented in Figure 3.11, a, exhibits a distribution in grain size in the range of 1–5 μm. Presence of a small amount of inter- and intra-granular pores can be noted. When only 1 vol.% of ANFC is introduced into the matrix, a significant change in the microstructure occurs (Figure 3.11, b). Graphenated fillers result in formation of both nano-sized and abnormally grown elongated alumina grains. With increased percentage of the fillers, a grain size distribution becomes narrower, and a substantial decrease in grain size is registered. The grain refining effect of graphene has been reported in many works [33,67–71], and, evidently, hybrid graphenated fibers also replicate this

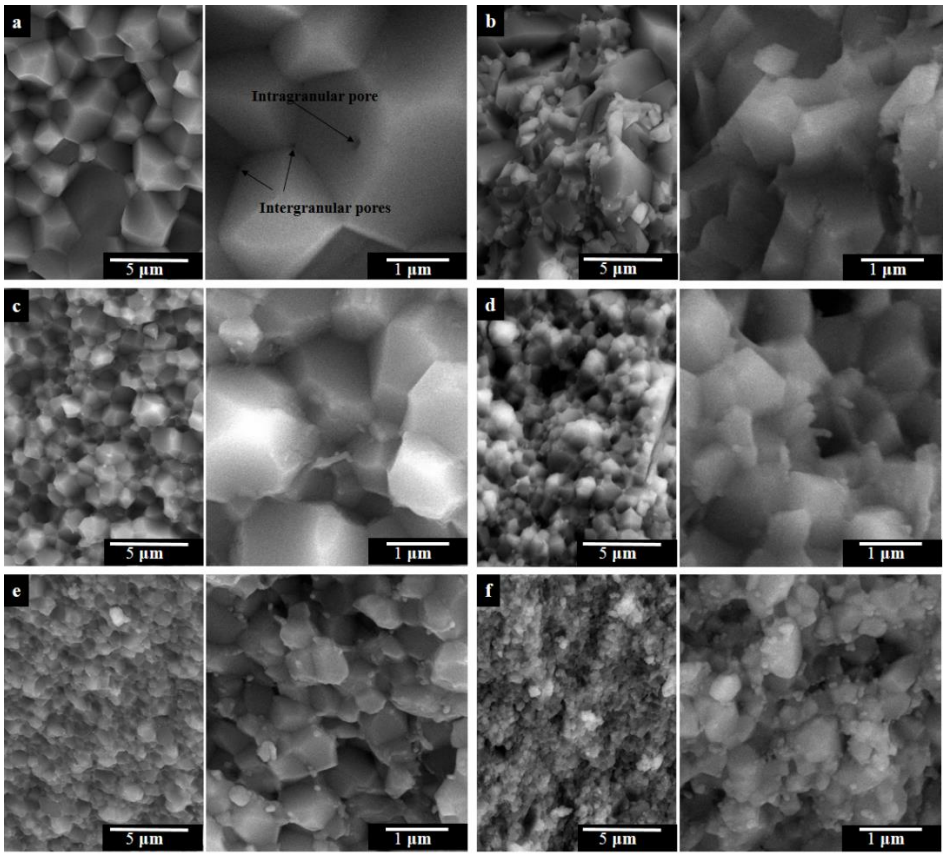

Figure 3.11 *FE-SEM images of the fracture surfaces of the sintered samples added by different amount of ANFC: a – A0, b – A1, c – A3, d – A5, e – A10, and f – A15 [Paper I]*

feature. Such refinement of the microstructure is attributed to the distribution of graphene layers throughout ceramic grain boundaries and preserving their migration during sintering. SEM observation at higher resolution reveals that graphene covered nanofibers are also located mainly in the grain boundaries or junctions of Al_2O_3 grains, preventing grain growth as shown in Figure 3.12. Some

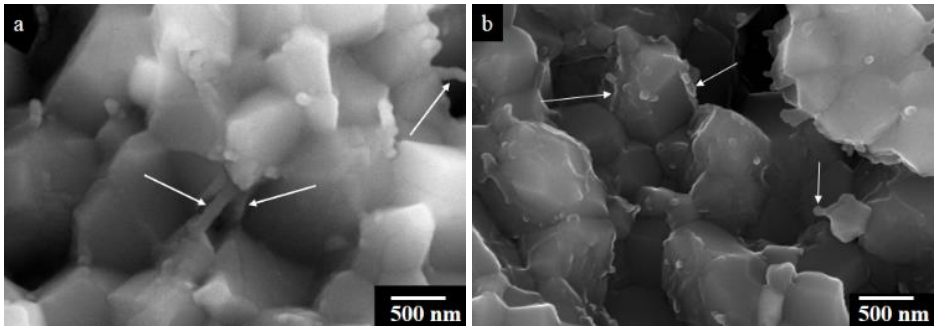

Figure 3.12 *FE–SEM images of the hybrid fibers in the a – A5 and b – A10 composites*

fibers are embedded into the alumina grains, and others are distributed along grain boundaries of the matrix. Hence, the mechanism of grain growth inhibition in case of the given fillers can be attributed to the same reason, as in a case of graphene or CNTs, namely, pinning grains together and impeding boundary diffusion [72].

3.3.4. Mechanical properties and wear performance of the produced composites

A composition, relative densities and the corresponding mechanical properties along with relative index of brittleness (RIB is a HV/IFT ratio divided by HV/IFT of pure alumina) for reference pure alumina and composites with different content of ANFC are summarized in Table 4. The hardness of composites with a content of fibers of 1-5 vol.% was increased by about 8-10% over the pure alumina, reaching its maximum value of HV1 1830 (17.95 GPa). While increase in hardness may be related to the grain refinement conditioned by supplementing composites with ANFCs, when the amount of additives reaches a certain concentration deteriorating full densification, the increased residual porosity exponentially reduces hardness of the material. Thus, the combined impact of these two effects is reflected by the variation in hardness.

Table 4 *Mechanical properties of the alumina/ANFC composites*

Composition	**ID**	**Carbon, wt%**	**Relative density, %**	**Vickers hardness HV1**	**IFT, MPa·m$^{0.5}$**	**RIB**
Al_2O_3	**A0**	0	>99	1670 ± 78	3.34 ± 0.1	1
Al_2O_3/1 vol.%ANFC	**A1**	~0.1	>99	1830 ± 93	3.91± 0.11	~0.93
Al_2O_3/3 vol.%ANFC	**A3**	~0.3	>99	1824 ± 33	5.4 ± 0.09	~0.67
Al_2O_3/5 vol.%ANFC	**A5**	~0.5	>99	1820 ± 45	5.6 ± 0.17	~0.65
Al_2O_3/10 vol.%ANFC	**A10**	~0.10	~98	1791 ± 67	5.03 ± 0.3	~0.71
Al_2O_3/15 vol.%ANFC	**A15**	~0.15	~96	1640 ± 98	3.3 ± 0.34	~1

The indentation fracture toughness value for the reference sample of alumina was measured to be 3.34 MPa·m$^{0.5}$. With ANFC additive, the fracture toughness of the composites is increased to the maximum value of 5.6 MPa·m$^{0.5}$ for the Al_2O_3/5 vol.% ANFC composite corresponding to an increase of approximately 68% as compared to the pure alumina. With further increase in filler amount, the IFT was found decreased due to a higher level of porosity and formation of nanofiber agglomerates and interconnected network that may act as weak interfaces [73]. Possible toughening mechanisms contributing to the increased toughness in the composites added by hybrid nanofibers are depicted in a schematic diagram shown in Figure 3.13.

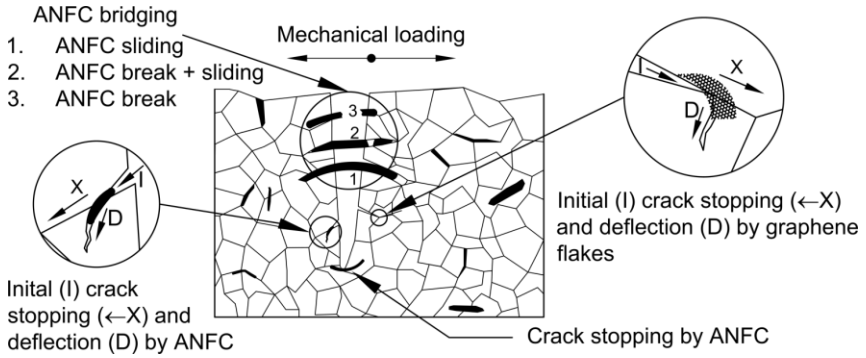

Figure 3.13 *Toughening mechanisms in the composites. [Paper II]*

Graphene is considered to be a promising candidate for solid lubrication to reduce the coefficient of friction between sliding surfaces at micro- and nano-scale. Intriguing results on reduction of wear rates for graphene reinforced ceramic-based nanocomposites have been reported in several studies [74–77]. The improved wear performance is believed to be a result of the simultaneously acting toughening mechanisms such as crack bridging, crack branching and crack deflection together with the formation of the protective tribofilm on the wear track. To study the effect of ANFCs on wear resistance of the composites, wear tests under mild and severe abrasive conditions have been carried out. Wear rates of the composites sliding against alumina ball with hardness of HV1450 are shown in Table 5 and the coefficients of friction (COF) as a function of sliding time in mild and severe conditions are shown in Figure 3.14 and Figure 3.15, respectively. Under the low applied load of 0.98 N, the composite with 1 vol.% of fibers exhibits minimal COF; the lowest value for the weight loss was observed for the composite A3 with a 60% reduction as compared to A0. The composite with 15 vol.% ANFC, due to its relatively high porosity, shows wear rate as high as that of the pure alumina. For more detailed analysis on wear performance see [Paper II].

Table 5 *Wear rates of alumina and alumina/ANFC composites in mild and severe conditions*

Composition	**ID**	**Carbon, wt%**	**Wear, mild cond., x10^{-9} mm^3/Nm**	**Wear, severe cond., x10^{-9} mm^3/Nm**
Al_2O_3	**A0**	0	11.1 ± 8.5	231.2 ± 149.6
Al_2O_3/1 vol.%ANFC	**A1**	~0.1	5.2 ± 1.4	15.6 ± 2.6
Al_2O_3/3 vol.%ANFC	**A3**	~0.3	4.0 ± 3.0	394.2 ± 196.8
Al_2O_3/5 vol.%ANFC	**A5**	~0.5	5.5 ± 2.9	853.2 ± 89.7
Al_2O_3/10 vol.%ANFC	**A10**	~0.10	4.4 ± 2.2	700.6 ± 105.8
Al_2O_3/15 vol.%ANFC	**A15**	~0.15	12.1 ± 4.5	468.9 ± 39.7

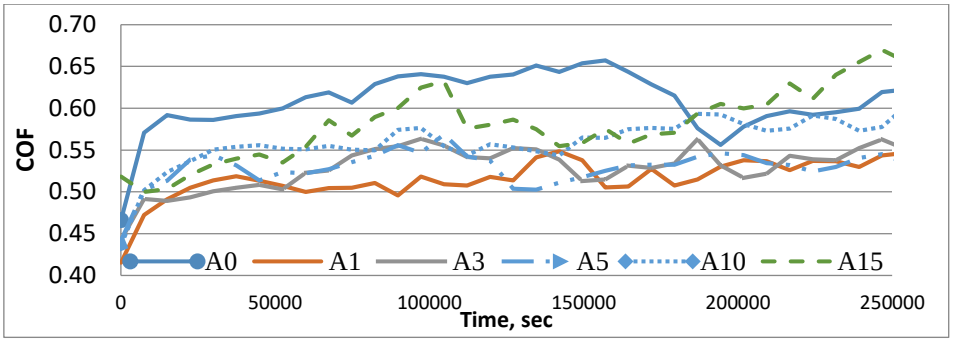

Figure 3.14 *Coefficient of friction as a function of time of the composites in mild test conditions [Paper II]*

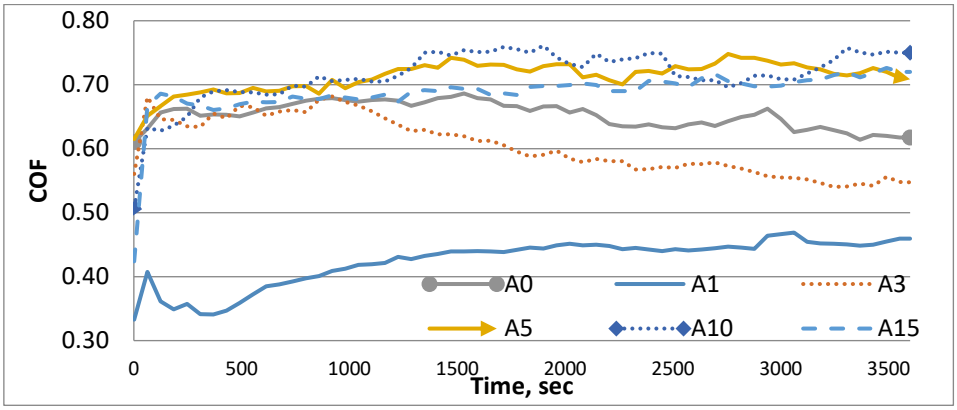

Figure 3.15 *Coefficient of friction as a function of time of the composites in severe test conditions [Paper II]*

To sum up, composites added by the fibers covered with graphene containing additives starting from 10 vol.% demonstrate mediocre mechanical and tribological properties because of their relatively high residual porosity due to poor sinterability of mixture of metal oxides and carbon. Composites A3 and A5 proved to have improved both hardness and toughness and showed enhanced performance during mild wear test. Composite A1 shows the minimal among other materials COF ranged from 0.45 up to 0.5, also coupled with high hardness. One of the main microstructural features of this material is a structure combining large grains (up to 5 μm) with ultra-fine scaled ones (about 0.7 μm) together with nano-reinforcements of several nanometres in diameter and a huge aspect ratio of 10^2.

3.3.5. Electrical properties of the produced composites

In addition to the outstanding mechanical properties, graphene is also known for its high electrical conductivity. Addition of the graphene or CNT to alumina matrix leads to change of initially insulating behavior of Al_2O_3 to electrically conductive [33,35,45,78].The electrical conductivity of the composites as a function of filler percentage is depicted in Figure 3.16. Pure alumina has

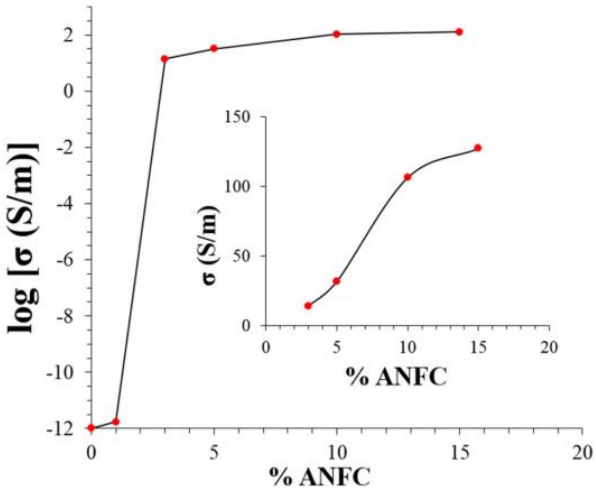

Figure 3.16 *Electrical conductivity of alumina/ANFC composites as a function of ANFC content [Paper I]*

conductivity below 10^{-12} S·m^{-1}. An increase in electrical conductivity by nearly 13 orders of magnitude is detected for the composite with 3 vol.% of fillers. Therefore, the percolation threshold for the alumina-based composites with graphene encapsulated nanofibers can be considered around or lower than 3 vol.%, which corresponds to only 0.3 or lower wt.% of graphene. With further addition of ANFC, the electrical conductivity is enhanced up to 127 S·m^{-1} for 15 vol.%. Noticing that in Al_2O_3/CNT composites the conductive phase content of at least 2wt.% burdened by significant deterioration of hardness is needed to reach the same level of conductivity, this result shows the unparalleled advantage of graphene-covered nanofibers as reinforcing phase in composites compared with other carbon materials. The homogeneous distribution of the fibers throughout the matrix enables an interconnected network of the conductive fillers containing only 10 wt.% of graphene, while the rest mass pertains to the alumina core. This allows a sample with as low graphene content as 0.3 wt.% to develop interconnected network of conductive phases, and therefore, to turn into electro-conductive material.

The results show the strategy of core-shell hierarchical fillers to be successful in homogeneous dispersion of conductive nano-additives throughout the matrix and enhancing conductivity of the composites, retaining high hardness of the original material and at the same time improving toughness and wear performance.

3.4. Synthesis and characterization of zirconia-based composites

In this section the synthesis of electroconductive zirconia-based composites doped by the hybrid graphene-augmented alumina nanofibers is reported. The composites added by 1, 3 and 5 vol.% of ANFC (further indicated as Z1, Z3 and Z5) have been consolidated by spark plasma sintering (SPS). Given fraction percentage was chosen based on the previous work on alumina-based composites,

which has shown the optimal amount of fillers to achieve fully dense (>99% relative density) bulk composites to be within 1 – 5 %. Results of this study are demonstrated in detail in Paper III.

3.4.1. Parameters of densification

The dilatometry curve of pure PSZ powder subjected to sintering in air with a constant heating rate of 5 °C·min^{-1} is shown in Figure 3.17. The material undergoes a total contraction of 27% with the largest portion of contraction in between approximately 900 °C and 1400 °C. A relative maximum shown by the shrinkage rate is at 1185 °C corresponding to the monoclinic to tetragonal phase transformation of PSZ powder. The highest rate of densification, determined by the absolute minimum of shrinkage derivative in the dilatometry curve, is reached at approximately 1255 °C.

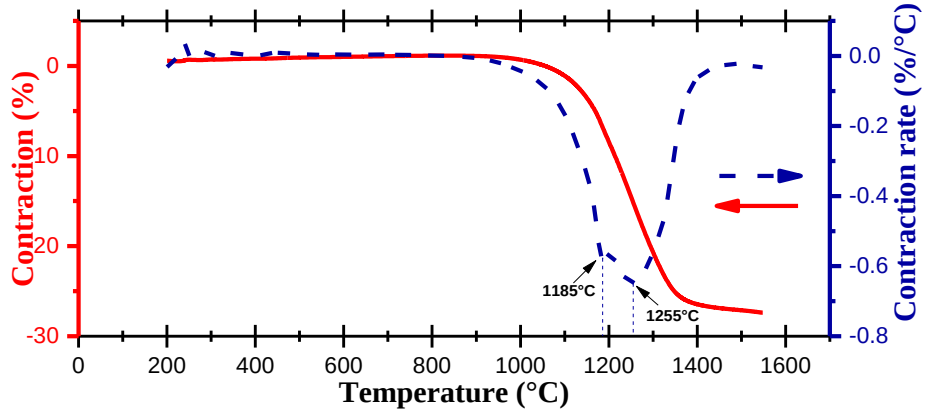

Figure 3.17 *Dilatometry curves of PSZ powder [Paper III]*

A temperature of 1250 °C, pressure of 40 MPa and holding time 5 minutes were chosen for the SPS processing as it yielded close to full density (>99%) reference sample.

3.4.2. Composition and structural integrity of graphene

XRD observation of the sintered specimens revealed no significant effect of the sintering process on the constituents of the composites. The XRD pattern presented in Figure 3.18 shows no other phases except for ZrO_2, demonstrating no reaction between graphene and zirconia. It should be also noted that zirconia has retained its tetragonal phase after sintering.

Tetragonal zirconia polycrystalline phase was also recognised in the Raman spectrum of the samples by the presence of peaks at 146 cm^{-1}, 259 cm^{-1}, 319 cm^{-1}, 464 cm^{-1}, 607 cm^{-1} and 641 cm^{-1}[79,80], as shown in Figure 3.19. Other peaks, seen at the higher shifts of Raman spectra, are related to graphene structures, and correspond to the peaks also found in Raman spectra of the hybrid nanofibers encapsulated in graphene layers as described in Section 3.1.1. For the sintered composites these peaks are located at around 1350 cm^{-1}(D), 1600 cm^{-1}(G),

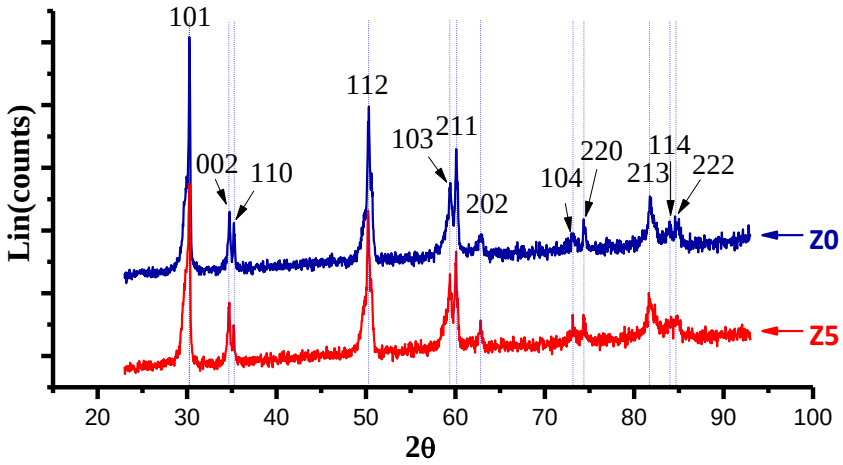

Figure 3.18 *XRD patterns of PSZ reference sample (Z0) and composite sample (Z5) correspond to tetragonal zirconia.*

2690 cm^{-1}(2D), 2940 cm^{-1}(D+G) and 3250 cm^{-1}(2D'), showing slight upshift in a second-order spectrum compared to the pristine fiber. The upshift can be explained by the mechanical restriction of the freedom of C-C vibrations in graphene layers imposed by zirconia matrix [81]. Peaks were found exhibiting lower intensity as compared to the graphenated fibers due to a small fraction of graphene in the sintered materials. However, the peak intensity ratio for the D band and the G band (I_D/I_G) being between 1.6 and 1.8, is close to initial I_D/I_G ratio calculated for the fibers (~1.6), which confirms the integrity of the initial graphene structure in the composites after ultrasonification, milling and SPS processing. The presence of few-layered graphene within the sintered samples is also confirmed by the Raman map showing the intensity ratio I_{2D}/I_G, insert in Figure 3.19.

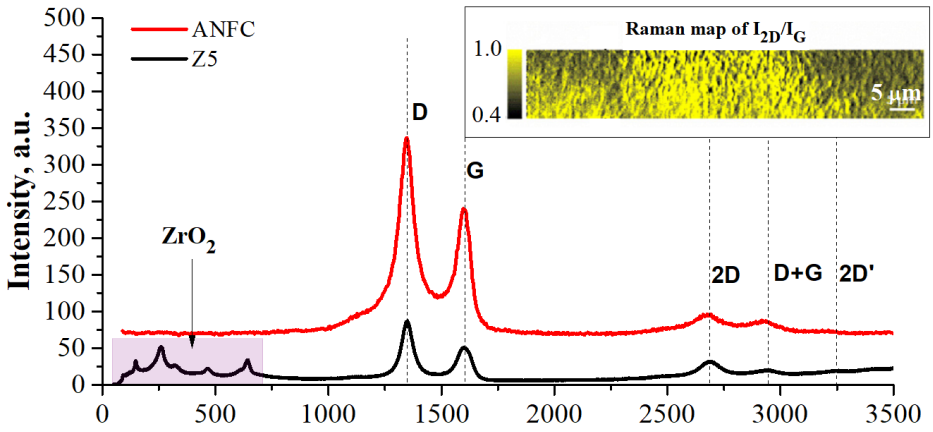

Figure 3.19 *Raman spectrum of the pristine ANFC and the composite (Z5)*

The DTA/TG analysis of the sintered samples was carried out in order to get quantitative assessment of graphene content in the bulk material. Samples were preliminarily crushed into powders to allow better access of oxygen during heating. As expected, the TG curve of reference zirconia sample shows no mass change during heating up to 1200 °C. The TG curves of the composites added by hybrid fillers indicate mass loss in the temperature interval between 420 °C and 620 °C, which is in good agreement with the oxidation temperatures reported for the multi-walled carbon nanotubes in air [82]. DTA and TG curves obtained from the Z5 sample are presented in Figure 3.20. Mass losses of 0.33% and 0.20% were detected for the specimens Z5 and Z3, correspondingly. For the material with only 1 vol.% of graphenated hybrid nanofibers content (0.07 wt.% of graphene) the obtained results were in the range of an experimental error (~0.02%).

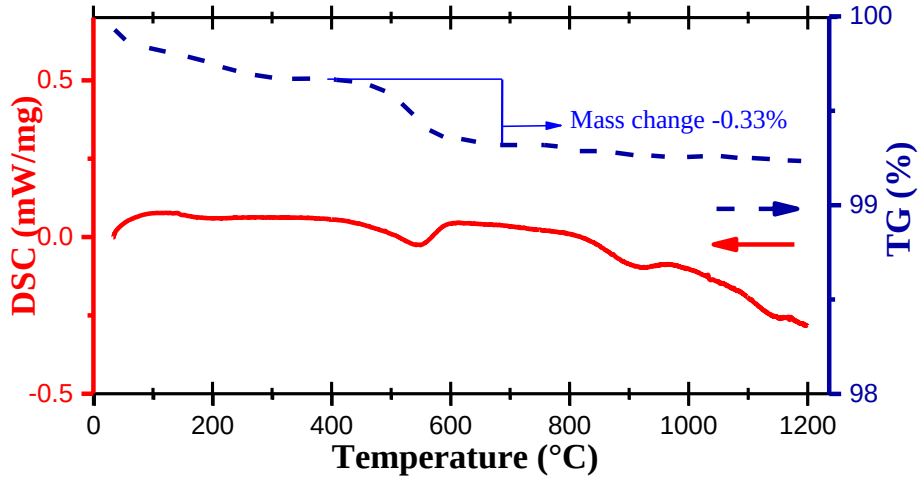

Figure 3.20 *DTA/TG curves for Z5 specimen*

3.4.3. Microstructure of the composites

FE-SEM micrographs taken from the fractured surfaces of composites doped with ANF are shown in Figure 3.21. Homogenous distribution of fillers throughout the nearly pore-free zirconia microstructures with narrow grain size distribution can be observed. Fibers are located between the grain boundaries and in junctions of zirconia grains (pointed out with arrows), their debonding and pull-outs are visible on the fractured surface. Zirconia grains exhibit a mixed (transgranular and intergranular) fracture mode.

In contrast to the widely reported grain growth inhibition by different types of graphene structures when added to alumina [70,83] or silicon nitride matrix [84,85], an incorporation of graphenated additives into the partially stabilized zirconia matrix up to 5 vol.% did not result in any noticeable suppression in grain size and/or morphology. Similar results have been reported for reduced graphene oxide reinforced zirconia composites [22]. A large increase in grain size can be detected in zirconia samples with the processing temperature

rising above 1350 °C, and only at this point the refining effect of CNTs added to the composite is noticeable, as it have been found in [86]. The grain size for both pure zirconia sample and those doped with CNTs remains in same level after annealing at temperatures up to 1350 °C.

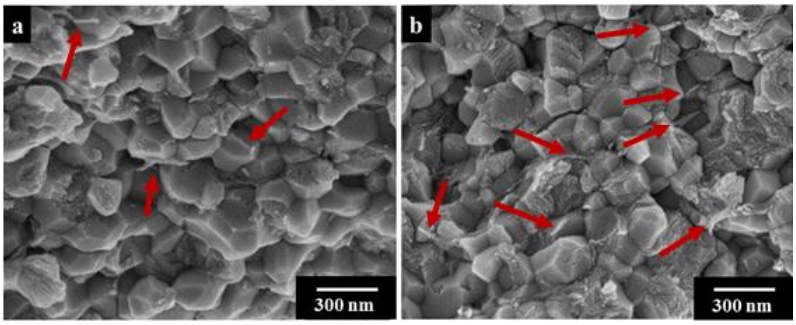

Figure 3.21 *FE-SEM images of fracture surface of the composites: a – Z3 and b – Z5; red arrows denote ANFC*

3.4.4. Mechanical properties of the produced composites

Mechanical properties and density of the materials tested at room temperature are demonstrated in Table 6. All the samples attained density of >98%, though the hybrid fillers seem to slightly hinder densification, leading to a more porous structure (with minimum relative density of 98% measured for Z5 sample).

Table 6 *Mechanical properties of the monolithic zirconia and composites added by the graphenated nano fibers*

Composition	ID	Carbon, wt.% / vol.%	Relative density, %	Vickers Hardness, GPa	IFT, $MPa \cdot m^{0.5}$
ZrO_2	**Z0**	0	~99	14.0 ± 0.3	5.73 ± 0.1
ZrO_2/1 vol.%ANFC	**Z1**	~0.07 / ~0.19	>98	13.86 ± 0.3	6.25 ± 0.1
ZrO_2/3 vol.%ANFC	**Z3**	~0.20 / ~0.54	>98	13.75 ± 0.2	6.91 ± 0.2
ZrO_2/5 vol.%ANFC	**Z5**	~0.34 / ~0.91	~98	13.4 ± 0.4	5.77 ± 0.3

Unlike the alumina matrix composites, the hardness of zirconia-based composites undergoes slight reduction when the portion of the additives is increasing. As a grain size refinement usually plays an important role in enhancement of the hardness of materials, lack of positive effect on hardness in zirconia can be explained by the absence of grain size reduction. At the same time, slight decrease in hardness is expected, as it is in compliance with the decrease in density of the samples. Nevertheless, it should be noted that changes in hardness were found not exceeding ~5% as compared to the pure zirconia sample.

In terms of indentation fracture toughness, hybrid graphenated fibers were exhibiting recognizable improvement. An approximate 20% increase in fracture toughness over monolithic ZrO_2 is achieved by adding 3 vol.% ANFC. Fracture toughness increased with increasing the contents of fillers up to 3 vol.%, then decreased again when the ANFC content reached 5 vol.%. SEM micrographs of

indentation-induced cracks in 5 vol.% ANFC added zirconia composites are shown in Figure 3.22. The general crack appearance in the Z5 composite compared to Z0 is shown in Figure 3.22, b. The monolithic ZrO_2 material exhibits typical "brittle" crack propagation; the cracks in the samples added with graphenated fillers demonstrate bridging, pulled-out fibers, and crack deflections.

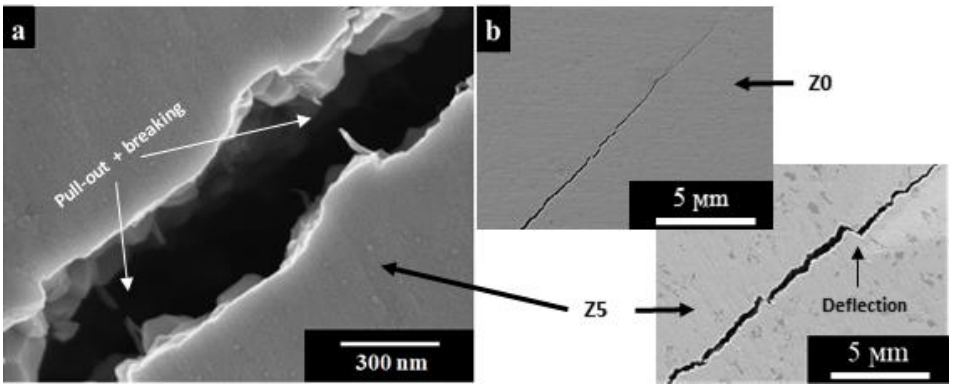

Figure 3.22 *SEM images of the indentation induced cracks.*

3.4.5. Electrical properties of the produced composites

The electrical conductivity of the zirconia-based composites added by ANFC was measured as a function of the graphene content (Table 7). Pure zirconia and the Z1 composite added by 1 vol.% (~0.07 wt.% graphene) ANFC was found exhibiting a dielectric behaviour at room temperature with electrical resistivity as high as $10^{10}\,\Omega\cdot$m. However, incorporation of 3 vol.% of additives (~0.2 wt.% graphene) significantly increased the electrical conductivity up to ~21 $S\cdot m^{-1}$ (about 11 orders of magnitude). Further improvement in the electrical conductivity of the composite to a value of ~58 $S\cdot m^{-1}$ is demonstrated after increasing fillers content up to 5 vol.% (~0.34 wt.% graphene).

In this work, it is shown that insulating material, such as zirconia, can be turned into conductive material with conductivity exceeding requirement for EDM by adding as small amount of carbon as 0.2 wt.%, deposited around alumina nanofiber cores. The fibers deliver interconnected network, which the electrical current can pass through. Furthermore, this enhancement in conductivity can be achieved without compromising the initial mechanical properties. Electrical conductivity and hardness in percentages of the hardness of reference sample of the electrically conductive composites obtained in this work are shown in Table 7. Results of hardness and conductivity of different

Table 7 *Electrical conductivity of the zirconia composites obtained in this work*

ID	C wt.%	C vol.%	Conductivity, $S\cdot m^{-1}$	Fillers	Hardness,%
Z3	0.20	0.54	21	CVD-ed graphene (on alumina nanofiber core)	98
Z5	0.34	0.91	57		96

electroconductive zirconia composites added by different carbon structure fillers reported in cited literature are summarized in Table 8. To our knowledge, results of present work show the best combination of electrical conductivity and hardness of the PSZ composites added by low carbon content below 1 wt.%.

Table 8 *Summary of electrical conductivity of zirconia composites added by different carbon-based fillers of content below 1 wt.%*

Ref.	wt.%	vol.%	Conductivity, $S \cdot m^{-1}$	Fillers	Hardness, %
[68]	1		9	exfoliated graphene	106
[32]	0.1	0.4	1	SWCNT	98
	0.5	1.7	150		88
[87]	0.82		6	pyrolized carbon	-
[22]	(0.23)	0.6	10^{-7}	RGO	96
	(0.6)	1.8	10^{-7}		89
	(1)	3	20		89
[88]	0.25		5	MWCNT	-
	0.5		59		-
	1		13		-
[89]	1.07		952	CNF	60
[39]	(0.67)	2	630	CNF/HP	59
	(0.67)	2	391	CNF/SPS	70
[90]	0.5		10^{-7}	MWCNT	101
[91]	0.5		~20	MWCNT	91
[92]	0.3		10^{-10}	GO in-situ reduced during SPS	96
	0.4		10^{-10}		97
	1		3.5		96
[24]	(0.33)	1	10^{-10}	GNP	103
	(0.84)	2.5	10^{-10}		94

CONCLUSIONS

In this work, a novel approach to electroconductive oxide ceramic added by hybrid graphenated nanofibers is demonstrated. Processing of the alumina and zirconia-based composites without deterioration of hardness and with increase in fracture toughness by incorporation of the conductive fillers representing oxide ceramic nanofibers covered by multi-layered graphene (ANFC) has shown success.

Based on this study the following can be concluded:

(i) The novel approach to tremendously increasing the electroconductivity of otherwise dielectric oxide ceramics is developed;

(ii) The procedure for homogeneous dispersion of nano-fillers throughout the alumina and zirconia matrices, which guaranteed a percolation threshold for graphene content as low as 0.2-0.3 wt.%, is developed;

(iii) The highly electroconductive alumina/ANFC and PSZ/ANFC composites with low load of ANFC are designed and produced with the help of the SPS technique. Alumina-based ceramic composites were fabricated at the temperature of 1380 °C during the dwell time of 10 min under the pressure of 40 MPa with the addition of the graphenated fibers in the content range from 1 to 15 vol.%. The material of full density (>99 %) with increased indentation toughness, non-deteriorated hardness and suitable electrical conductivity allowing EDM processing are produced by adding 3 vol.% of ANFC corresponding to 0.3 % of carbon.

(iv) Partially stabilized zirconia-based ceramic composites with density >98 % were fabricated at the temperature of 1250 °C during the dwell time of 5 min under the pressure of 40 MPa with the addition of the graphenated fibers in the content range from 1 to 5 vol.%. An increase in electroconductivity does not deteriorate the mechanical properties.

(v) The gradual grain refinement in the alumina-based composites with the increase of ANFC content is evidenced. In zirconia-based composites, an increase in ANFC concentration does not yield significant effect on either grain size or morphology.

(vi) Addition of 1 vol.% of the graphenated fillers is not enough to form conductive network, meaning the percolation threshold for the ANFC should be between 1 and 3 vol.%.

REFERENCES

[1] Rice, P.M., On the Origins of Pottery. – *Journal of Archaeological Method and Theory*, 1999, 6 (1), 1–54. DOI:10.2307/40035280.

[2] Schneemann, K., Abrasion and Erosion, in: *Ullmann's Encyclopedia of Industrial Chemistry*, 2000, Weinheim, Germany: Wiley-VCH Verlag GmbH & Co. KGaA, 1–26. DOI:10.1002/14356007.b01_09.

[3] Matrenin, S.V., Slosman, A.I., *Техническая керамика: Учебное пособие [Technical ceramics: Textbook]*. 2004 Tomsk, Publishing house TPU. [WWW] http://window.edu.ru/resource/551/75551/files/mechanical_engineering.pdf (accessed October 23, 2017).

[4] Reh, H., Current Classification of Ceramic Materials, in: F. Händle (Ed.), *Extrusion in Ceramics. Engineering Materials and Processes*, 2009, Berlin, Heidelberg: Springer, 35–57. DOI:https://doi.org/10.1007/978-3-540-27102-4_3.

[5] de Faoite, D., Browne, D.J., Chang-Díaz, F.R., Santon, K.T., A review of the processing, composition and temperature- dependent mechanical and thermal properties of dielectric technical ceramics. – *Materials Science*, 2012, 47 (10), 4211–4235. DOI:10.1007/s10853-011-6140-1.

[6] Levin, I., Brandon, D., Metastable Alumina Polymorphs: Crystal Structures and Transition Sequences. – *Journal of the American Ceramic Society*, 1998, 81 (8), 1995–2012. DOI:10.1111/j.1151-2916.1998.tb02581.x.

[7] Munz, D., Fett, T., Overview and Basic Properties, in: *Ceramics*, 1999 Springer, Berlin, Heidelberg, 1–7. DOI:10.1007/978-3-642-58407-7_1.

[8] Rahaman, M.N., Yao, A., Bal, B.S., Garino, J.P., Ries, M.D., Ceramics for Prosthetic Hip and Knee Joint Replacement. – *Journal of the American Ceramic Society*, 2007, 90 (7), 1965–1988. DOI:10.1111/j.1551-2916.2007.01725.x.

[9] Aluminum Oxide (Alumina) Ceramics & Properties. *Marketech International Inc.* [WWW] https://mkt-intl.com/materials/ceramic-materials/aluminum-oxide/ (accessed May 30, 2017).

[10] Kelly, P.M., Rose, L.R.F., The martensitic transformation in ceramics - Its role in transformation toughening. – *Progress in Materials Science*, 2002, 47 (5), 463–557. DOI:10.1016/S0079-6425(00)00005-0.

[11] Evans, A.G., Heuer, A.H., Review — Transformation Toughening in Ceramics: Martensitic Transformations in Crack-Tip Stress Fields. – *Journal of the American Ceramic Society*, 1980, 63 (5–6), 241–248.

DOI:10.1111/j.1151-2916.1980.tb10712.x.

[12] Jin, X.J., Martensitic transformation in zirconia containing ceramics and its applications. – *Current Opinion in Solid State and Materials Science*, 2005, 9 (6), 313–318. DOI:10.1016/j.cossms.2006.02.012.

[13] Daculsi, G., History of development and use of the bioceramics and biocomposites, in: I.V. Antoniac (Ed.), *Handbook of Bioceramics and Biocomposites*, 2016 Springer, 3–22. DOI:10.1007/978-3-319-12460-5_2.

[14] Rühle, M., Evans, A.G., High toughness ceramics and ceramic composites. – *Progress in Materials Science*, 1989, 33 (2), 85–167. DOI:10.1016/0079-6425(89)90005-4.

[15] Kelly, J.R., Denry, I., Stabilized zirconia as a structural ceramic: An overview. – *Dental Materials*, 2008, 24 (3), 289–298. DOI:10.1016/j.dental.2007.05.005.

[16] Hussey, R.J., Wilson, J., *Advanced Technical Ceramics Directory and Databook*. 1998. DOI:10.1007/978-1-4419-8662-7.

[17] Schwartz, R., Ceramics, Electronic Properties and Material Structure, in: *Kirk-Othmer Encyclopedia of Chemical Technology*, 2000, Hoboken, NJ, USA: John Wiley & Sons, Inc., 1–13. DOI:10.1002/0471238961.0512050319030823.a01.

[18] Richerson, D.W., Electrical Behavior, in: *Modern Ceramic Engineering: Properties, Processing, and Use in Design*, 2nd ed., 1992 CRC Press, 204–250.

[19] Carter, C.B., Norton, M.G., *Ceramic Materials: Science and Engineering*. 2007 Springer.

[20] Köbel, S., Plüschke, J., Vogt, U., Graule, T.J., $MoSi_2$-Al_2O_3 electroconductive ceramic composites. – *Ceramics International*, 2004, 30 (8), 2105–2110. DOI:10.1016/j.ceramint.2003.11.015.

[21] Ishida, A., Matsubara, H., Furukawa, K., Miyayama, M., Yanagida, H., Computer simulation of percolation structure in composites. – *Nippon Seramikkusu Kyokai Gakujutsu Ronbunshi*, 1995, 103 (10), 996–999.

[22] Shin, J., Hong, S., Fabrication and properties of reduced graphene oxide reinforced yttria-stabilized zirconia composite ceramics. – *Journal of the European Ceramic Society*, 2013, 34 (5), 1297–1302. DOI:10.1016/j.jeurceramsoc.2013.11.034.

[23] Jankovský, O., Šimek, P., Sedmidubský, D., Huber, Š., Pumera, M., Sofer, Z., Towards highly electrically conductive and thermally insulating graphene nanocomposites: Al2O3 –graphene. – *RSC Advances*, 2014,

4 (15), 7418–7424. DOI:10.1039/C3RA45069D.

[24] Gallardo-López, A., Márquez-Abril, I., Morales-Rodríguez, A., Muñoz, A., Poyato, R., Dense graphene nanoplatelet/yttria tetragonal zirconia composites: Processing, hardness and electrical conductivity. – *Ceramics International*, 2017, 43 (15), 11743–11752. DOI:10.1016/j.ceramint.2017.06.007.

[25] Iijima, S., Helical microtubules of graphitic carbon. – *Nature*, 1991, 354, 56–58. DOI:10.1038/354056a0.

[26] Treacy, M.M.J., Ebbesen, T.W., Gibson, J.M., Exceptionally high Young's modulus observed for individual carbon nanotubes. – *Nature*, 1996, 381, 678–680. DOI:10.1038/381678a0.

[27] Ruoff, R.S., Lorents, D.C., Mechanical and thermal properties of carbon nanotubes. – *Carbon*, 1995, 33 (7), 925–930. DOI:10.1016/0008-6223(95)00021-5.

[28] Bandaru, P.R., Electrical Properties and Applications of Carbon Nanotube Structures. – *Journal of Nanoscience and Nanotechnology*, 2007, 7 (4), 1239–1267. DOI:10.1166/jnn.2007.307.

[29] Yi, J., Xue, W.J., Xie, Z.P., Dai, S., Cheng, H., Fracture mechanism of a fracture-resistant CNT/alumina nanocomposite at cryogenic temperature. – *Ceramics International*, 2015, 41 (10), 13908–13911. DOI:10.1016/j.ceramint.2015.08.065.

[30] Sikder, P., Sarkar, S., Biswas, K.G., Das, S., Basu, S., Das, P.K., Improved densification and mechanical properties of spark plasma sintered carbon nanotube reinforced alumina ceramics. – *Materials Chemistry and Physics*, 2016, 170, 99–107. DOI:10.1016/j.matchemphys.2015.12.024.

[31] Garmendia, N., Santacruz, I., Moreno, R., Obieta, I., Zirconia-MWCNT nanocomposites for biomedical applications obtained by colloidal processing. – *Journal of Materials Science: Materials in Medicine*, 2010, 21 (5), 1445–1451. DOI:10.1007/s10856-010-4023-7.

[32] Shin, J.-H., Hong, S.-H., Microstructure and mechanical properties of single wall carbon nanotube reinforced yttria stabilized zircona ceramics. – *Materials Science and Engineering: A*, 2012, 556, 382–387. DOI:10.1016/j.msea.2012.07.001.

[33] Fan, Y., Wang, L., Li, J.J., Li, J.J., Sun, S., Chen, F., Chen, L., Jiang, W., Preparation and electrical properties of graphene nanosheet/Al2O3 composites. – *Carbon*, 2010, 48 (6), 1743–1749. DOI:10.1016/j.carbon.2010.01.017.

[34] Li, J., Östling, M., Prevention of Graphene Restacking for Performance Boost of Supercapacitors—A Review. – *Crystals*, 2013, 3 (1), 163–190. DOI:10.3390/cryst3010163.

[35] Zhan, G.D., Kuntz, J.D., Garay, J.E., Mukherjee, A.K., Electrical properties of nanoceramics reinforced with ropes of single-walled carbon nanotubes. – *Applied Physics Letters*, 2003, 83 (6), 1228–1230. DOI:10.1063/1.1600511.

[36] Guo-Dong Zhan and Amiya K. Mukherjee, Carbon nanotube reinforced alumina-based ceramics with novel mechanical, electrical, and thermal properties. – *International Journal of Applied Ceramic Technology*, 2004, 1 (2), 161–171. DOI:10.1111/j.1744-7402.2004.tb00166.x.

[37] Kumari, L., Zhang, T., Du, G.H., Li, W.Z., Wang, Q.W., Datye, A., Wu, K.H., Synthesis, microstructure and electrical conductivity of carbon nanotube-alumina nanocomposites. – *Ceramics International*, 2009, 35 (5), 1775–1781. DOI:10.1016/j.ceramint.2008.10.005.

[38] Michálek, M., Sedláček, J., Parchoviansky, M., Michálková, M., Galusek, D., Mechanical properties and electrical conductivity of alumina/MWCNT and alumina/zirconia/MWCNT composites. – *Ceramics International*, 2014, 40 (1, part B), 1289–1295. DOI:10.1016/j.ceramint.2013.07.008.

[39] Dusza, J., Blugan, G., Morgiel, J., Kuebler, J., Inam, F., Peijs, T., Reece, M.J., Puchy, V., Hot pressed and spark plasma sintered zirconia/carbon nanofiber composites. – *Journal of the European Ceramic Society*, 2009, 29 (15), 3177–3184. DOI:10.1016/j.jeurceramsoc.2009.05.030.

[40] Borrell, A., Rocha, V.G., Torrecillas, R., Fernández, A., Improvement of carbon nanofibers/ZrO_2 composites properties with a zirconia nanocoating on carbon nanofibers by sol-gel method. – *Journal of the American Ceramic Society*, 2011, 94 (7), 2048–2052. DOI:10.1111/j.1551-2916.2010.04354.x.

[41] Duszová, A., Dusza, J., Tomášek, K., Blugan, G., Kuebler, J., Microstructure and properties of carbon nanotube/zirconia composite. – *Journal of the European Ceramic Society*, 2008, 28 (5), 1023–1027. DOI:10.1016/j.jeurceramsoc.2007.09.011.

[42] Ahmad, I., Yazdani, B., Zhu, Y., Recent Advances on Carbon Nanotubes and Graphene Reinforced Ceramics Nanocomposites. – *Nanomaterials*, 2015, 5 (1), 90–114. DOI:10.3390/nano5010090.

[43] Pei, S., Cheng, H.M., The reduction of graphene oxide. – *Carbon*, 2012, 50 (9), 3210–3228. DOI:10.1016/j.carbon.2011.11.010.

[44] Fan, Y., Jiang, W., Kawasaki, A., Highly conductive few-layer

graphene/Al_2O_3 nanocomposites with tunable charge carrier type. – *Advanced Functional Materials*, 2012, 22 (18), 3882–3889. DOI:10.1002/adfm.201200632.

[45] Centeno, A., Rocha, V.G., Alonso, B., Fernández, A., Gutierrez-Gonzalez, C.F., Torrecillas, R., Zurutuza, A., Graphene for tough and electroconductive alumina ceramics. – *Journal of the European Ceramic Society*, 2013, 33 (15–16), 3201–3210. DOI:10.1016/j.jeurceramsoc.2013.07.007.

[46] König, W., Dauw, D.F., Levy, G., Panten, U., EDM-Future Steps towards the Machining of Ceramics. – *CIRP Annals - Manufacturing Technology*, 1988, 37 (2), 623–631. DOI:10.1016/S0007-8506(07)60759-8.

[47] Ji, R., Liu, Y., Diao, R., Xu, C., Li, X., Cai, B., Zhang, Y., Influence of electrical resistivity and machining parameters on electrical discharge machining performance of engineering ceramics. – *PLOS ONE*, 2014, 9 (11). DOI:10.1371/journal.pone.0110775.

[48] Pachaury, Y., Tandon, P., An overview of electric discharge machining of ceramics and ceramic based composites. – *Journal of Manufacturing Processes*, 2017, 25, 369–390. DOI:10.1016/j.jmapro.2016.12.010.

[49] Malek, O., González-Julián, J., Vleugels, J., Vanderauwera, W., Lauwers, B., Belmonte, M., Carbon nanofillers for machining insulating ceramics. – *Materials Today*, 2011, 14 (10), 496–501. DOI:10.1016/S1369-7021(11)70214-0.

[50] Gadow, R., Landfried, R., Kern, F., Electrical Discharge Machining (EDM) of High-Performance Ceramics, in: O.N. Lee W., Gadow R., Mitic V. (Ed.), *Proceedings of the III Advanced Ceramics and Applications Conference*, 2016, Paris: Atlantis Press, 25–32. DOI:10.2991/978-94-6239-157-4_2.

[51] Singh, M.A., Sarma, D.K., Hanzel, O., Sedláček, J., Šajgalík, P., Machinability analysis of multi walled carbon nanotubes filled alumina composites in wire electrical discharge machining process. – *Journal of the European Ceramic Society*, 2017, 37 (9), 3107–3114. DOI:10.1016/j.jeurceramsoc.2017.03.058.

[52] Chen, Y.F., Bi, J.Q., Yin, C.L., You, G.L., Microstructure and fracture toughness of graphene nanosheets/alumina composites. – *Ceramics International*, 2014, 40 (9, part A), 13883–13889. DOI:10.1016/j.ceramint.2014.05.107.

[53] Kvetková, L., Duszová, A., Hvizdoš, P., Dusza, J., Kun, P., Balázsi, C., Fracture toughness and toughening mechanisms in graphene platelet reinforced Si_3N_4 composites. – *Scripta Materialia*, 2012, 66 (10), 793–796. DOI:10.1016/j.scriptamat.2012.02.009.

[54] Tokita, M., *Spark Plasma Sintering (SPS) Method, Systems, and Applications*.2nd ed. 2013, Oxford: Academic Press. DOI:10.1016/B978-0-12-385469-8.00060-5.

[55] Guillon, O., Gonzalez-Julian, J., Dargatz, B., Kessel, T., Schierning, G., Räthel, J., Herrmann, M., Field-assisted sintering technology/spark plasma sintering: Mechanisms, materials, and technology developments. – *Advanced Engineering Materials*, 2014, 16 (7), 830–849. DOI:10.1002/adem.201300409.

[56] Aghayan, M., Hussainova, I., Gasik, M., Kutuzov, M., Friman, M., Coupled thermal analysis of novel alumina nanofibers with ultrahigh aspect ratio. – *Thermochimica Acta*, 2013, 574, 140–144. DOI:10.1016/j.tca.2013.10.010.

[57] Niihara, K., Morena, R., Hasselman, D.P.H., Evaluation of K_{Ic} of brittle solids by the indentation method with low crack-to-indent ratios. – *Journal of Materials Science Letters*, 1982, 1 (1), 13–16. DOI:10.1007/BF00724706.

[58] Wu, C.C., Rice, R.W., Porosity Dependence of Wear and Other Mechanical Properties on Fine-Grain $A1_2O_3$ and B_4C. – *Proceedings of the 9th Annual Conference on Composites and Advanced Ceramic Materials: Ceramic Engineering and Science Proceedings*, 1985, 6 (7/8), 977–994. DOI:10.1002/9780470320280.ch51.

[59] Kuphaldt, T., Kelvin (4-wire) resistance measurement, in: *Lessons In Electric Circuits: Volume I - DC*, 5th ed., 2006, 282–289. [WWW] https://www.allaboutcircuits.com/assets/pdf/direct-current.pdf.

[60] Jorio, A., Raman Spectroscopy in Graphene-Based Systems: Prototypes for Nanoscience and Nanometrology. – *ISRN Nanotechnology*, 2012, 2012, 1–16. DOI:10.5402/2012/234216.

[61] Bokobza, L., Bruneel, J.-L., Couzi, M., Raman Spectra of Carbon-Based Materials (from Graphite to Carbon Black) and of Some Silicone Composites. – *C*, 2015, 1, 77–94. DOI:10.3390/c1010077.

[62] Ferrari, A.C., Raman spectroscopy of graphene and graphite: Disorder, electron-phonon coupling, doping and nonadiabatic effects. – *Solid State Communications*, 2007, 143 (1–2), 47–57. DOI:10.1016/j.ssc.2007.03.052.

[63] Katagiri, G., Ishida, H., Ishitani, A., Raman spectra of graphite edge planes. – *Carbon*, 1988, 26 (4), 565–571. DOI:10.1016/0008-6223(88)90157-1.

[64] Sadezky, A., Muckenhuber, H., Grothe, H., Niessner, R., Pöschl, U., Raman microspectroscopy of soot and related carbonaceous materials:

Spectral analysis and structural information. – *Carbon*, 2005, 43 (8), 1731–1742. DOI:10.1016/j.carbon.2005.02.018.

[65] Saito, R., Hofmann, M., Dresselhaus, G., Jorio, A., Dresselhaus, M.S., Raman spectroscopy of graphene and carbon nanotubes. – *Advances in Physics*, 2011, 60 (3), 413–550. DOI:10.1080/00018732.2011.582251.

[66] Mahajan, A., Kingon, A., Kukovecz, Á., Konya, Z., Vilarinho, P.M., Studies on the thermal decomposition of multiwall carbon nanotubes under different atmospheres. – *Materials Letters*, 2013, 90, 165–168. DOI:10.1016/j.matlet.2012.08.120.

[67] He, T., Li, J., Wang, L., Zhu, J., Jiang, W., Preparation and Consolidation of Alumina/Graphene Composite Powders. – *Materials Transactions*, 2009, 50 (4), 749–751. DOI:10.2320/matertrans.MRA2008458.

[68] Kwon, S.-M., Lee, S.-J., Shon, I.-J., Enhanced properties of nanostructured ZrO_2–graphene composites rapidly sintered via high-frequency induction heating. – *Ceramics International*, 2015, 41 (1), 835–842. DOI:10.1016/j.ceramint.2014.08.042.

[69] Yazdani, B., Xia, Y., Ahmad, I., Zhu, Y., Graphene and carbon nanotube (GNT)-reinforced alumina nanocomposites. – *Journal of the European Ceramic Society*, 2015, 35 (1), 179–186. DOI:10.1016/j.jeurceramsoc.2014.08.043.

[70] Liu, J., Yang, Y., Hassanin, H., Jumbu, N., Deng, S., Zuo, Q., Jiang, K., Graphene-Alumina Nanocomposites with Improved Mechanical Properties for Biomedical Applications. – *ACS Applied Materials and Interfaces*, 2016, 8 (4), 2607–2616. DOI:10.1021/acsami.5b10424.

[71] Liu, J., Yan, H., Jiang, K., Mechanical properties of graphene platelet-reinforced alumina ceramic composites. – *Ceramics International*, 2013, 39 (6), 6215–6221. DOI:10.1016/j.ceramint.2013.01.041.

[72] Liu, Y., Huang, J., Niinomi, M., Li, H., Inhibited grain growth in hydroxyapatite-graphene nanocomposites during high temperature treatment and their enhanced mechanical properties. – *Ceramics International*, 2016, 42 (9), 11248–11255. DOI:10.1016/j.ceramint.2016.04.038.

[73] Porwal, H., Tatarko, P., Grasso, S., Khaliq, J., Dlouhý, I., Reece, M.J., Graphene reinforced alumina nano-composites. – *Carbon*, 2013, 64, 359–369. DOI:10.1016/j.carbon.2013.07.086.

[74] Porwal, H., Tatarko, P., Saggar, R., Grasso, S., Kumar Mani, M., Dlouhý, I., Dusza, J., Reece, M.J., Tribological properties of silica-graphene nano-platelet composites. – *Ceramics International*, 2014, 40 (8, part A), 12067–12074. DOI:10.1016/j.ceramint.2014.04.046.

[75] Gutierrez-Gonzalez, C.F., Smirnov, A., Centeno, A., Fernández, A., Alonso, B., Rocha, V.G., Torrecillas, R., Zurutuza, A., Bartolome, J.F., Wear behavior of graphene/alumina composite. – *Ceramics International*, 2015, 41 (6), 7434–7438. DOI:10.1016/j.ceramint.2015.02.061.

[76] Yazdani, B., Xu, F., Ahmad, I., Hou, X., Xia, Y., Zhu, Y., Tribological performance of Graphene/Carbon nanotube hybrid reinforced Al_2O_3 composites. – *Scientific Reports*, 2015, 5 (1), 11579. DOI:10.1038/srep11579.

[77] Kim, H.J., Lee, S.-M., Oh, Y.-S., Yang, Y.-H., Lim, Y.S., Yoon, D.H., Lee, C., Kim, J.-Y., Ruoff, R.S., Unoxidized Graphene/Alumina Nanocomposite: Fracture- and Wear-Resistance Effects of Graphene on Alumina Matrix. – *Scientific Reports*, 2015, 4 (1), 5176. DOI:10.1038/srep05176.

[78] Kumari, L., Zhang, T., Du, G.H., Li, W.Z., Wang, Q.W., Datye, A., Wu, K.H., Synthesis, microstructure and electrical conductivity of carbon nanotube-alumina nanocomposites. – *Ceramics International*, 2009, 35 (5), 1775–1781. DOI:10.1016/j.ceramint.2008.10.005.

[79] Kim, D.-J., Jung, H.-J., Raman Spectroscopy of Tetragonal Zirconia Solid Solutions. – *Journal of the American Ceramic Society*, 1993, 76 (8), 2106–2108. DOI:https://doi.org/10.1111/j.1151-2916.1993.tb08341.x.

[80] Valmalette, J.C., Isa, M., Size effects on the stabilization of ultrafine zirconia nanoparticles. – *Chemistry of Materials*, 2002, 14 (12), 5098–5102. DOI:10.1021/cm021233n.

[81] Giulianini, M., Motta, N., Polymer Self-assembly on Carbon Nanotubes, in: *Self-Assembly of Nanostructures*, 2012, New York, NY: Springer New York, 1–72. DOI:10.1007/978-1-4614-0742-3_1.

[82] Osswald, S., Havel, M., Gogotsi, Y., Monitoring oxidation of multiwalled carbon nanotubes by Raman spectroscopy. – *Journal of Raman Spectroscopy*, 2007, 38, 728–736. DOI:10.1002/jrs1686.

[83] Nieto, A., Huang, L., Han, Y.H., Schoenung, J.M., Sintering behavior of spark plasma sintered alumina with graphene nanoplatelet reinforcement. – *Ceramics International*, 2015, 41 (4), 5926–5936. DOI:10.1016/j.ceramint.2015.01.027.

[84] Belmonte, M., González-Julián, J., Miranzo, P., Osendi, M.I., Spark plasma sintering: A powerful tool to develop new silicon nitride-based materials. – *Journal of the European Ceramic Society*, 2010, 30 (14), 2937–2946. DOI:10.1016/j.jeurceramsoc.2010.01.025.

[85] Belmonte, M., Nistal, A., Boutbien, P., Román-Manso, B., Osendi, M.I., Miranzo, P., Toughened and strengthened silicon carbide ceramics by

adding graphene-based fillers. – *Scripta Materialia*, 2016, 113, 127–130. DOI:10.1016/j.scriptamat.2015.10.023.

[86] Milsom, B., Viola, G., Gao, Z., Inam, F., Peijs, T., Reece, M.J., The effect of carbon nanotubes on the sintering behaviour of zirconia. – *Journal of the European Ceramic Society*, 2012, 32 (16), 4149–4156. DOI:10.1016/j.jeurceramsoc.2012.07.028.

[87] Fukumura, Y., Pattanayak, D.K., Wanghui, C., Shirai, T., Fuji, M., Wang, F., In situ zirconia / carbon network composite fabricated by gelcast following reduction-sintering. – *Journal of the Ceramic Society of Japan*, 2012, 120 (8), 347–350. DOI:10.2109/jcersj2.120.347.

[88] Ukai, T., Sekino, T., Hirvonen, A.T., Tanaka, N., Kusunose, T., Nakayama, T., Niihara, K., Preparation and Electrical Properties of Carbon Nanotubes Dispersed Zirconia Nanocomposites. – *Key Engineering Materials*, 2006, 317–318, 661–664. DOI:10.4028/www.scientific.net/KEM.317-318.661.

[89] Duszová, A., Dusza, J., Tomášek, K., Morgiel, J., Blugan, G., Kuebler, J., Zirconia/carbon nanofiber composite. – *Scripta Materialia*, 2008, 58 (6), 520–523. DOI:10.1016/j.scriptamat.2007.11.002.

[90] Mazaheri, M., Mari, D., Schaller, R., Bonnefont, G., Fantozzi, G., Processing of yttria stabilized zirconia reinforced with multi-walled carbon nanotubes with attractive mechanical properties. – *Journal of the European Ceramic Society*, 2011, 31 (14), 2691–2698. DOI:10.1016/j.jeurceramsoc.2010.11.009.

[91] Melk, L., Antti, M.L., Anglada, M., Material removal mechanisms by EDM of zirconia reinforced MWCNT nanocomposites. – *Ceramics International*, 2015, . DOI:10.1016/j.ceramint.2015.12.120.

[92] Solís, N.W., Peretyagin, P., Torrecillas, R., Fernández, A., Menéndez, J.L., Mallada, C., Díaz, L.A., Moya, J.S., Electrically conductor black zirconia ceramic by SPS using graphene oxide. – *Journal of Electroceramics*, 2017, 38 (1), 119–124. DOI:10.1007/s10832-017-0076-z.

ACKNOWLEDGEMENTS

I would like to thank my supervisor Prof. Irina Hussainova, for the encouragement, support and priceless guidance, which made this work possible. I would like to thank Prof. Miguel A. Rodriguez, who supported me greatly and was always willing to help.

I am very grateful to my all my colleagues, especially Marina Aghayan, Roman Ivanov, Der-Liang Yung, Janis Baroninš, Tatevik Minasyan and Ali Saffar for their friendship, help and support. I would also like to thank my foreign colleagues whose support and help made my being on the conferences and research stays to go smooth and memorable.

Many thanks to Domingo Pérez-Coll, Fernando Rubio-Marcos, Valdek Mikli, Rainer Traksmaa, Mart Viljus, Hans Vallner, Birgit Maaten and Olga Volobujeva for their assistance and technical help.

The project would have been impossible without the financial support of institutional research funding IUT 19–29 of the Estonian Ministry of Education and Research, Archimedes targeted grant AR12133 (NanoCom), Estonian Research Council under the personal research grant PUT1093 (I. Hussainova) and European Social Fund's Doctoral Studies and Internationalization Programme DoRa, which is carried out by Foundation Archimedes. This work has been partially supported by graduate school „Functional materials and technologies" receiving funding from the European Social Fund under project 1.2.0401.09-0079 in Estonia. This work has been partially supported by ASTRA "TUT Institutional Development Program for 2016-2022" Graduate School of Functional Materials and Technologies (2014-2020.4.01.16- 0032).

I would like to thank my family and friends for their support, understanding and patience.

ABSTRACT

Electroconductive oxide ceramics with hybrid graphenated nanofibers

Doping ceramic composites with graphene or carbon nanotubes can impressively increase their electrical conductivity. However, high conductivity usually comes at the cost of deteriorated hardness, because the amount of fillers needed to achieve it is high and the nano-fillers are prone to tangling and/or agglomeration due to van der Waals forces.

The aim of this work was to minimize the problem associated with degradation of hardness of the electroconductive ceramic/graphene composite by providing a good dispersion of graphene. An original approach to solving this problem was developed. The proposed solution was to introduce the graphene into the ceramics using a supporting carrier. The goal of it was to obtain a material with reduced to the lowest possible fraction of carbon and with a considerably high electrical conductivity at the same time. In this way, a novel type of hybrid graphene/ceramic nano-fillers – alumina nanofibers with diameter of 7 ± 3 nm, coated by 2-3 layers of graphene (ANFC) – were developed.

A simple powder processing route by ultrasound and attrition milling using ethanol as media was used to prepare precursor powder mixtures. The ceramic/ANFC composites were consolidated with the help of Spark Plasma Sintering (SPS) technique. The optimal sintering conditions for the composites were determined. The microstructure, phase composition, mechanical, tribological and electrical properties of the obtained composites were characterized.

The first part of the research was focused on alumina/ANFC composites. Composites with the content of ANFC from 1 vol.% up to 15 vol.% (which corresponds to 0.1 up to 1.5 wt.% of graphene) were produced. The study of the microstructure of the composites revealed the effect of grain growth inhibition induced by the addition of ANFC. The hardness of composites with a content of fibers of 1-5 vol.% was increased by about 8-10% over the pure alumina, reaching its maximum value of HV1 1830 (17.95 GPa). The indentation fracture toughness of the composites was increased to the maximum value of 5.6 $MPa \cdot m^{0.5}$ for the Al_2O_3/5 vol.% ANFC composite corresponding to an increase of approximately 68% as compared to the pure alumina. The series of tribological wear tests showed that the composites with 3 and 5 vol.% of ANFC had improved performance during mild wear test. The Al_2O_3/1 vol.%ANFC composite proved to have the best of all the obtained composites tribological performance during severe wear tests with the minimal coefficient of friction ranged from 0.45 up to 0.5. An increase in electrical conductivity by nearly 13 orders of magnitude was detected for the composite with 3 vol.% of fillers (0.3 wt.% graphene). Further addition of ANFC led to subsequent growth of the electrical conductivity reaching up to 127 $S \cdot m^{-1}$ at 15 vol.%.

The second part of the research referred to zirconia/ANFC composites. Based on previous results for alumina matrix composites, the zirconia/ANFC compositions were narrowed down to optimal percentages from 1 vol.% up to 5 vol.% (which corresponds to 0.07 up to 0.34 wt.% of graphene). No significant effect of the ANFC fillers on the microstructure of the composites was detected. Unlike the alumina matrix composites, the hardness of zirconia-based composites underwent slight reduction (but no more than 5%) with the increase in filler amount up to 5 vol.%. The highest indentation fracture toughness of 6.9 $MPa \cdot m^{0.5}$, being approximately a 20% increase over the monolithic zirconia, was reached for the ZrO_2/3 vol.%ANFC. The electrical conductivity for the samples with 3 and 5 vol.% ANFC increased 11 orders of magnitude up to 21 and 57 $S \cdot m^{-1}$, respectively. To our knowledge, results of present work show the best combination of electrical conductivity and hardness of the zirconia composites added low carbon content below 1 wt.%.

In this work, it was shown that insulating materials, such as alumina and zirconia, can be turned into conductive material with conductivity exceeding a requirement for Electrical Discharge Machining (EDM) (which is a minimum ~1 $S \cdot m^{-1}$) by adding as small amount of carbon as 0.2 wt.%, deposited to the alumina nanofiber cores, as a part of hybrid filler. Great advantages of the proposed approach are the ease of distribution of the graphene into the ceramic matrix; low percolation point with relatively high values of the electrical conductivity at the lowest contents of graphene (below 0.5 wt.%) and preservation or even improvement of hardness. Also, it should be mentioned that the process of the ANFC production is relatively easy and cost-effective.

KOKKUVÕTE

Elektrijuhtiva oksiid-grafeenkiudkeraamika tehnoloogia ja püsivus

Süsiniku lisamine grafeeni või süsinik-nanotorude näol keraamilistesse komposiitidesse võib suurendada tunduvalt nende elektrijuhtivust. Suure juhtivusega kaasneb tavaliselt väiksem kõvadus, sest selle saavutamiseks vajalike täiteainete kogus on suur ning *van der Waalsi* jõudude tõttu nanotäiteained kalduvad haakuma ja/või aglomeeruma.

Töö eesmärk oli arendada ja saada elektrijuhtivusega oksiidkeraamikat, mis muidu on dielektriline, ja lahendada elektrijuhtiva oksiid-grafeenkiudkeraamika kõvaduse vähenemisega seotud probleeme, tulenevalt grafeeni kõrgest dispersiooniastmest. Probleemi lahendamiseks on kavandatud originaalne lähenemisviis – sisestada grafeen keraamikasse tugiainete abil. Eesmärk oli saada materjal, mis sisaldab minimaalse fraktsiooniga süsinikku ja millel on samaaegselt märkimisväärselt kõrge elektrijuhtivus. Sel viisil töötati välja uudne oksiidkomposiitkeraamika hübriidnanotäiteained – alumiiniumoksiidi nanokiudud läbimõõduga 7 ± 3 nm, mis on kaetud 2-3 grafeeni kihiga (*Aluminiumoxide Nanofibers Carbon*, ANFC).

Lähtepulbersegude valmistamiseks kasutati lihtsat peenestamist ultraheli- ja hõõrdjahvatusega etanooli keskkonnas. ANFC-keraamika komposiidid valmistati sädeplasmapaagutusmeetodit (*Spark Plasma Sintering* (SPS)) kasutades. Määrati saadud komposiitide optimaalsed paagutustingimused, iseloomustati saadud komposiitide mikrostruktuuri, faasikoostist, mehaanilisi, triboloogilisi ja elektrilisi omadusi.

Uuringu esimene osa keskendub alumiiniumoksiid-ANFC komposiitidele. Valmistati komposiidid ANFC sisaldusega alates 1 mahu% kuni 15 mahu% (mis vastab grafeeni massi% 0,1 kuni 1,5). Komposiitide mikrostruktuuri uurimine näitas ANFC lisamisega esilekutsutud terakasvu inhibitsiooni mõju. Grafeenkiudu sisaldava (1-5 mahu%) komposiitide kõvadus ületas 8-10 % võrra puhta alumiiniumoksiidi oma, ulatudes kuni 1830 HV1-ni (17,95 GPa). Komposiitide indenteerimispurunemissitkus ulatus kuni 5,6 MPa·m0,5, alumiiniumoksiidkomposiidi 5 mahu% ANFC sisalduse korral, mis vastab ligikaudu 70%-lisele kasvule võrreldes puhta alumiiniumoksiidiga. Triboloogilised kulumiskatsed näitasid 3 ja 5 mahu% ANFC sisaldusega komposiitidel head kulumiskindlust. Alumiiniumoksiidi baasil mahu% ANFC sisaldusega komposiit osutus kõigist saadud komposiitidest parima kulumiskindlusega rasktingimustes kulumiskatsel. Minimaalne hõõrdetegur oli vahemikus 0,45 – 0,5 kolme mahu% grafeentäiteainega (0,3 mahu%) komposiidi puhul, samas elektrijuhtivus suurenes ligikaudu 13 suurusjärgu võrra. ANFC-kiudude edasine lisamine tõi kaasa keraamika elektrijuhtivuse edasise kasvu, ulatudes kuni 127 $S \cdot m^{-1}$ 15 mahu% ANFC puhul.

Uuringu teine osa käsitleb tsirkooniumdioksiidi/ANFC komposiite. Tulenevalt alumiiniumoksiidmaatrikskomposiitide eelnevatest tulemustest piirduti tsirkooniumdioksiidi/ANFC komposiitides optimaalsete protsendimääradega – alates 1 mahu% kuni 5 mahu% (mis vastab grafeeni sisaldusele 0,07 kuni 0,34 massi%). ANFC täiteainete olulist mõju komposiitide mikrostruktuurile ei tuvastatud. Erinevalt alumiiniumoksiidmaatrikskomposiitidest, toimus tsirkooniumdioksiidipõhiste komposiitide kõvaduse kerge vähenemine (kuni 5 %) täiteaine koguse suurenemisega kuni 5 mahu%-ni. Suurimaks indenteerimispurunemissitkus saavutati ZrO_2 / 3 mahu% ANFC puhul 6,9 MPa · $m^{0,5}$, mis ületab umbes 20 % monoliitse tsirkooniumdioksiidi tugevust. 3 ja 5-mahu% ANFC komposiitide elektrijuhtivus suurenes 11 suurusjärgu võrra, vastavalt kuni 21 ja 57 $S \cdot m^{-1}$. Senised töötulemused näitavad, et tsirkooniumdioksiidi komposiitide elektrijuhtivuse ja kõvaduse parim kombinatsioon on madal grafeenkiudude sisalduse korral (alla 1 massi%).

Töös on näidatud, et keraamilisi isolatsioonimaterjale, nagu alumiiniumoksiid ja tsirkooniumdioksiid, saab muuta elektrijuhtivaks materjaliks, mille juhtivus ületab nõutavat elektrilahendusseadmetele (on minimaalselt ~ 1 $S \cdot m^{-1}$), lisades väikeses koguses süsinikku (kui 0,2 massi%), ladestatuna alumiiniumoksiidist nanokiusüdamikule hübriidse täiteainena. Kavandatud lähenemisviisi eelised on: (1) ühtlane grafeeni jaotuse tagamine keraamilises maatriksis; (2) madal perkolatsioonipunkt suhteliselt suure elektrijuhtivuse väärtustel grafeeni madalaima sisalduse juures (alla 0,5 massi%) ja (3) kõvaduse säilimine või isegi tõus. Samas aga tuleb mainida, et ANFC kiudude tootmisprotsess on suhteliselt lihtne ja kulutõhus.

CURRICULUM VITAE

1. Personal data

Name	Maria Drozdova
Date and place of birth	03.01.1988, Tallinn, Estonia
E-mail address	maria.drozdova@aol.com

2. Education

Graduation year	Educational institution	Education (Programme/degree)
2013	Saint-Petersburg State University	Specialist degree in Mechanics
2007	Lasnamäe Gümnaasium	Highschool

3. Language competence/skills (fluent, average, basic skills)

Language	Level
Russian	Native
English	Fluent
Estonian	Good
Korean	Good
Spanish	Basic

4. Professional employment

Period	Organisation	Position
2013-…	Tallinn University of Technology	Early Stage Researcher
2011-2013	Laboratory for Strength of Materials, Saint-Petersburg State University	Junior Researcher

5. Activities

Period	Organisation	Position
2008-2013	The pedagogical student group “Skazka”	Member
2008-2013	Faculty of Mathematics and Mechanics Trade Union	Member
2008	BEST Estonia	Participant

6. Research visits

Period	Organisation
09.10.2017 – 12.10.2017	Institute of Materials Research, Slovak Academy of Science (Slovakia, Košice)
13.03.2016 - 20.03.2016	Instytut Zawansowanych Technologii Wytwarzania (Poland, Krakow)
31.10.2014 - 20.11.2014	Institute of Ceramics and Glasses, Spanish Academy of Science (Spain, Madrid)
05.01.2014 - 01.07.2014	Institute of Ceramics and Glasses, Spanish Academy of Science (Spain, Madrid)

7. Special courses

Period	Educational or other organisation
27.09.2016-28.09.2016	Short Course on Graphene/Ceramic Composites
05.09.2016-06.09.2016	FMTDK summer school “New Trends in Chemistry, Physics, Material Scinece and Environmental Technology”
07.07.2017-09.07.2017	Summer school “Innovative technologies in the field of ceramic manufacturing”

ELULOO KIRJELDUS

1. Isikuandmed

Ees- ja perekonnanimi	Maria Drozdova
Sünniaeg ja –koht	03.01.1988, Tallinn, Eesti
E-posti aadress	maria.drozdova@aol.com

2. Hariduskäik

Lõpetamise aeg	**Õppeasutus**	**Haridus (eriala/kraad)**
2013	Saint-Petersburg State University	Specialisti kraad Mehaanikas
2007	Lasnamäe Gümnaasium	Highschool

3. Keelteoskus (alg-, kesk- või kõrgtase)

Keel	**Tase**
Vene	Emakeel
Inglise	Kõrg
Eesti	Kesk
Korea	Kesk
Hispaania	Alg

4. Töökogemus

Töötamise aeg	**Tööandja nimetus**	**Ametikoht**
2013-…	Tallinna Tehnikaülikool, Tallinn, Eesti	Nooremteadur
2011-2013	Materjalide tugevuslabor, Peterburi Riiklik Ülikool, Peterburi, Venemaa	Nooremteadur

5. Tegevus

Periood	Asutus	Ametikoht
2008-2013	Pedagoogiline üliõpilasmalev “Skazka”	Liige
2008-2013	Matemaatika ja mehaanika teaduskonna ametiühing	Liige
2008	BEST Estonia	Osaleja

6. Välismaal teadustöö

Periood	Asutus
09.10.2017 – 12.10.2017	Institute of Materials Research, Slovak Academy of Science (Slovakia, Košice)
13.03.2016 - 20.03.2016	Instytut Zawansowanych Technologii Wytwarzania (Poland, Krakow)
31.10.2014 - 20.11.2014	Institute of Ceramics and Glasses, Spanish Academy of Science (Spain, Madrid)
05.01.2014 - 01.07.2014	Institute of Ceramics and Glasses, Spanish Academy of Science (Spain, Madrid)

7. Täiendusõpe

Periood	Asutus
27.09.2016-28.09.2016	Grafeeni/keraamiliste komposiidide lühike kursus
05.09.2016-06.09.2016	FMTDK suvekool “New Trends in Chemistry, Physics, Material Scinece and Environmental Technology”
07.07.2017-09.07.2017	Suvekool “Innovative technologies in the field of ceramic manufacturing”

OTHER PUBLICATIONS

1. A. Shishkin, **M. Drozdova**, V. Kozlov, I. Hussainova, D. Lehmhus, Vibration-Assisted Sputter Coating of Cenospheres: A New Approach for Realizing Cu-Based Metal Matrix Syntactic Foams. *Metals*. 7 (2017) 16. DOI:10.3390/met7010016.
2. S. Belyaev, **M. Drozdova**, N. Frolova, V. Pilyugin, N. Resnina, V. Slesarenko, V. Zeldovich, Structure and properties of TiNi alloy subjected to severe plastic deformation and subsequent annealing. *Materials Science Forum*. 739 (2013) 518–524. DOI:10.4028/www.scientific.net/MSF.738-739.518.

APPROBATION

1. 9th International Conference of DAAAM Baltic, INDUSTRIAL ENGINEERING, 24-26 April 2014, Tallinn, Estonia
2. Materials Engineering 2014, 22-23 October 2014, Kaunas, Lithuania
3. 14th Conference of the European Ceramic Society (ECerS2015) 21-25 June 2015, Toledo, Spain.
4. The 11th International Conference of Pacific Rim Ceramic Societies(PacRim-11) 30 August – 4 September 2015, Jeju, Korea
5. Eleventh Conference for Young Scientists in Ceramics (SM-2015), 21-24 -October 2015, Novi Sad, Serbia
6. 24th International Baltic Conference in Engineering Materials & Tribology (BALTMATTRIB 2015), 5-6 November 2015, Tallinn, Estonia
7. International Workshop on Graphene/Ceramic Composites (WGCC), 28-30 September 2016, Cuenca, Spain
8. 15th Conference & Exhibition of the European Ceramic Society (ECerS2017), 9-13 July 2017, Budapest, Hungary

Paper I. **Drozdova, M.**, Hussainova, I., Pérez-Coll, D., Aghayan, M., Ivanov, R., Rodríguez, M.A., Drozdova, M., Pérez-Coll, D., Aghayan, M., Ivanov, R., Rodríguez, M.A., A novel approach to electroconductive ceramics filled by graphene covered nanofibers. – *Materials and Design*, 2016, 90, 291-298. DOI:10.1016/j.matdes.2015.10.148.

Materials and Design 90 (2016) 291–298

Contents lists available at ScienceDirect

Materials and Design

journal homepage: www.elsevier.com/locate/jmad

A novel approach to electroconductive ceramics filled by graphene covered nanofibers

M. Drozdova [a], I. Hussainova [a,b,*], D. Pérez-Coll [c], M. Aghayan [a], R. Ivanov [a], M.A. Rodríguez [c]

[a] Tallinn University of Technology, Ehitajate 5, 19180 Tallinn, Estonia
[b] ITMO University, Kronverksky 49, St. Petersburg, 197101, Russian Federation
[c] Instituto de Cerámica y Vidrio, CSIC, 28049, Madrid, Spain

ARTICLE INFO

Article history:
Received 2 October 2015
Received in revised form 26 October 2015
Accepted 27 October 2015
Available online 29 October 2015

Keywords:
Nanofibers
Graphene
Alumina
Composites
SPS
Electroconductivity

ABSTRACT

In this study, a novel approach to processing electrically conductive and comparatively cost-effective ceramics by incorporation of the graphene coated oxide ceramic nanofibers into alumina matrix is presented. The conductive fillers are produced by chemical vapour deposition of a few-layered graphene shells on a dielectric substrate of alumina nanofibers of 7–10 nm in diameter and an exceptional aspect ratio of 10^7. Our approach allows utilizing the advantages of reinforcement by fibres and high conductivity of graphene through homogeneous dispersion of the fibres within alumina matrix. The composites are densified using spark plasma sintering at 1380 °C with 40 MPa pressure for 10 min. It is shown that addition of 0.3 wt.% of graphene results in increase in electroconductivity of 13 orders of magnitude as compared to the monolithic alumina. Moreover, a low graphene loading does not result in deterioration of hardness of the produced hierarchically structured composites. The strategy proposed in this work can be extended to other insulating materials to produce advanced composites suitable for high-precision electrical discharge machining.

1. Introduction

The potential for a wide variety of applications of advanced ceramics has triggered significant research activities on development of new classes of ceramic composites with tailorable properties. The main limiting factors for even wider ceramics usage are mechanical unreliability and poor electrical conductivity, which make the materials difficult to be processed to required shape. To fully employ outstanding mechanical properties of ceramic materials in a variety of applications, ease of shaping is one of the principal necessities. Electro-discharge machining allows producing complex-shaped parts; however, this operation can only be applied to electroconductive materials.

Recently the research interest in electroconductive and relatively tough ceramics has been focused on carbon nanotubes (CNT) and graphene reinforced materials [1–5]. The significant improvements in mechanical and electrical properties have been continuously reported. For example, Fan et al. [5] reported an improvement of about 100% in fracture toughness and 20% in flexural strength with the addition of 1.0 wt.% single walled carbon nanotubes to alumina matrix; Centeno et al. [3] demonstrated at least 8 orders of magnitude decrease in electrical resistivity with addition of 0.22 wt.% of graphene. Due to high conductivity and high surface area of graphene nanosheets, the percolation threshold for conductive carbon-containing nanocomposites is calculated to be below 1.0 wt.% [6]. Thus, the problems associated with deterioration of some mechanical properties for such composites can be minimized by reducing the graphene-based filler content to the lowest appropriate amount while keeping conductivity considerably high. For example, for effective application of electro-discharge machining (EDM) the required electrical conductivity should be higher than 0.3–1 S m^{-1} [3,7]. As the percolation threshold depends on degree of filler distribution within a matrix, a proper dispersion of the conductive additives remains one of the challenges for commercial production of the conductive ceramics.

To provide qualitative dispersion, either powder or colloidal processing are mainly used [4]. Graphene surface functionalization is often required for the preparation of stable suspensions for composites production. In this study, we propose a novel type of electroconductive nanofillers that can be easily and uniformly distributed within the matrix of a host material with the help of a simple powder-processing route. Such kind of nanofillers represents oxide ceramics nanofibers with diameter of several nanometers covered by multi-layered graphene shells utilizing the advantages of reinforcement by fibres and high conductivity of graphene.

Another key challenge is to produce graphene of high quality. Usually two well-developed methods, namely high energy milling of graphite [6–8] and modified Hummer's method for obtaining graphene from graphite oxide [9,10] are used to produce graphene out of commercially available graphite. The major problem associated with both methods is uncontrollable quality of the graphene sheets [4]. Among other methods,

* Corresponding author at: Tallinn University of Technology, Ehitajate 5, 19180 Tallinn, Estonia.
E-mail address: irina.hussainova@ttu.ee (I. Hussainova).

http://dx.doi.org/10.1016/j.matdes.2015.10.148
0264-1275/

chemical vapour deposition (CVD) has been demonstrated as a suitable process for a cost effective synthesis of large area graphene sheets mostly on metallic substrates [11]. In this work for the first time we propose a CVD graphene deposition directly onto an insulating substrate of alumina (Al_2O_3) nanofibers to be used as a conductive filler for insulating oxide ceramic.

Although many reports on graphene-metal oxide composites have recently been published, there is still a challenge in terms of processing and manufacturing of mechanically reliable and electroconductive composite. Recently, Fan et al. [5] reported fabrication of a fully dense graphene nanosheets — Al_2O_3 composite by ball milling and spark plasma sintering (SPS). Indeed, conventional sintering techniques require relatively long processing time at high temperatures that may result in degradation of nano-carbons. SPS allows lowering the sintering temperature and shortening the dwell times and preserves the integrity of the graphenated nanofillers [12,13].

In this study, for the first time we propose a strategy for production of electroconductive hierarchically structured alumina by easily upscalable method using SPS technique. Commercially available α-Al_2O_3 powder is taken as an example to elucidate a strategy of utilizing hybrid structure of alumina nanofibers covered by multi-layered graphene for the preparation of metal oxide electroconductive composite with addition of only 0.3 wt.% of carbon.

2. Experimental procedure

2.1. Deposition of a few layered graphene onto alumina nanofibers

The shells of graphene layers were grown on the surface of alumina nanofibers (ANF) of 7–10 nm in diameter and a huge aspect ratio of 10^7, as described in [14], with the help of a hot-wall chemical vapour deposition (CVD) of carbon at atmospheric pressure as detailed in [15,16]. Fig. 1 shows the SEM and HR-TEM images of the structures produced *via* one-step catalyst-free chemical vapour deposition procedure at temperature of 1000 °C during 20 min in a mixture of nitrogen (N_2) gas flowing at a rate of 500 cm^3/min and methane (CH_4) flowing at a rate of 50 cm^3/min.

2.2. Processing

Appropriate amount of graphene covered alumina nanofibers (ANFC) has been dispersed in ethanol by a stick ultrasound (Hielscher UP400S) for 1 h at 400 W and 24 kHz following the procedure outlined in [17]. The obtained suspension was treated in attrition mill for 1 h in ethanol with zirconia balls of 3 mm in diameter in order to attain deagglomeration of the fibres bundles. Then different amount of α-alumina nano-powder (Taimei TMDAR, Japan) with an average particle size of 100 nm was added to the suspension and treated for an hour to prepare composites with 1 wt.%, 3 wt.%, 5 wt.%, 10 wt.% and 15 wt.% ANFC. The suspension mixtures were dried at 65 °C for 24 h and sieved through 100 μm sieve for the further investigation. Pure alumina nanopowder was used as a reference material to study the effect of nanofiller addition on microstructure, electrical and mechanical properties of alumina.

The bulk ceramics were prepared using SPS technique (Dr. Sinter SPS-510CE, Japan). Two grammes of the ANFC-Al_2O_3 powder mixtures were loaded into a 10 mm inner diameter graphite die with a sheet of graphitic paper placed between the punch and the powder. The mixtures were sintered at 1350, 1380 and 1400 °C with simultaneous application of 40 MPa pressure for a dwell time of 10 min. Heating rate was

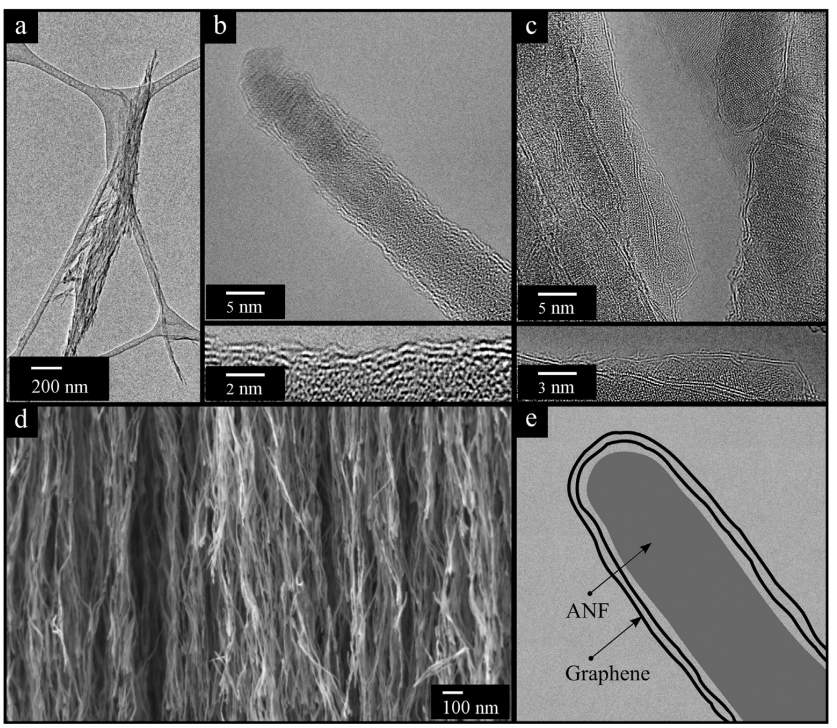

Fig. 1. (a, b, c) — TEM images of the alumina nanofibers covered by a few layers of graphene; (d) — SEM image of the fibres covered by graphene; and (e) — the schematic representation of the nanofiller.

set to 200 °C/min between 600 and 1000 °C and then 100 °C/min. The sintering was conducted in N_2 atmosphere.

2.3. Characterization

Application of high temperatures during sintering makes the thermal behaviour of the fillers and matrix materials to be a key factor for the production of a defect free bulk. The thermal behaviour of ANFC has been studied elsewhere [17]. Differential thermal and thermogravimetric analyses (DTA/TG) (SETARAM, SETSYS 16/18, France) were carried out in order to determine the amount of graphene in the sintered samples.

Identification of phases in the sintered samples was carried out by X-ray diffraction using a Bruker diffractometer (D8) with CuKα radiation. For microstructural characterization of the fillers and bulks, a transmission electron microscope (TEM/STEM JEOL2100F) operating at 200 kV and equipped with a field emission electron gun providing a point resolution of 0.19 nm and a field emission scanning electron microscope (HITACHI S-4700, Japan) were used.

The density of the samples after sintering was measured by a conventional geometric method. To study the effect of fillers on mechanical properties, the Vickers hardness and indentation fracture toughness (IFT) of the composites were determined by the Vickers hardness tester Indentec 5030 SKV. The IFT was determined by the measurement of the crack lengths produced by Vickers indentations (49 N) following the procedure proposed by Anstis [23]. Modulus of elasticity (E) needed for calculation of the IFT was previously measured for a pure alumina produced under the same conditions by the impulse excitation technique (IET) according to ASTM-E1876. Assuming insignificant effect of alumina nanofibers onto the modulus of elasticity of alumina matrix composite, the obtained value of 380 GPa was used to determine toughness of materials with density higher than 99%. It is well established fact that modulus of elasticity is usually decreased with increasing porosity; therefore, an estimation of modulus for the less dense materials was made following the dependence $E \approx E_0 \times e^{-bP}$, where E_0 is the modulus of material with no porosity, P is the volume fraction of porosity, and b is a characteristic number, which is equal to 3 in the case of spherical pores [24].

The hardness was measured under the applied load was 49.03 N (HV_5) and holding time 10 s. The reported numbers represent the averaged values of at least 10 indentations.

Room temperature electrical properties were studied by a dc-four probe method. A potentiostat/galvanostat (Autolab PGSTAT 302 N) was used in galvanostatic mode to supply the current through the external electrodes and to record the voltage drop between the inner electrodes. The electrical conductivity was calculated from the experimental resistances obtained by the slope of the V–I curves in the range of 10–100 mA.

3. Results and discussion

3.1. Processing

FESEM images of the dried suspension containing 1 wt.%, 3 wt.%, 5 wt.% and 15 wt.% of ANFCs are shown in Fig. 2.

A dilatometric study of the alumina powder was carried out up to 1550 °C using 5 °C/min as heating rate in air. The study aims at rough estimation of the maximum temperature during the first SPS experiments. The onset and endset temperatures have been determined from the dilatometric curves shown in Fig. 3. The shrinkage begins at 940 °C and ends at about 1400 °C. The total contraction of the sample is 14%. The minimum peak of derivative of the dilatometric curve corresponds to the temperature of the highest rate of densification that is reached at approximately 1290 °C.

To find out the optimal sintering temperature for alumina-ANFC nanocomposites, a set of tests has been performed. It was established that the nearly full density (>99% of theoretical density) can be reached at 1380 °C for the alumina reference material, whereas its relative density decreases at lower temperatures of sintering. For composites added by 10 and 15 wt.% of ANFC, the application of neither lower nor higher temperatures resulted in poreless bulks. It should be noted that for all temperatures an increase in the amount of ANFC in the composite mixture leads to evident decrease in density. Therefore, an optimal sintering temperature for the further study was considered 1380 °C. Nevertheless, nanofillers content up to 5 wt.% did not significantly affect the densification behaviour of the nanocomposites. Table 1 shows the bulk and relative densities of the materials. Pure alumina and composites added

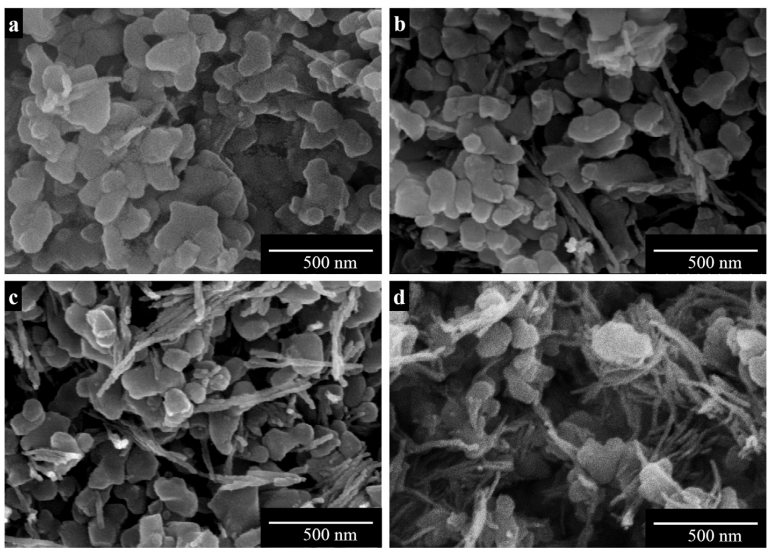

Fig. 2. FE–SEM images of composite powders with different percentages of alumina nanofibers covered by multi-layers of graphene (ANFC): (a) 1 wt.%, (b) 3 wt.%, (c) 5 wt.%, and (d) 15 wt.% of ANFC in Al_2O_3 matrix.

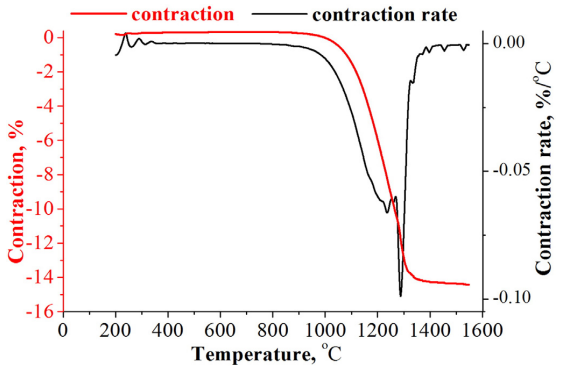

Fig. 3. Dilatometry of the alumina powder carried out at 5 °C/min up to 1550 °C.

by less than 10 wt.% of nanofibers exhibit higher than 99% density, whereas for the composites with 10 wt.% and 15 wt.% of ANFCs density decreases down to 97% and 95%, correspondingly.

3.2. Microstructural characterization

To examine the microstructural features of the composites, the fractured surfaces of the samples were studied, Fig. 4a, b. Homogeneous distribution of the nanofibers, which are de-bonded and pulled out from the matrix, may be seen from the micrographs displayed in Fig. 4. The microstructure of the pure alumina presents homogenous grain size distribution in the range of 1–5 μm, Fig. 5a, with the presence of a small amount of inter- and intra-granular pores. The main mechanism of fracture for the pure alumina is intergranular crack propagation. Addition of only 1 wt.% of fibres greatly affects the microstructure (Fig. 5b). Al_2O_3-1 wt.% ANFC composite has uneven grain size distribution with the presence of both submicron and abnormally grown elongated grains. The evolution of the grain size in the sintered material containing different amount of nanofillers can be observed from Fig. 5. Evidently, increasing the amount of ANFC results in a significant decrease in a grain size. Similar behaviour was noticed by Liu et al. [1] for alumina-graphene platelets (GPL) composites produced by SPS. The refinement of the microstructure was explained by the distribution of GPLs throughout ceramic grain boundaries and preservation their migration during sintering. Similar to GPLs, graphene covered nanofibers are also distributed between alumina particles and may prevent grain growth.

The X-ray diffraction pattern (obtained for the sample with the highest amount of ANFC (15%) on the verge of the XRD detection limits) shows only the peaks of alumina detecting no second phase formation and indicating no significant reaction between graphene and alumina under selected processing parameters, Fig. 6.

To precise the amount of C in the composites under consideration, the DTA–TG analysis of the sintered samples was performed. As an example, Fig. 7 presents TG and DTA curves for Al_2O_3-10 wt.% ANFC material. The TG curve shows a continuous insignificant weight loss (~0.1%) up to 420 °C, which is caused by the elimination of impurities from the surface of the sample. The sharp decrease in weight (1% of the remained mass) between 420 and 620 °C is accompanied with the exothermic effect and is associated with the oxidation of the so-called "graphitized carbon". The same effect at this temperature range was determined in our previous work [17] in TG curve of ANFC. Thus, the amount of carbon in Al_2O_3-10wt.% ANFC composite is determined to be around 1 wt.%; therefore, each 1 wt.% of graphene covered nanofibers adds approximately 0.1 wt.% of carbon to the composites.

Table 1
Bulk and relative density of the alumina-ANFC composites sintered at 1380 °C.

Percentages of ANFC, wt.%	0	1	3	5	10	15
Density, g/cm^3	3.94	3.96	3.95	3.95	3.84	3.77
Relative density, %	99.4	99.9	99.7	99.8	96.9	95.1

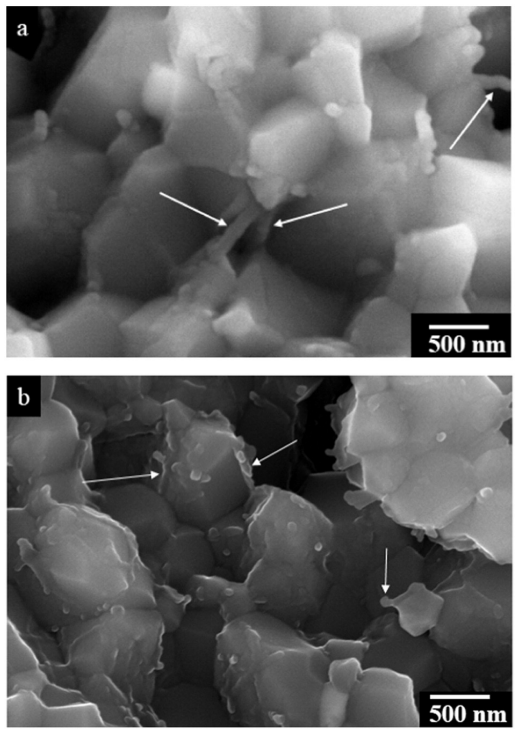

Fig. 4. FE–SEM images of the ANFCs in the composites: (a) Al_2O_3-5 wt.% ANFC, (b) Al_2O_3-10 wt.% ANFC.

Raman spectroscopy was used to confirm the structural integrity of the graphene in the alumina matrix after sintering (Fig. 8). The defect-derived D-band (~1350 cm^{-1}), the structure derived G-band (~1600 cm^{-1}) and the G′ band at ~2700 cm^{-1} were observed for the sintered Al_2O_3-15 wt.% ANFC specimen. Raman intensities of D and G bands are compared for the sample filled by ANFCs and the bundle of untreated ANFC. The similar I_D/I_G ratio for ANFC and the sintered composite sample indicates that the nanostructure of graphene is maintained during the powder mixing and sintering processes.

3.3. mechanical properties

The numbers of Vickers hardness of the monolithic alumina and ANFC-added composites are displayed in Fig. **9**. The hardness of Al_2O_3-1 wt.% ANFC composite has increased by 24% over the pure alumina, reaching its maximum value of 1764 HV_5 (17.3 GPa); the hardness of the materials with 3 and 5 wt.% of the ANFCs just slightly exceeds the hardness of unfilled alumina.

Therefore, the addition of the nanofibers covered by multi-layered graphene does not critically influence such an important mechanical property as hardness. However, further increase in ANFC content results in hardness degradation. This behaviour can be related to the combined impact of two effects: grain refinement and increased residual porosity. Grain growth inhibition is conditioned by supplementing alumina with

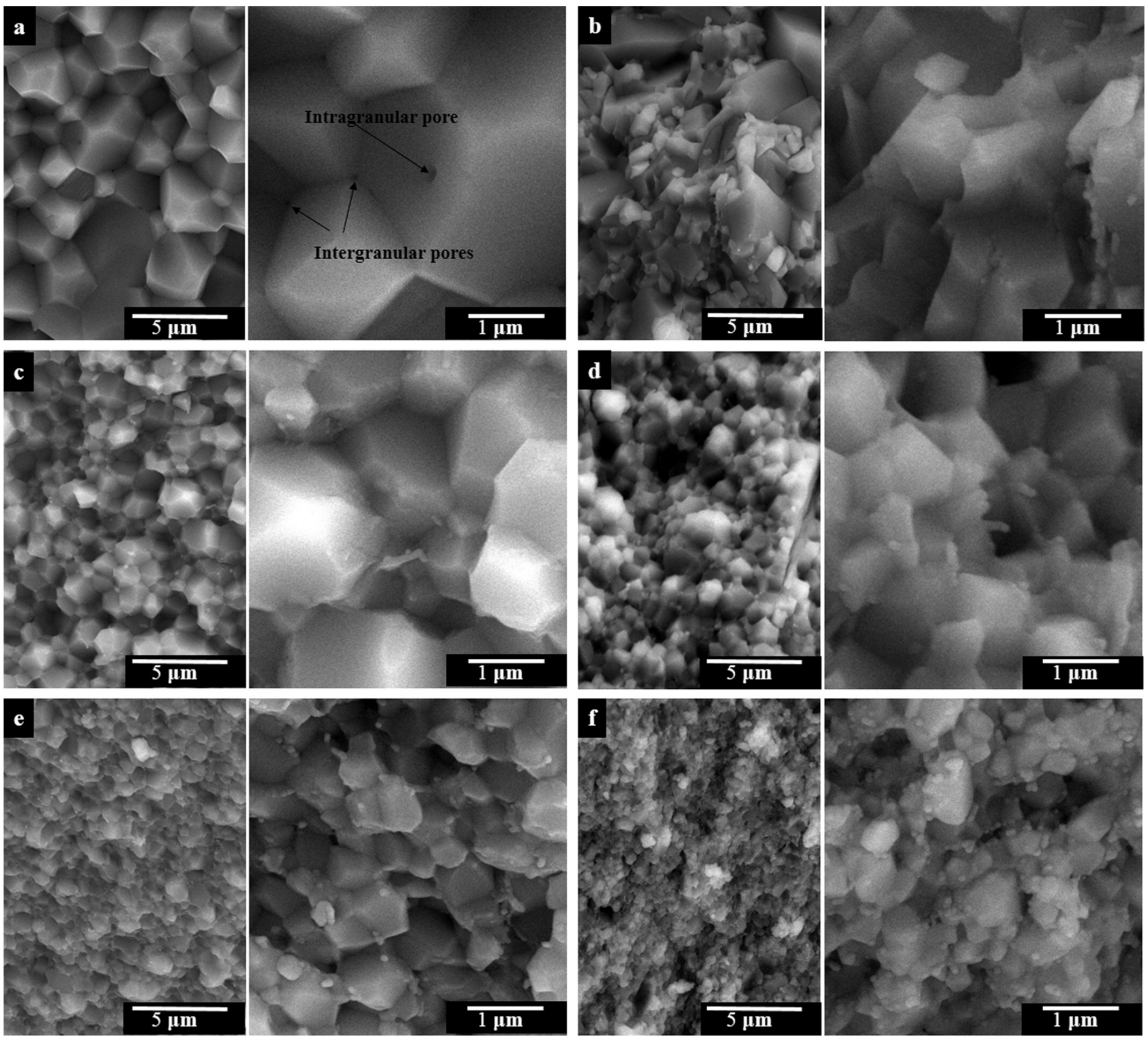

Fig. 5. FE–SEM images of fracture surfaces of the sintered samples of Al_2O_3 with different amount of ANFC: (a) without ANFC, (b) 1 wt.%, (c) 3 wt.%, (d) 5 wt.%, (e) 10 wt.%, (f) 15 wt.% ANFC.

the ANFCs. From the other side, increase in porosity level usually exponentially reduces hardness of the materials [18].

The indentation fracture toughness value for the reference sample of pure alumina was measured to be 3.31 MPa $m^{1/2}$ that was increased with incorporation of nanofillers into the matrix. The IFT reached a maximum value of 5.54 MPa $m^{1/2}$ for the Al_2O_3-5 wt% ANFC composite corresponding to an increase of approximately 40% as compared to pure alumina. The IFT slightly decreased for graphene loading higher than

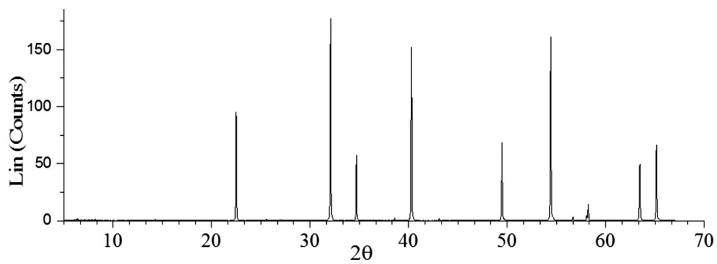

Fig. 6. XRD pattern of sintered Al_2O_3-15 wt.% ANFC sample.

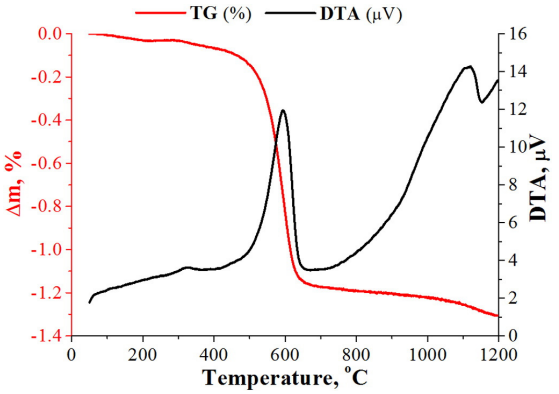

Fig. 7. TG and DTA curves of sintered Al_2O_3-10wt.% ANFC sample.

5 wt.% down to 4.6 MPa $m^{1/2}$ for the Al2O3-15 wt.% ANFC that may be associated with porosity and formation of an inter-connected network of the graphene shell covered nanofibers that may act as a weak interfaces [25].

3.4. Electrical properties

The electrical conductivity of the ceramic composites was measured as a function of the carbon content (Table 2). It was demonstrated that both pure alumina and the alumina filled with 1 wt.% of alumina nanofibers covered by multi-layered graphene shell, which is approximately equal to 0.1 wt.% of graphene in the material, show dielectric behaviour at a room temperature with a conductivity that does not exceed 10^{-12} S m^{-1}.

Incorporation of only 3 wt.% of ANFC, which is approximately equal to 0.3 wt.% of graphene, results in a significant increase in the electrical conductivity (about 13 orders of magnitude) exhibiting a conductivity of ~14 S m^{-1}. Therefore, three wt.% of ANFCs give an interconnected network of the conductive fillers throughout the bulk material, suggesting that the percolation threshold is reached for ~0.3 wt.% graphene addition. A higher amount of conductive nanofillers to the Al_2O_3 matrix produces a continuous increase in conductivity from ~32 S m^{-1} for 5 wt.% ANFC to ~106 S/m for 10 wt.% ANFC. Such kind of behaviour well agrees with the general trend for the conductivity observed by other research groups for different types and morphologies of carbon-based additives in Al_2O_3 ceramic matrix [3,5,19,20] However, when the filler loading increased up to 15 wt.%, the increase in conductivity is less pronounced, reaching a value of ~127 S m^{-1}. This can be explained by the microstructural changes, Fig. 5, where the introduction

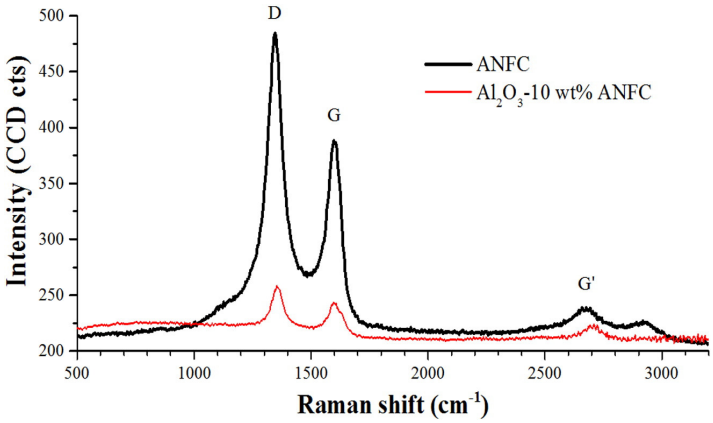

Fig. 8. Raman spectrum of alumina nanofibers covered by multi-layered graphene (ANFC) and sintered Al_2O_3-15 wt.% ANFC composite.

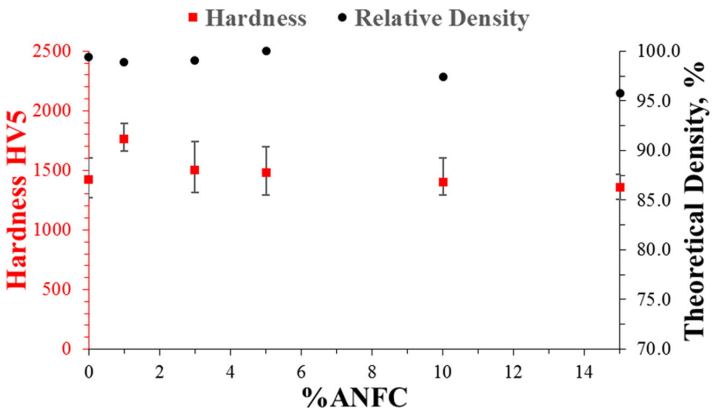

Fig. 9. Hardness and theoretical density of alumina-ANFC composites sintered at 1380 °C as functions of ANFC contents.

Table 2
Electrical conductivity of alumina-ANFC nanocomposites.

Percentages of ANFC, wt%	0	1	3	5	10	15
Graphene content, wt%	0	0.1	0.3	0.5	1	1.5
Resistivity, Ω·m	10^{12}	$5.8°10^{11}$	$7.1°10^{-2}$	$3.1°10^{-2}$	$9.4°10^{-3}$	$7.9°10^{-3}$
Conductivity, S m^{-1}	10^{-12}	$1.7°10^{-12}$	14	32	106	127

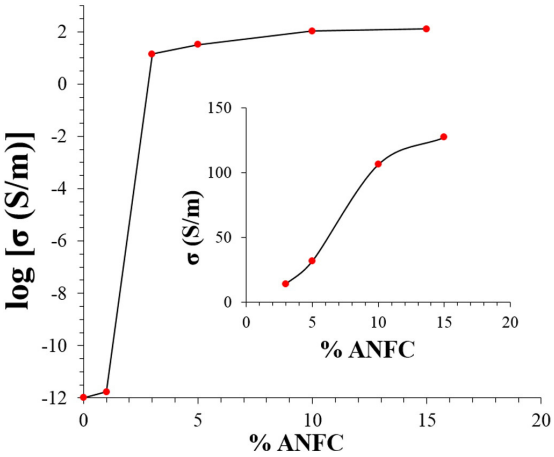

Fig. 10. Electrical conductivity of ANFC/Al2O3 samples as a function of the ANFC load.

of higher contents of ANFC at the grain boundaries produces a systematic deterioration in densification preventing the grain growth process and providing extended grain boundary regions. This can result in the effective reduction of the density of the conducting phase at grain boundaries decreasing the number of conductive paths [21]. Moreover, a high content of nanofillers is responsible for some agglomeration of the ANFC phase, resulting in a non-homogeneous distribution at grain boundaries [23]. On the other hand, although the samples with 15 wt.% ANFC still show high values of densification (~96% of the theoretical density), the porosity could also contribute to slight increase in the effective length for the electrical transport harming the conductivity. Consequently, the higher content of conductive phase in high-loaded samples is partially countered by the smaller grain size and the lower density leading to the effective "smoothing" in further increase in conductivity, Fig. 10.

Table 3 summarizes some results on the conductivity of the ceramic composites reported in the literature for different carbon-based nanofillers in the Al_2O_3 matrix. Inam et al. [21] reported that the use of carbon nanotubes as a filler improved the electrical behaviour compared to carbon black due to a better dispersion of the CNTs and the tendency of the carbon black to agglomerate. On the other hand, the use of graphene nanosheets exhibits substantial increase in conductivity once the fillers network percolation is achieved for the samples with a quite low values of additive load [2,3,5] possibly because of the higher contact area between the sheets of the 2-dimensional graphene as compared to the 1-dimensional carbon nanotubes [3]. As the percolation threshold depends on the degree of filler dispersion within the matrix, a wide range of conductive filler concentrations were reported for ceramic-based composites. The electrical properties analysed in the present study for different nanofiller loads show a very low percolation threshold (~0.3 wt.% graphene) needed for increasing the conductivity over 13 orders of magnitude compared to the monolithic alumina. Taking into consideration a low load of conductive phase, the results of the present study show the potential for opening a new avenue in developing electroconductive ceramic composites suitable for electrical discharge machining of otherwise insulating ceramics.

4. Conclusions

To summarize, a novel approach to prepare the electroconductive ceramic-based composites by incorporation of the conductive nanofibers of oxide ceramic covered by multi-layered graphene shell is demonstrated for the case of alumina. The feasibility of the graphene coated alumina nanofibers to serve as the additive for producing electroconductive ceramics of enhanced toughness is shown in this study. Well dispersed and fully dense (>99% of theoretical density) composites of alumina and alumina nanofibers covered by multi-layered graphene shells were produced by powder processing and densified using SPS at 1380 °C with 40 MPa pressure for 10 min. An increase in electro-conductivity of 13 orders of magnitude as compared to the monolithic alumina is achieved at as low load of carbon as only ~0.3 wt.%, which correspond to 3 wt.% of the nanofillers. Moreover, an increase in hardness of the composites with ≤10 wt.% nanofillers was approximately 20% while an improvement in an indentation fracture toughness was 40% for the composites containing 5 wt.% graphene covered nanofibers; therefore, an increase in conductivity does not result in deterioration of the mechanical properties. Slight decrease in hardness for materials with more than 10 wt.% of graphenated nanofibers can be attributed to increase in porosity level due to a poor densification of the materials. The strategy proposed in the current study can easily be extended to other insulating ceramics.

Acknowledgements

This research was supported by European Social Fund's Doctoral Studies and Internationalization Programme DoRa, which is carried out by Foundation Archimedes; as well as Archimedes funded project NanoCom AR12133, and institutional research funding IUT 19–29 of the Estonian Ministry of Education and Research. The

Table 3
Electrical conductivity of alumina-carbon nanocomposites.

Reference	Processing method	Temp., °C	Filler type	Conduct. (S m^{-1})
Inam et al. [21]	SPS	1800	2 wt.% carbon black	30
Inam et al. [21]	SPS	1800	2 wt.% carbon nanotubes	125
Zhang et al. [22]	Pressureless sintering	1500	1 vol.% multi-wall carbon nanotubes (~0.53 wt.%)	2.2×10^{-12}
Wang et al. [2]	SPS	1300	2 wt.% graphene nanosheets	172
Centeno et al. [3]	SPS	1500/1300	0.16 wt.% graphene	0.1
Centeno et al. [3]	SPS	1500/1300	0.22 wt.% graphene	6.7
Centeno et al. [3]	SPS	1500/1300	0.45 wt.% graphene	11.1
Fan et al. [5]	SPS	1300	0.6 vol.% graphene (~0.35 wt.%)	30
Fan et al. [5]	SPS	1300	2.35 vol.% graphene (~1.35 wt.%)	1038.15
Present work	SPS	1380	0.3–1.5 wt.% graphene	14–127

authors would like to thank Dr. Fernando Rubio-Marcos from Instituto de Cerámica y Vidrio, CSIC, Spain, for his excellent assistance in TEM imaging.

References

[1] J. Liu, H. Yan, K. Jiang, Mechanical properties of graphene platelet-reinforced alumina ceramic composites, Ceram. Int. 39 (2013) 6215–6221, http://dx.doi.org/10.1016/j.ceramint.2013.01.041.
[2] K. Wang, Y. Wang, Z. Fan, J. Yan, T. Wei, Preparation of graphene nanosheet/alumina composites by spark plasma sintering, Mater. Res. Bull. 46 (2011) 315–318, http://dx.doi.org/10.1016/j.materresbull.2010.11.005.
[3] A. Centeno, V.G. Rocha, B. Alonso, A. Fernández, C.F. Gutierrez-Gonzalez, R. Torrecillas, et al., Graphene for tough and electroconductive alumina ceramics, J. Eur. Ceram. Soc. 33 (2013) 3201–3210, http://dx.doi.org/10.1016/j.jeurceramsoc.2013.07.007.
[4] H. Porwal, S. Grasso, M.J. Reece, Review of graphene–ceramic matrix composites, Adv. Appl. Ceram. 112 (2013) 443–454, http://dx.doi.org/10.1179/174367613X13764308970581.
[5] Y. Fan, W. Jiang, A. Kawasaki, Highly conductive few-layer graphene/Al 2O 3 nanocomposites with tunable charge carrier type, Adv. Funct. Mater. 22 (2012) 3882–3889, http://dx.doi.org/10.1002/adfm.201200632.
[6] Y. Fan, L. Wang, J. Li, J. Li, S. Sun, F. Chen, et al., Preparation and electrical properties of graphene nanosheet/Al2O3 composites, Carbon N Y 48 (2010) 1743–1749, http://dx.doi.org/10.1016/j.carbon.2010.01.017.
[7] W. König, D.F. Dauw, G. Levy, U. Panten, EDM-Future steps towards the machining of ceramics, Annals CIRP 37 (2) (1988) 623–631.
[8] P. Kun, O. Tapasztó, F. Wéber, C. Balázsi, Determination of structural and mechanical properties of multilayer graphene added silicon nitride-based composites, Ceram. Int. 38 (2012) 211–216, http://dx.doi.org/10.1016/j.ceramint.2011.06.051.
[9] T. Zhou, F. Chen, K. Liu, H. Deng, Q. Zhang, J. Feng, et al., A simple and efficient method to prepare graphene by reduction of graphite oxide with sodium hydrosulfite, Nanotechnology 22 (2011) 045704, http://dx.doi.org/10.1088/0957-4484/22/4/045704.
[10] Y. Zhu, S. Murali, W. Cai, X. Li, J.W. Suk, J.R. Potts, et al., Graphene and graphene oxide: synthesis, properties, and applications, Adv. Mater. 22 (2010) 3906–3924, http://dx.doi.org/10.1002/adma.201001068.
[11] A.N. Obraztsov, Chemical vapour deposition: making graphene on a large scale, Nat. Nanotechnol. 4 (2009) 212–213, http://dx.doi.org/10.1038/nnano.2009.67.
[12] Z. Munir, U. Anselmi-Tamburini, M. Ohyanagi, The effect of electric field and pressure on the synthesis and consolidation of materials: a review of the spark plasma sintering method, J. Mater. Sci. 41 (2006) 763–777, http://dx.doi.org/10.1007/s10853-006-6555-2.
[13] I. Hussainova, M. Drozdova, M. Aghayan, R. Ivanov, D. Pérez-Coll, Graphene covered alumina nanofibers as toughening agent in alumina ceramics, Adv. Sci. Technol. 88 (2014) 49–53, http://dx.doi.org/10.4028/www.scientific.net/AST.88.49.
[14] M. Aghayan, I. Hussainova, M. Gasik, M. Kutuzov, M. Friman, Coupled thermal analysis of novel alumina nanofibers with ultrahigh aspect ratio, Thermochim. Acta 574 (2013) 140–144, http://dx.doi.org/10.1016/j.tca.2013.10.010.
[15] I. Hussainova, R. Ivanov, S.N. Stamatin, I.V. Anoshkin, E.M. Skou, A.G. Nasibulin, A few-layered graphene on alumina nanofibers for electrochemical energy conversion, Carbon N Y 88 (2015) 157–164, http://dx.doi.org/10.1016/j.carbon.2015.03.004.
[16] R. Ivanov, V. Mikli, J. Kübarsepp, I. Hussainova, Direct CVD growth of foliated graphene closed shells on alumina nanofibers, Key Eng. Mater. 674 (2016) 77–80, http://dx.doi.org/10.4028/www.scientific.net/KEM.674.77.
[17] R. Ivanov, I. Hussainova, M. Aghayan, M. Drozdova, D. Pérez-Coll, M.A. Rodríguez, Graphene-encapsulated aluminium oxide nanofibers as a novel type of nanofillers for electroconductive ceramics, J. Eur. Ceram. Soc. 35 (2015) 4017–4021, http://dx.doi.org/10.1016/j.jeurceramsoc.2015.06.011.
[18] F.J. Paneto, J.L. Pereira, J.O. Lima, E.J. Jesus, L.A. Silva, E. Sousa Lima, et al., Effect of porosity on hardness of Al2O3–Y3Al5O12 ceramic composite, Int. J. Refract. Met. Hard Mater. 48 (2015) 365–368, http://dx.doi.org/10.1016/j.ijrmhm.2014.09.010.
[19] L. Kumari, T. Zhang, G.H. Du, W.Z. Li, Q.W. Wang, A. Datye, et al., Synthesis, microstructure and electrical conductivity of carbon nanotube-alumina nanocomposites, Ceram. Int. 35 (2009) 1775–1781, http://dx.doi.org/10.1016/j.ceramint.2008.10.005.
[20] K. Hirota, Y. Takaura, M. Kato, Y. Miyamoto, Fabrication of carbon nanofiber(CNF)-dispersed Al2O3 composites by pulsed electric-current pressure sintering and their mechanical and electrical properties, J. Mater. Sci. 42 (2007) 4792–4800, http://dx.doi.org/10.1007/s10853-006-0830-0.
[21] F. Inam, H. Yan, D.D. Jayaseelan, T. Peijs, M.J. Reece, Electrically conductive alumina-carbon nanocomposites prepared by spark plasma sintering, J. Eur. Ceram. Soc. 30 (2010) 153–157, http://dx.doi.org/10.1016/j.jeurceramsoc.2009.05.045.
[22] S.C. Zhang, W.G. Fahrenholtz, G.E. Hilmas, E.J. Yadlowsky, Pressureless sintering of carbon nanotube-Al2O3 composites, J. Eur. Ceram. Soc. 30 (2010) 1373–1380, http://dx.doi.org/10.1016/j.jeurceramsoc.2009.12.005.
[23] G.R. Anstis, P. Chantikul, B.R. Lawn, D.B. Marshall, A critical-evaluation of indentation techniques for measuring fracture-toughness.1. Direct crack measurements, J. Am. Ceram. Soc. 64 (9) (1981) 533–538.
[24] C.C. Wu, R.W. Rice, Porosity dependence of wear and other mechanical fine-grain Al2O3 and B4C, Ceram. Eng. Sci. Proc. 6 (1985) 977–994.
[25] H. Porwal, P. Tatarko, S. Grasso, J. Khaliq, I. Dlouhy, M.J. Reece, Graphene reinforced alumina nano-composites, Carbon 64 (2013) 359–369, http://dx.doi.org/10.1016/j.carbon.2013.07.086.

Paper II. Hussainova, I., Baronins, J., **Drozdova, M.**, Antonov, M., Wear performance of hierarchically structured alumina reinforced by hybrid graphene encapsulated alumina nanofibers. – *Wear*, 2016, 368–369, 287–295. DOI:10.1016/j.wear.2016.09.028.

Wear 368-369 (2016) 287–295

Contents lists available at ScienceDirect

Wear

journal homepage: www.elsevier.com/locate/wear

Wear performance of hierarchically structured alumina reinforced by hybrid graphene encapsulated alumina nanofibers

Irina Hussainova [a,b,*], Janis Baronins [a], Maria Drozdova [a], Maksim Antonov [a]

[a] Department of Materials Engineering, Tallinn University of Technology, Ehitajate tee 5, 19086 Tallinn, Estonia
[b] ITMO University, Kronverksky 49, St. Petersburg 197101, Russian Federation

ARTICLE INFO

Article history:
Received 30 May 2016
Received in revised form
28 September 2016
Accepted 29 September 2016
Available online 1 October 2016

Keywords:
Alumina
Nanofibres
Graphene
Sliding wear
Coefficient of friction

ABSTRACT

Nowadays, the lightweight composites with superior mechanical and tribological properties to be used for several applications in automotive and aerospace industries attract much research interest. Graphene added into ceramic-based composites is believed to positively contribute into sliding wear resistance of materials. To study an effect of graphenated fillers, dry sliding wear behaviour of spark plasma sintered alumina and its hierarchically structured composites reinforced by hybrid graphene encapsulated alumina nanofibres were tested against alumina at a reciprocating mode under mild (0.98 N) and severe (4.90 N) loading conditions for 72 h and 1 h, respectively. The tests were conducted at an average velocity of 0.006 m s^{-1} in air for the composites with different content (0 – 15 wt%) of the fillers corresponding to 0 – 1.5 wt% of graphene. Benchmarked against the pure alumina, the composites added with 1 – 5 wt% of hybrid nanofibres exhibited at least threefold higher wear resistance under mild conditions along with insignificant change in coefficient of friction; whilst under severe conditions, the wear resistance was found to increase up to 90% along with a decrease in the coefficient of friction only for the composite added by 1 wt% of fibres. Wear reduction for the composites with a low content of hybrid nanofibres might be attributed to increase in hardness together with increase in indentation fracture toughness. The relative index of brittleness is shown to serve as a wear performance indicator only under mild environment.

1. Introduction

Structural ceramic materials are an actively developed field of research for advanced engineering applications due to their excellent properties such as high temperature stability, chemical inertness, high strength, and good wear performance. Alumina (Al_2O_3) is one of the most attractive ceramics owing to its high hardness and compressive strength, good bio-compatibility and oxidation resistance, combined with relatively low density. These properties ensure its application as seals rings, medical prosthesis, laser tubes, electronic substrates, thermocouple tubes, electric insulators, etc. [1–3]. However, monolithic ceramics tend to be mechanically unreliable, which limits their wide use in applications where damage tolerance is a main requirement [1–4]. Therefore, a wide range of reinforcing and/or toughening agents such as fibres, carbon nanotubes and, recently, graphene nanoplatelets have been incorporated into ceramic matrices in attempt to produce tough and damage tolerant ceramic-matrix composites [4–7]. As graphene has demonstrated exceptionally high mechanical properties (for example, 2 nm graphene sheet exhibits an ultimate tensile strength of 130 GPa, spring constants in the region of 1–5 N m^{-1} and a Young's modulus of 0.5–1.0 TPa [7] along with strains exceeding 20% [8]), a tremendous number of research works concentrate on development of graphene reinforced composites of increased toughness and damage resistance [9–11].

Despite of an impressive amount of studies on alumina/graphene composites exploiting different approaches for introducing a wide variety of carbon structures starting with an exfoliated graphene, graphene oxide, reduced graphene oxide and un-oxidized graphene platelets [5,12,13], the studies on tribological performance of these composites are still quite limited; moreover, the novel type of hierarchically structured materials added by nanofibers encapsulated by graphene is tested for the first time. In fact, several works have documented reduction of wear rates for graphene nanoplatelets reinforced ceramic-based nanocomposites [10,11,14,15]. The high wear performance has been reported to attribute to crack deflection, crack bridging and crack branching together with the formation of a protective tribofilm on the wear track. Such reinforcement related effects as debond, pull-out and

* Corresponding author.
E-mail address: irina.hussainova@ttu.ee (I. Hussainova).

http://dx.doi.org/10.1016/j.wear.2016.09.028
0043-1648/

rupture of graphene nanosheets from ceramic matrix have been proposed as one of the main toughening mechanisms [14–17].

Kim et al. [10] has reported on a wear behaviour of the alumina and exfoliated graphene/alumina composite showing a decrease in wear rate by 91.5% with increase in graphene content up to 1.0 vol% when tested against WC counterbody at a load of 25 N and sliding speed of 100 mm s^{-1}; the remarkable improvements in wear resistance of the composites were proposed to be related to a less degree of grains pull-out during wear test. The wear rate has changed from close to severe wear regime (2.12×10^{-4} mm^3 N^{-1} m^{-1} for pure alumina) to approximately mild wear regime reaching wear rate of 1.87×10^{-5} mm^3 N^{-1} m^{-1} for 1.0 vol% of graphene containing alumina composites.

Gutierrez-Gonzalez et al. [14] has prepared a graphene/alumina composites using a colloidal mixture of graphene oxide and Al_2O_3 followed by subsequent spark plasma sintering under vacuum and reported on about 50% lower wear rate and ~10% reduction in the coefficient of friction (CoF) with adding 0.22 wt% of graphene platelets into the alumina matrix. Yazdani et al. [11] has studied the tribological performance of graphene/carbon hybrid reinforced Al_2O_3 composites and has found that graphene nanoplatelets are playing the important role in the formation of the tribofilm, while carbon nanotubes contribute to an improvement of the fracture toughness and a prevention the alumina grains from being pulled-out during the wear tests.

Herein, we report on the synthesis of alumina – based composites reinforced by the alumina nanofibres wrapped by several layers of non-functionalized graphene using a hot wall chemical vapour deposition (CVD) technique with a subsequent spark plasma sintering (SPS) of the bulks demonstrating enhanced hardness, toughness, and wear resistance. In this work, the sliding wear performance of the recently developed hierarchically structured alumina composites with various contents of hybrid graphene encapsulated alumina nanofibers is thoroughly analysed under different testing conditions. The wear mechanisms and influence of graphene content on the wear rate is reported along with change in mechanical properties of the materials produced.

2. Materials and methods

2.1. Materials

Commercially available α-alumina nanosized powder *TAIMICRON TM-DAR* with an average particle size of 100 nm (*TAIMEI CHEMICALS Co., Ltd.*, Japan) was used as a matrix material. The alumina nanofibres of 50 ± 2 mm in length and average single fibre diameter of 7 ± 2 nm described in detail in our previous work [18], Fig. 1a, were encapsulated into multi-layered graphene shells with the help of the recently developed one-step CVD process at temperature of 1000 °C and atmospheric pressure in a flow of two gases: ethylene (C_2H_4) with a flow rate of 10 cm^3/min and hydrogen (H_2) with a flow rate of 360 cm^3/min [19,20], Fig. 1a-insert. Our approach allows utilizing the advantages of reinforcement by fibres and high mechanical properties of graphene through homogeneous dispersion of the fibres within the alumina matrix.

The mixture suspensions of Al_2O_3 powder with addition of 0, 1, 3, 5, 10 and 15 wt% alumina nanofibres covered by graphene (ANFG), which correspond to graphene content of around 0, 0.1, 0.3, 0.5, 1.0 and 1.5 wt% [5], respectively, were treated in attrition mill with zirconia balls of 3 mm in diameter for 1 hour for fibres de-agglomeration, then dried at 65 °C for 24 h and sieved in 100 μm sieve. The composites were densified using spark plasma sintering (*Dr. Sinter SPS-510CE*, Japan) at 1380 °C with 40 MPa pressure for 10 min; the fracture surface of the composite with 15 wt% of ANFG is shown in Fig. 1b. The produced tablets with 50 mm in diameter were categorized according to concentration of the reinforcing constituents.

2.2. Experimental

The bulk density of the prepared composites was measured using Archimedes' method and their theoretical density was estimated assuming a rule of mixtures and taking the density of Al_2O_3 and graphene to be 3.98 and 2.1 g/cm^3, respectively. Results of at least five measurements were averaged.

Identification of phases in the sintered samples was carried out by X-ray diffraction using a Bruker diffractometer (D8) with CuKα radiation. Microstructural characterization of the composites was performed by scanning electron microscopy (SEM) imaging with

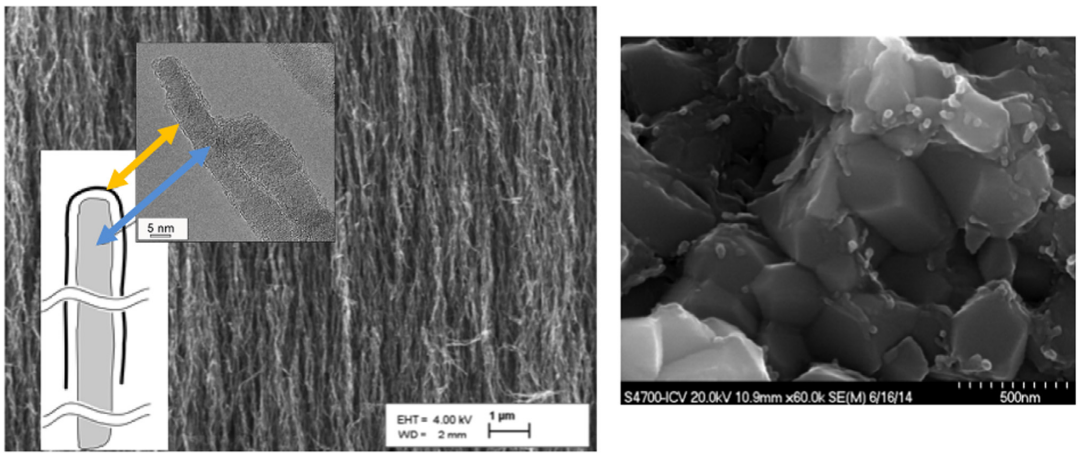

Fig. 1. (a) SEM image of a network of alumina nanofibres encapsulated into graphene wrap as shown in inserts: schematically drawn and TEM image (blue arrow – the alumina core; and yellow arrow – graphene layer grown on the surface of Al_2O_3 core fibre); (b) a fractured surface of the composite of Al_2O_3/ANFG with 15 wt% load of ANFG.

Table 1
Sliding wear test conditions with constant load.

Parameter	Description	
Configuration	Ball-On-Plate	
Mode	Reciprocating	
Ball diameter, m	3×10^{-3}	
Ball material	Al_2O_3 (ISO 3290)	
Load, *N* (g)	0.98 (100), 4.90 (500)	
Amplitude, m	1×10^{-3}	
Frequency, Hz	3	
Linear velocity, m s^{-1}	0.006	
Atmosphere	Air, 23 ± 2 °C, relative humidity $30 \pm 5\%$	
	Mild regime	**Severe regime**
	0.98 N (100 g)	**4.90 N (500 g)**
Duration, min (h)	4320 (72)	60 (1)
Number of repetitive sliding events (motions) at the same point on the track, times	1555200	21600
Wear path length, m	1555.2	21.6
Hertzian stress, GPa	1.65	2.83

HITACHI TM-1000 and *Zeiss EVO MA-15* system with LaB_6 cathode in secondary electron mode, applying an accelerating voltage of 10–15 kV and 6.5–8.5 mm working distance. Raman spectra of the graphenated structures were obtained with Raman spectroscopy (*Horiba Jobin Yvon LabRAM* 300) with laser excitation energy of 514 nm.

The Vickers hardness and indentation fracture toughness (IFT) were determined by the measurement of the crack lengths produced by Vickers indentations with a load of 9.8 N for 10 s (*Zwick/Roell ZHU/Z2.5*, Ulm, Germany). At least five equally spaced indents were recorded for each specimen and values were averaged. Calculation of the fracture toughness was done using the equation according to [21].

Wear experiments were carried out with a Universal Micro Materials Tester (*UMT-2*) from *CETR* (now *Bruker*) in a reciprocating mode with a stationary ball located above specimen that assumes wear debris keeping at the vicinity of a wear scar. At least three tests were performed for each specimen. It is worthy to mention that according to our recent study on influence of the counterbody ball position on wear rate, the development of the protective tribolayer is highly affected by the possibility for wear debris to escape the wear track [22]. Some kind of self-healing of tribomaterial was observed through the embedment of the entrapped wear debris to the track in the case of a high level of loading system inertia. As the result of the embedment, a high level of vibration was detected [23].

Moreover, as a running-in is an initial surface and subsurface conditioning process and is important not only for the materials in contact, but also for the system in which they reside [24,25], the present work executing a non-conformal (ball-on-plate) tribotest applies a long enough test duration, which enables the tribosystem to reach a steady-state regime.

Prior to the wear test, surfaces of the specimens were polished using *Buehler Vector* and *Buehler Beta Grinder-Polisher* device setups with a diamond polishing disc (*Apex DGD*) down to 0.5 μm and then cleaned with acetone and ethylene alcohol. The main conditions of the testing setup are given in Table 1. Taking into consideration structural oxide ceramics, the upper limit for mild wear regime of $\leq 10^{-6}$ mm^3 N^{-1} m^{-1} and for severe wear regime typically of $\geq 10^{-4}$ mm^3 N^{-1} m^{-1} was proposed in [26] and ensured in the present work, Table 1. The alumina balls (*Red-Hill Balls*, Czech Republic) with a hardness HV10 ≈ 1450 and roughness R_a=0.02 μm were used as counterbodies against the pre-polished specimens to provide ceramic – ceramic composite tribocontact with a similar value of hardness to observe a wear resistance of new composites and an influence of solid lubrication by graphene on CoF.

The selected conditions reflect situation often observed in modern devices containing ceramic moving and static parts (gears, twin gears, bearings, sliding contacts, etc.). In some cases, lubrication by liquids is limited, especially if device has to work in high purity environment (any presence of contaminating medium should be avoided) or at high temperature. Therefore, high hardness, solid lubrication, similar thermal expansion of parts in contact (dimensional stability) and stable performance in a wide range of temperatures are required.

The friction force transferred to a load cell was recorded throughout the tests. The cross-sectional areas of wear tracks of the samples were measured using a *Bruker Contour GT-K0+* profilometer and the specific wear rate W ($mm^3 \cdot N^{-1} \cdot m^{-1}$) was calculated by using the following equation (Eq. (1)):

$$W = \frac{\Delta V}{F_N \cdot L} \tag{1}$$

where ΔV is a wear volume, mm^3; F_N is an applied load, N; and L is a sliding distance, m.

Standard deviations for COF and wear volume were calculated by using the Eq. (2):

$$Stdev = \sqrt{\frac{\sum (x - \bar{x})^2}{(n-1)}} \tag{2}$$

where x is a measured COF or wear, mm^3; $\bar{x}$ is an average COF or wear, mm^3; n is a number of repeated measurements for each test.

3. Results and discussion

3.1. Mechanical properties and microstructural features

As wear behaviour of materials is closely attributed to their mechanical properties, Table 2 summarises the chemical composition, relative densities and the corresponding mechanical properties along with relative index of brittleness (RIB) for different composites and reference pure alumina prepared by SPS technique. It is well documented that wear resistance of ceramic based composites is affected by both hardness and fracture toughness [27,28,29], therefore the RIB defined as the HV/IFT ratio divided by

Table 2
Properties of the composites.

Composition	ID	Carbon, wt%	Relative density, %	Vickers hardness	IFT, MPa $m^{1/2}$	RIB
Al_2O_3	**A0**	0	> 99	1670 ± 78	3.34 ± 0.1	1
Al_2O_3/1 wt%ANFG	**A1**	~0.1	> 99	1830 ± 93	3.91 ± 0.11	~0.93
Al_2O_3/3 wt%ANFG	**A3**	~0.3	> 99	1824 ± 33	5.4 ± 0.09	~0.67
Al_2O_3/5 wt%ANFG	**A5**	~0.5	> 99	1820 ± 45	5.6 ± 0.17	~0.65
Al_2O_3/10 wt%ANFG	**A10**	~1.0	~98	1791 ± 67	5.03 ± 0.3	~0.71
Al_2O_3/15 wt%ANFG	**A15**	~1.5	~96	1640 ± 98	3.3 ± 0.34	~1

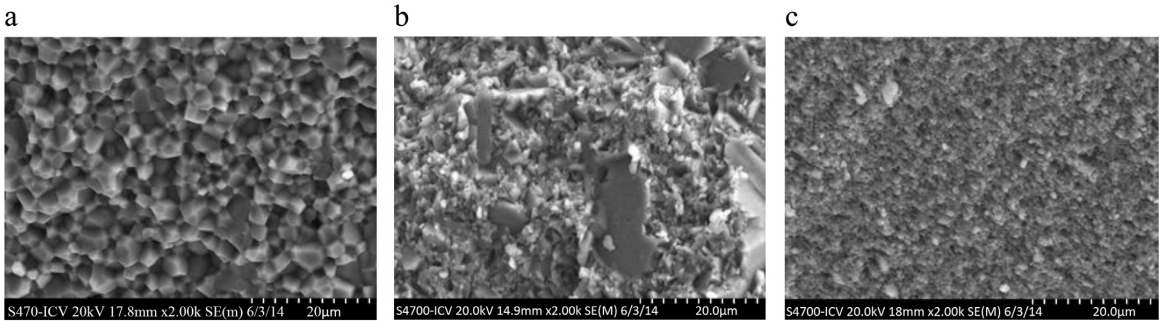

Fig. 2. SEM images of fractured surfaces of (a) pure alumina; (b) Al_2O_3/1 wt%ANFG composite, and (c) Al_2O_3/15 wt%ANFG composite.

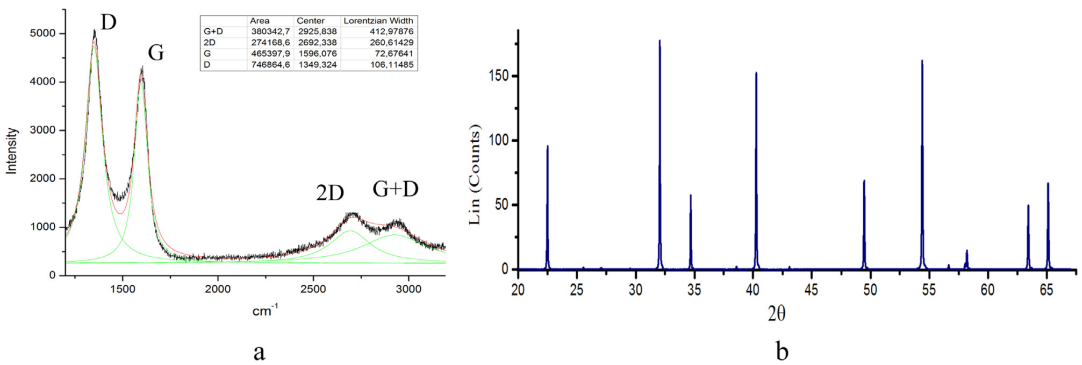

Fig. 3. The microstructural features of the Al_2O_3/15 wt%ANFG composite: (a) – Raman spectrum; and (b) – XRD pattern.

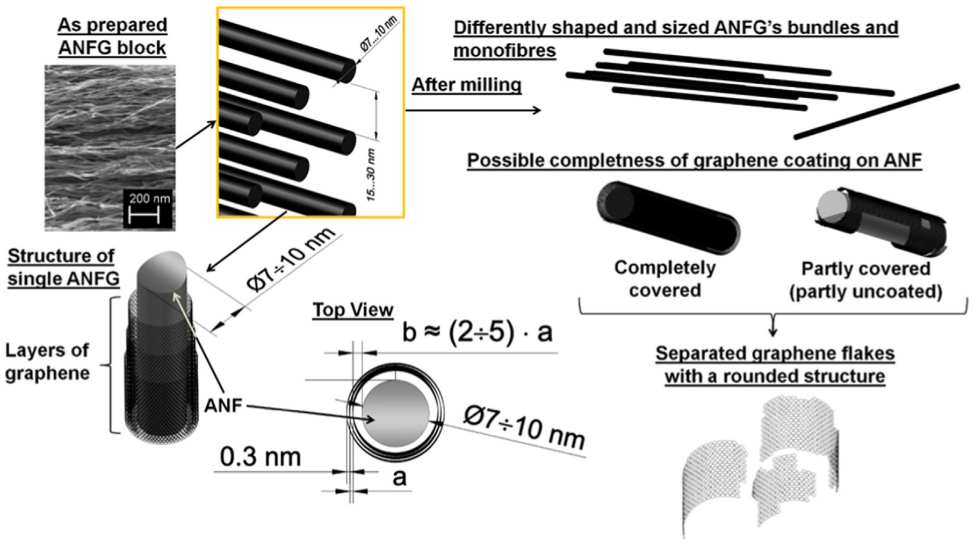

Fig. 4. Schematic of graphenated nanofibres presented in the composites.

index of brittleness of pure alumina.

Fig. 2 shows the representative SEM images of the fractured surfaces of pure alumina and specimens A1 and A15; their hierarchical structure is reflected by the presence of both micro- and nano-sized grains along with nano-scaled inclusions of high aspect ratio of about 10^3. Substantial reduction in grain size with increase in graphene content is well recognized and discussed in detail in [5]. The Raman spectrum of the sintered A15 composite confirms that the graphene is well-dispersed in the ceramic matrix and there was no damage to the graphene during the ball milling and sintering process, Fig. 3a. The 2D band of the A15 composite splits into two peaks and was numerically fitted by two Lorentzian line

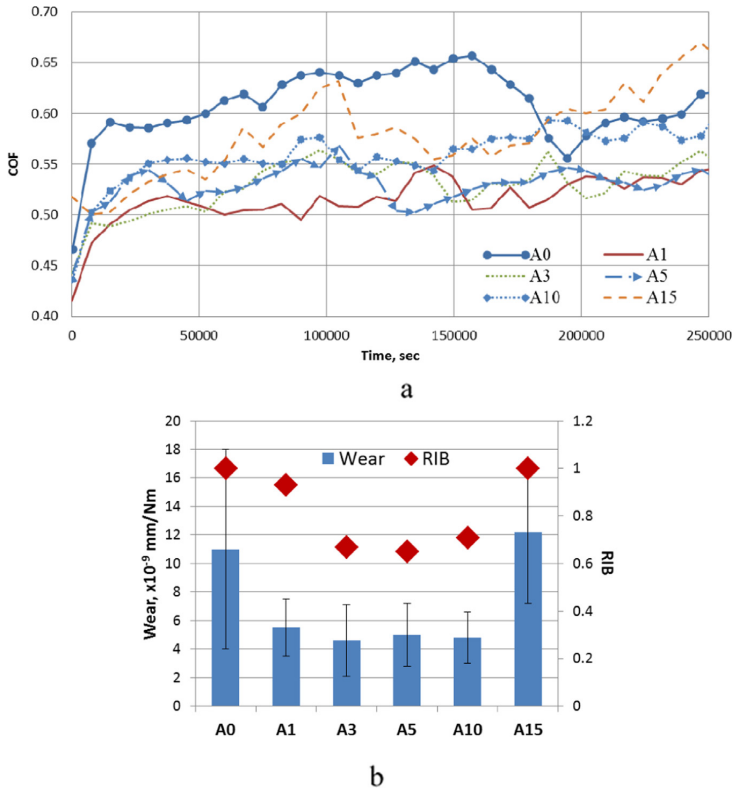

Fig. 5. (a) Coefficient of friction as a function of sliding time; and (b) wear rates (mm^3/NM) of the composites in mild environment along with RIBs.

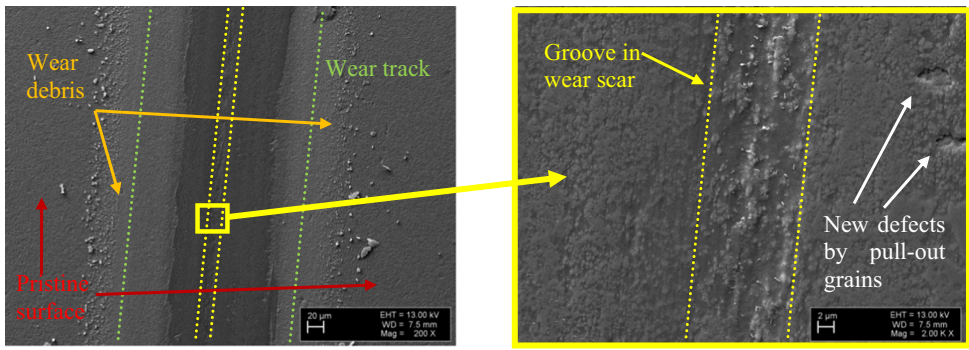

Fig. 6. SEM images of the wear track produced at the surface of Al_2O_3 – 15 wt% ANFG composite under the applied load of 0.98 N during 72 h.

shapes as shown in Fig. 3a and insert, which refers to a few-layer graphene dispersed in a matrix material [30].

The typical peaks of α-Al_2O_3 were detected in all specimens in their XRD profiles (Fig. 3b), without any detectable carbide phases, indicating no significant reactions between carbon and the alumina matrix during the process of densification.

It is worth to mention that in this work, we report on the development of ceramic-based composite reinforced with fibres covered by untreated graphene, which did not undergo any further oxidation or reduction process to improve bonding with the matrix material. Remarkably, the addition of only 3–5 wt% of graphenated fibres, which correspond to 0.3–0.5 wt% of graphene, was observed to increase the indentation fracture toughness by 62–68%, respectively. Fig. 4 shows a schematic diagram of nanoadditives used, indicating that the nanofibres encapsulated by the nanometre-thick graphene layers (ANFG) may represent both single fibre or agglomerated bundles of fibre; moreover, during milling and mixing procedure, the tiny graphene platelets may be released from the surface of the alumina nanofibres.

It is well documented that interphases can significantly affect the mechanical properties of composites [1,10,31]. In all probability, the force required to pull out a graphene sheet is expected to be somewhat higher than pulling out a nanofibre due to its large specific surface area and the wrapping/anchoring of graphene

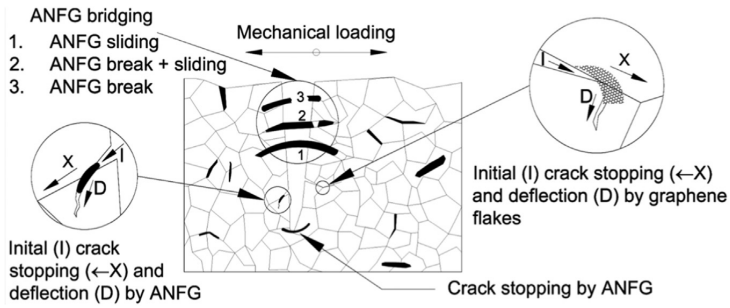

Fig. 7. Schematic diagram of toughening mechanisms for the composites.

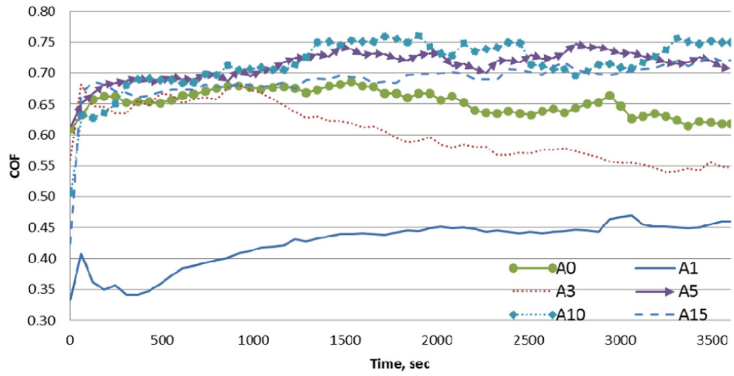

a

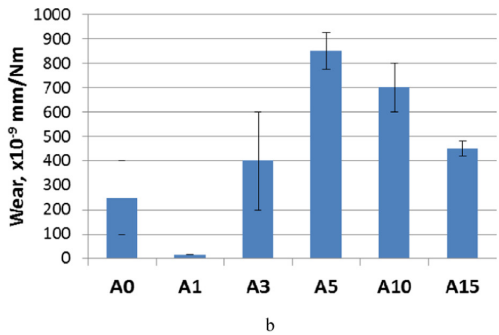

b

Fig. 8. (a) Coefficient of friction as a function of sliding time; and (b) wear rates (mm^3/NM) of the composites in severe environment.

around fibre. Therefore, the simultaneous improvement in fracture toughness and hardness is apparent at all composites with exception of A15 which lower mechanical properties are attributed to a lower degree of densification and a higher degree of fibres agglomeration combined with the weak interphases. Nevertheless, the RIB is decreased assuming the materials to be more damage tolerant as compared to the pure alumina.

3.2. Mild wear test

The evidence to date suggests that a ceramic is useful as a commercial tribological component when provides the specific wear rate less than 10^{-6} mm^3/Nm, which is the upper limit for the mild wear [26]. Fig. 5a shows the representative cumulative curves of CoF as a function of time, and Fig. 5b compares the wear rates of the composites under consideration obtained during the long duration tests (72 h) under a mild load of 0.98 N or 100 g along with indication of the RIB. Under the low applied load, the composite A1 shows the minimal CoF; the lowest value for the weight loss was observed for the composite A3 with a 60% reduction as compared to A0. The composite with 15 wt% ANFG shows as high wear rate as the pure alumina because of relatively high porosity. It should be noted that the deviation in total wear is about twofold higher for the pure alumina as compared to A15 and about sixfold higher as compared to A1.

Large fluctuations in CoF for all materials may be explained by releasing of large particles (wear debris) from the worn surface. Generally, two kinds of wear debris can be recognized at and around wear track: the smeared debris at the middle of the wear track, and the randomly distributed pulled-out particles at the

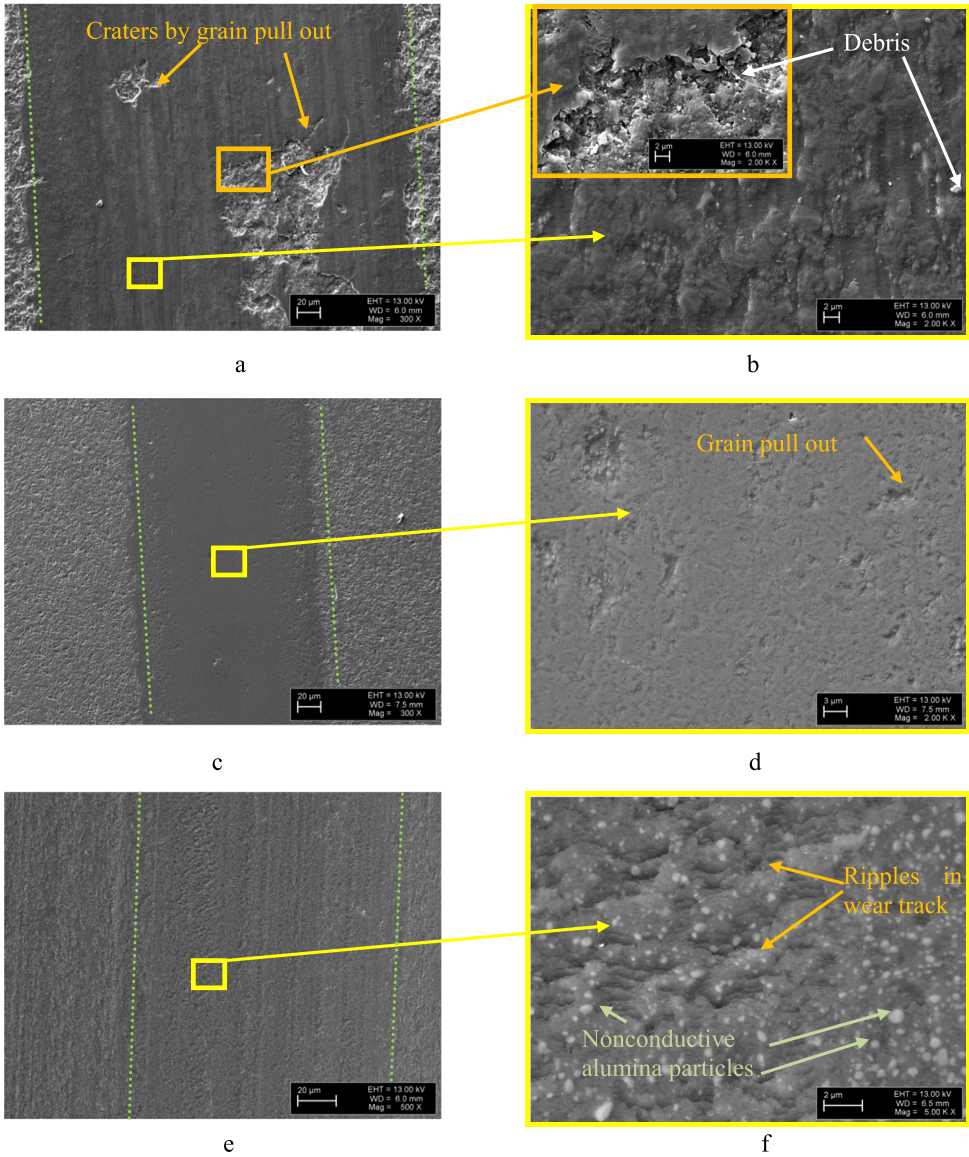

Fig. 9. SEM images of wear tracks of: (a–b) – A0; (c–d) – A1; and (e–f) – A15 composites.

edge of the track. Fig. 6 gives the representative SEM image of the wear track produced in A15.

Collation of wear rates with RIBs of composites shows the tendency of wear reduction with decrease in relative index of brittleness. In our work, the maximal toughening effect was obtained for composites with a low content of hybrid reinforcements (3–5 wt%) corresponding to only 0.3–0.5 wt% of graphene that is much lower concentration needed for toughening as compared to CNTs added alumina [10]. It should be noted that after milling double reinforcement by ANFG together with graphene nanoplatelets may serve as a mechanism of increase in fracture toughness, Fig. 4. A schematic diagram indicating toughening mechanisms of the composites added by hybrid nanofibers is giving in Fig. 7.

3.3. Severe wear test

The evolution of the CoF for severe regime of wear is shown in Fig. 8a giving the cumulative curves for each specimen. Composites with a content of ANFG from 0 and 3 wt% exhibit relative stabilization in CoF at the first 1000 s with a further tendency for decrease. Fig. 8b shows the wear rates for a short duration (1 h) tests under a severe load (4.90 N). According to the wear track profile, Fig. 9, the content of the additives plays a critical role in the tribological properties. The worn volume significantly decreased for the composite with 1 wt% ANFG, however adding 3 and a higher wt% ANFGs deteriorates the wear resistance and drastically increases the wear rate (Fig. 8b). Therefore, adding up to 1 wt% ANFG (or 0.1 wt% graphene) into the alumina matrix results in

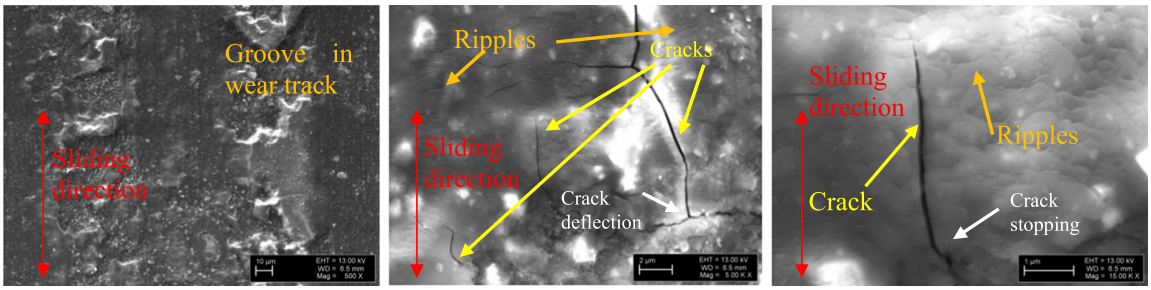

Fig. 10. SEM images of abrasive groove on the surface of A3 with 3 wt% ANFG.

significant improvement in the wear performance, resulting in over 90% reduction in the wear rate as benchmarked against the pure Al_2O_3.

For both regimes, the composite A1 shows the minimal among other materials CoF ranged from 0.45 up to 0.5. One of the main microstructural features of this material is obviously pronounced hierarchical structure combing large grains (up to 5 μm) with ultra-fine scaled ones (up to 0.7 μm) together with nano-reinforcements of several nanometres in diameter and a huge aspect ratio of 10^3.

Fig. 9 gives the SEM images of the wear track profiles for pure alumina and composites under consideration. Fig. 9a exhibits the removed fragments produced by grain pull-outs along with micro-seized wear debris on the worn surface of pure alumina. Under 4.9 N sliding load, there are no pronounced grains pull-outs for A1–A15, that may be attributed to the lower RIBs as compared with A0 and change in wear mechanism at severe sliding stresses and strains. However, the grove traces in Fig. 10 indicate a deformation controlled wear behaviour and microcracking due to weakened grain boundaries between alumina and graphene. The wear tracks for the reinforced materials are narrower and looks much smoother as compared to pure alumina. The formation of ripples, perpendicular orientated to sliding direction, on the worn surface with a density about 4–6 ripples per μm^{-1} is well recognized for all composites.

The formation of the nanometre and micrometre sized ripple patterns on the top of the material surface has been previously reported for different materials and processes [26,32,33]. The ripples are thought to be amorphous and represent a thin amorphous tribofilm developed on the surface of many ceramics [26].

However, addition of a higher amount of ANFG ($\geq$ 3 wt%) led to micro- and nano-chipping as well as development of intergranular cracks. Although adding of graphene platelets is believed to reduce residual stresses in bulk alumina [14,34] and, therefore, reduce the probability of grains/chips pull-out, this concept is well working only for the mild wear, whilst relatively weak interfaces between alumina and graphene result in intensive cracking under a high load. The high density of interfaces prevents dislocations motion and provides cracks deflection, therefore, ensure materials with a high strength and a high fracture toughness of, nevertheless, quite low relative index of brittleness, Table 1, that may serve as an indicator for assessment the mild wear of ceramics reinforced by graphenated nanostructures.

However, under sever wear conditions these mechanisms are not as effective as under a low loading. Frictional pull-out of fibres occurred in classical composites may not be the only toughening mechanism in hybrid fibres reinforced ceramics. The role of interfaces is clearly realized, however, the exact mechanism of graphene interaction with oxide matrix is not yet well understood. Physically, an interface is a complex transitional area between a reinforcement and a matrix. It is known that carbon nanotubes (CNT) do not create a strong bond to ceramic, and their interactions are due to van der Waals forces, which is much weaker than covalent bonds. This leads to sliding of CNTs in the ceramic-matrix when subjected to loading. In [35] a micromechanics model is provided to predict the interfacial behaviour of multiwall carbon nanotubes and the crystal lattice structure of α-alumina. The result shows that there is a maximum value (0.68 GPa) of tensile stress under the biggest strain (0.686%) that the matrix can afford; the ultimate stress afforded by van der Waals interaction is achieved when the strain rate is 0.0091%, and the interfacial slip begins to occur. Taken into consideration that graphene encapsulated alumina nanofibre may represent multiwall CNT with alumina core, this values could give a limiting conditions when composite material still can ensure significant improvements in wear resistance. Control of interface chemistry and tailoring smart microstructures are essential steps for producing exceptionally tough, strong and wear resistant composites [36].

The presence or absence of the specific graphene nanolayer on the worn surface of the composite is neither confirmed nor disregarded in this work.

4. Conclusions

Reinforcement with hybrid graphene encapsulated alumina nanofibres (ANFG) results in simultaneous improvement in indentation fracture toughness and hardness of all composites with exception of composite with 15 wt% ANFG, which lower mechanical properties are attributed to a lower degree of densification. The relative index of brittleness (RIB) is decreased for all composites assuming the materials to be more damage tolerant as compared to pure alumina.

The sliding wear performance of the hierarchically structured alumina reinforced by hybrid nanofibres was studied using ball-on-plate technique. The composites added by 1–10 wt% of ANFGs, corresponding to 0.1–1.0 wt% of graphene, exhibited significant increase of 50–60% in wear resistance under the mild wear conditions (load 0.98 N); whilst the coefficient of friction remained almost unchanged showing a high degree of fluctuations.

Under sever wear conditions (load 4.9 N), only the composite added by 1 wt% ANFG showed the remarkable improvement in wear resistance of 90% together with a well recognizable reduction in CoF as benchmarked against the pure alumina. For the composites with a content of ANFG from 3 to 10 wt%, the formation of ripples with a density about 4 to 6 ripples per μm^{-1} and micrometre sized cracks in the wear track are the main mechanisms responsible for wear behaviour.

The RIB can serve as a useful tool for assessment of wear performance of composites while only operating under mild environment.

These recently developed materials, possessing relatively high fracture toughness combined with high hardness while still quite low relative index of brittleness, showed the promising wear performance to be adapted as a wear resistant materials for many different applications where enhanced wear resistance is required.

Acknowledgements

This work was supported by research grant PUT1063 (to I. Hussainova) of the Estonian Research Council, TallinnUniversity of Technology young researcher basic financing B56 (Maksim Antonov), as well as institutional research funding IUT19–29 of the Estonian Ministry of Education and Research. The authors would like to thank PhD M. Viljus for the help with SEM imaging.

References

[1] H. Porwal, S. Grasso, M.J. Reece, Review of graphene–ceramic matrix composites, Adv. Appl. Ceram. 112 (2013) 443–454, http://dx.doi.org/10.1179/174367613X13764308970581.

[2] S. Grasso, H. Yoshida, H. Porwal, Y. Sakka, M. Reece, Highly transparent α-alumina obtained by low cost high pressure SPS, Ceram. Int. 39 (2013) 3243–3248, http://dx.doi.org/10.1016/j.ceramint.2012.10.012.

[3] H. Belghalem, M. Hamidouche, L. Gremillard, G. Bonnefont, G. Fantozzi, Thermal shock resistance of two micro-structured alumina obtained by natural sintering and SPS, Ceram. Int. 40 (2014) 619–627, http://dx.doi.org/10.1016/j.ceramint.2013.06.045.

[4] J. Liu, H. Yan, K. Jiang, Mechanical properties of graphene platelet-reinforced alumina ceramic composites, Ceram. Int. 39 (2013) 6215–6221, http://dx.doi.org/10.1016/j.ceramint.2013.01.041.

[5] M. Drozdova, I. Hussainova, D. Pérez-Coll, M. Aghayan, R. Ivanov, M. A. Rodríguez, A novel approach to electroconductive ceramics filled by graphene covered nanofibers, Mater. Des. 90 (2016) 291–298, http://dx.doi.org/10.1016/j.matdes.2015.10.148.

[6] H. Porwal, P. Tatarko, S. Grasso, J. Khaliq, I. Dlouhý, M.J. Reece, Graphene reinforced alumina nano-composites, Carbon N Y 64 (2013) 359–369, http://dx.doi.org/10.1016/j.carbon.2013.07.086.

[7] M. Berdova, A. Pyymaki Perros, W. Kim, J. Riikonen, T. Ylitalo, J. Heino, et al., Corrigendum: exceptionally strong and robust millimeterscale graphene–alumina composite (2014 Nanotechnology 25 355701), Nanotechnology 25 (2014) 439501, http://dx.doi.org/10.1088/0957-4484/25/43/439501.

[8] L. Gong, I.A. Kinloch, R.J. Young, I. Riaz, R. Jalil, K.S. Novoselov, Interfacial stress transfer in a graphene monolayer nanocomposite, Adv. Mater. 22 (2010) 2694–2697, http://dx.doi.org/10.1002/adma.200904264.

[9] M. Drozdova, D. Pérez-Coll, M. Aghayan, R. Ivanov, M.A. Rodríguez, I. Hussainova, Hybrid graphene/alumina nanofibers for electrodonductive zirconia, Key Eng. Mater. 674 (2016) 15–20, http://dx.doi.org/10.4028/www.scientific.net/KEM.674.15.

[10] H.J. Kim, S.-M. Lee, Y.-S. Oh, Y.-H. Yang, Y.S. Lim, D.H. Yoon, et al., Unoxidized graphene/alumina nanocomposite: fracture- and wear-resistance effects of graphene on alumina matrix, Sci. Rep. 4 (2014) 5176, http://dx.doi.org/10.1038/srep05176.

[11] B. Yazdani, F. Xu, I. Ahmad, X. Hou, Y. Xia, Y. Zhu, Tribological performance of Graphene/Carbon nanotube hybrid reinforced Al2O3 composites, Sci. Rep. 5 (2015) 11579, http://dx.doi.org/10.1038/srep11579.

[12] W. Kim, H.-S. Oh, I.-J. Shon, The effect of graphene reinforcement on the mechanical properties of Al2O3 ceramics rapidly sintered by high-frequency induction heating, Int. J. Refract. Met. Hard Mater. 48 (2015) 376–381, http://dx.doi.org/10.1016/j.ijrmhm.2014.10.011.

[13] F. Inam, H. Yan, D.D. Jayaseelan, T. Peijs, M.J. Reece, Electrically conductive alumina–carbon nanocomposites prepared by Spark Plasma Sintering, J. Eur. Ceram. Soc. 30 (2010) 153–157, http://dx.doi.org/10.1016/j.jeurceramsoc.2009.05.045.

[14] C.F. Gutierrez-Gonzalez, A. Smirnov, A. Centeno, A. Fernández, B. Alonso, V. G. Rocha, et al., Wear behavior of graphene/alumina composite, Ceram. Int. 41 (2015) 7434–7438, http://dx.doi.org/10.1016/j.ceramint.2015.02.061.

[15] H. Porwal, P. Tatarko, R. Saggar, S. Grasso, M. Kumar Mani, I. Dlouhý, et al., Tribological properties of silica–graphene nano-platelet composites, Ceram. Int. 40 (2014) 12067–12074, http://dx.doi.org/10.1016/j.ceramint.2014.04.046.

[16] L.S. Walker, V.R. Marotto, M.A. Rafiee, N. Koratkar, E.L. Corral, Toughening in graphene ceramic composites, ACS Nano 5 (2011) 3182–3190, http://dx.doi.org/10.1021/nn200319d.

[17] Y.-F. Chen, J.-Q. Bi, C.-L. Yin, G.-L. You, Microstructure and fracture toughness of graphene nanosheets/alumina composites, Ceram. Int. 40 (2014) 13883–13889, http://dx.doi.org/10.1016/j.ceramint.2014.05.107.

[18] M. Aghayan, I. Hussainova, M. Gasik, M. Kutuzov, M. Friman, Coupled thermal analysis of novel alumina nanofibers with ultrahigh aspect ratio, Thermochim. Acta 574 (2013) 140–144, http://dx.doi.org/10.1016/j.tca.2013.10.010.

[19] R. Ivanov, I. Hussainova, M. Aghayan, M. Drozdova, D. Pérez-Coll, M. A. Rodríguez, et al., Graphene-encapsulated aluminium oxide nanofibers as a novel type of nanofillers for electroconductive ceramics, J. Eur. Ceram. Soc. 35 (2015) 4017–4021, http://dx.doi.org/10.1016/j.jeurceramsoc.2015.06.011.

[20] R. Ivanov, V. Mikli, J. Kübarsepp, I. Hussainova, Direct CVD growth of multilayered graphene closed shells around alumina nanofibers, Key Eng. Mater. 674 (2016) 77–80, http://dx.doi.org/10.4028/www.scientific.net/KEM.674.77.

[21] B.R. Lawn, D.B. Marshall, Hardness, toughness, and brittleness: an indentation analysis, J. Am. Ceram. Soc. 62 (1979) 347–350, http://dx.doi.org/10.1111/j.1151-2916.1979.tb19075.x.

[22] M. Antonov, J. Pirso, A. Vallikivi, D. Goljandin, I. Hussainova, The effect of fine erodent retained on the surface during erosion of metals, ceramics, plastic, rubber and hardmetal, Wear 354–355 (2016) 53–68, http://dx.doi.org/10.1016/j.wear.2016.02.018.

[23] M. Antonov, I. Hussainova, E. Adoberg, Effect of loading system inertia on tribological behaviour of ceramic–ceramic, ceramic–metal and metal–metal dry sliding contacts, Tribol. Int. 65 (2013) 207–214, http://dx.doi.org/10.1016/j.triboint.2013.03.025.

[24] P.J. Blau, Running-in: art or engineering? J. Mater. Eng. 13 (1991) 47–53, http://dx.doi.org/10.1007/BF02834123.

[25] P.J. Blau, How common is the steady-state? The implications of wear transitions for materials selection and design, Wear (2014), http://dx.doi.org/10.1016/j.wear.2014.11.018.

[26] W.M. Rainforth, The wear behaviour of oxide ceramics – a review, J Mater. Sci. 39 (2004) 6705–6721, http://dx.doi.org/10.1023/B:JMSC.0000045601.49480.79.

[27] I. Hussainova, I. Jasiuk, M. Sardela, M. Antonov, Micromechanical properties and erosive wear performance of chromium carbide based cermets, Wear 267 (2009) 152–159, http://dx.doi.org/10.1016/j.wear.2008.12.104.

[28] A.R. Boccaccini, The relationship between wear behaviour and brittleness index in engineering ceramics and dispersion-reinforced ceramic composites, InterCeram Int Ceram. Rev. 48 (1999) 176–187.

[29] K. Kato, K. Adachi, Wear of advanced ceramics, Wear 253 (2002) 1097–1104, http://dx.doi.org/10.1016/S0043-1648(02)00240-5.

[30] A.C. Ferrari, J.C. Meyer, V. Scardaci, C. Casiraghi, M. Lazzeri, F. Mauri, et al., Raman spectrum of graphene and graphene layers, Phys. Rev. Lett. 97 (2006) 187401, http://dx.doi.org/10.1103/PhysRevLett.97.187401.

[31] I. Hussainova, A. Kolesnikova, M. Hussainov, A. Romanov, Effect of thermo-elastic residual stresses on erosive performance of cermets with core–rim structured ceramic grains, Wear 267 (2009) 177–185, http://dx.doi.org/10.1016/j.wear.2009.01.019.

[32] A. Socoliuc, E. Gnecco, R. Bennewitz, E. Meyer, Ripple formation induced in localized abrasion, Phys. Rev. B 68 (2003) 115416, http://dx.doi.org/10.1103/PhysRevB.68.115416.

[33] R.J.K. Wood, T.F. Jones, Investigations of sand–water induced erosive wear of AISI 304L stainless steel pipes by pilot-scale and laboratory-scale testing, Wear 255 (2003) 206–218, http://dx.doi.org/10.1016/S0043-1648(03)00095-4.

[34] K.V. Zakharchenko, J.H. Los, M.I. Katsnelson, A. Fasolino, Atomistic simulations of structural and thermodynamic properties of bilayer graphene, Phys. Rev. B 81 (2010) 235439, http://dx.doi.org/10.1103/PhysRevB.81.235439.

[35] T. Yan, G. Wei, Multiscale analysis of the interfacial mechanical behavior for composite of carbon nanotube and α -alumina, Adv. Mater. Sci. Eng. 2014 (2014) 1–7, http://dx.doi.org/10.1155/2014/237097.

[36] I. Hussainova, Microstructural design of ceramic–metal composites for tribological applications, Key Eng. Mater. 334–335 (2007) 125–128, http://dx.doi.org/10.4028/www.scientific.net/KEM.334-335.125.

Paper III. Hussainova, I., **Drozdova, M.**, Pérez-Coll, D., Rubio-Marcos, F., Jasiuk, I., Soares, J.A.N.T., Rodríguez, M.A., Electroconductive composite of zirconia and hybrid graphene/alumina nanofibers. – *Journal of the European Ceramic Society*, 2017, 37 (12), 3713–3719. DOI:10.1016/j.jeurceramsoc.2016.12.033.

Journal of the European Ceramic Society 37 (2017) 3713–3719

Contents lists available at www.sciencedirect.com

Journal of the European Ceramic Society

journal homepage: www.elsevier.com/locate/jeurceramsoc

Electroconductive composite of zirconia and hybrid graphene/alumina nanofibers

Irina Hussainova[a,c,d,*], Maria Drozdova[a], Domingo Pérez-Coll[b], Fernando Rubio-Marcos[b], Iwona Jasiuk[d], Julio A.N.T. Soares[e], Miguel A. Rodríguez[b]

[a] Tallinn University of Technology, Ehitajate tee 5, 19180 Tallinn, Estonia
[b] Instituto de Cerámica y Vidrio (CSIC), Campus Cantoblanco, 28049 Madrid, Spain
[c] ITMO University, Kronverksky 49, St. Petersburg, 197101, Russian Federation
[d] University of Illinois at Urbana-Champaign, 1206 Green St., Urbana, IL, 61801, USA
[e] Frederick Seitz Materials Research Laboratory, University of Illinois, 104 S Goodwin Ave., Urbana, IL 61801, USA

ARTICLE INFO

Article history:
Received 28 September 2016
Received in revised form
16 December 2016
Accepted 20 December 2016
Available online 26 December 2016

Keywords:
Zirconia
SPS
Nanofiber
Graphene
Electroconductivity

ABSTRACT

Novel type of hybrid nanofillers representing graphene encapsulated alumina nanofibres was selected as an additive to develop toughened electroconductive partially stabilized zirconia. The sinterability, mechanical and electrical properties of the produced nanocomposites were studied as function of the filler/graphene content. Composites containing just 0.6 vol.% of graphene corresponding to 3 vol.% of hybrid nanofibres exhibited high electroconductivity of 58 S/m without deterioration of mechanical properties. They also showed a slight toughening effect that is reflected by an increase in the indentation fracture toughness by 20% as compared to monolithic zirconia.

1. Introduction

Zirconium oxide (ZrO_2) or zirconia has been a widely used material in different industrial branches starting with solid oxide fuel cells, oxygen sensors, ceramic membranes and ending with structural and biomedical applications. However, despite many advantageous properties such as chemical inertness and biocompatibility, several issues still exist related to relatively low fracture toughness and abrasive wear resistance as well as difficulties in production of complex shapes which are necessary for high technology applications. To overcome these drawbacks, different approaches have recently been employed for enhancing the fracture toughness together with obtaining an electrically conductive material for its possible treatment using electrical discharge machining (EDM) [1]. One of the widely-accepted approaches is an incorporation of conductive fibres into a ceramic matrix [2,3]. Such kind of nanofillers deflect and/or bridge cracks, arresting them or at least limiting their fast propagation throughout a brittle matrix giving an additive value of electrical conductivity.

Over the last several years the nanosized allotropes of carbon, such as nanotubes (CNT) and graphene platelets (GNPs), have attracted a great attention as efficient reinforcement fillers for both oxide and non-oxide ceramics due to their good mechanical and electrical properties [4–7]. For example, the incorporation of either CNTs or GNPs into alumina (Al_2O_3) matrix composites has been shown to significantly enhance electrical conductivity up to extremely high value of 10,000 S m^{-1} [8], as well as to improve fracture toughness and flexural strength [3,4,9]. Lee et al. [10] reported an increase in K_{IC} values up to 10.5 MPa $m^{1/2}$ when 2 vol.% of reduced graphene oxide (rGOs) was added, which corresponds to an increment of ~150% as compared to monolithic ceramics. For zirconia, much less and somewhat contradictory results are reported. Shin et al. [11] achieved an increase in the fracture toughness of yttria stabilized zirconia (YSZ) ceramics by ~34% along with an improvement in electrical conductivity reaching 1.2×10^4 S/m when 4 vol.% of rGOs was added. The fracture toughness of 15.3 MPa $m^{1/2}$, as tested by a single-edge notched beam method, which reflects an increase of 61% as compared to GNPs-free yttria stabilized zirconia, is reported in [12].

* Corresponding author at: Tallinn University of Technology, Ehitajate tee 5, 19180 Tallinn, Estonia.
E-mail address: irina.hussainova@ttu.ee (I. Hussainova).

http://dx.doi.org/10.1016/j.jeurceramsoc.2016.12.033
0955-2219/

However, graphene or CNT content needed to get a substantial increase in electrical conductivity is comparatively high, which may result in considerable loss in mechanical and wear properties of the composite [2,8,13,14]. Moreover, when a powder metallurgy (PM) route is used for fabrication of a carbon/ceramic composite, the resulting material often exhibits lower than expected mechanical properties because of severe agglomeration of carbon nanostructures.

In the present study, the novel type of hybrid nanofillers representing alumina nanofibers of several nanometres in diameter encapsulated with multi-layered graphene shells and utilizing the advantages of reinforcement by fibres and high conductivity of graphene is added to the matrix of partially stabilized zirconia (PSZ). While the majority of the works on the ceramic–graphene composites apply a top–down approach to graphene production, such as exfoliating graphite/graphite oxide with high energy milling or colloidal processing of graphene or rGO, in this work a bottom-up method of hot-walled chemical vapour deposition (CVD) has been used for production of the conductive nanoreinforcements. The aim of this work is to sinter electrically conductive zirconia added by alumina/graphene hybrid fillers along with improving the mechanical properties provided by the monolithic zirconia. Benchmarked against the monolithic PSZ, the composites added with 1, 3 and 5 vol.% of graphene augmented alumina nanofibers have been consolidated by spark plasma sintering (SPS) technique to elucidate the influence of fillers onto microstructure, mechanical and electrical properties of the composites.

2. Materials and methods

2.1. Materials

Commercially available 3 mol% yttria partially stabilized zirconia powder (TZ-3Y-E, TOSOH, Japan; PSZ particles of ~40 nm) was used as a matrix material. The bundled network of graphene augmented alumina nanofibers, produced by controlled liquid phase oxidation, was deposited by carbon with the help of CVD method as described in detail elsewhere [15,16]. The fibres of 50 mm in length and average single fibre diameter of 7 ± 2 nm were encapsulated by several layers of graphene and used as the reinforcing fillers for production of electrically conductive fillers.

2.2. Processing

Details on the preparation of the nanocomposite powder mixtures to be consolidated can be found in the authors' previous work [3]. Briefly, the bundled fibres were grounded in a mortar and ultrasonicated in ethanol for 1 h to relieve agglomeration followed by ball milling with zirconia balls (3 mm diameter) for another hour. The ball milling provides sufficient shear forces needed for successful de-agglomeration that cannot be achieved with ultra-sonication alone. Subsequently the zirconia powder was gradually introduced into the suspension until achieving the desired composition and further milled for 1 h. The obtained powder mixture was dried at 65 °C for 24 h then sieved by 100 μm sieve. Compositions containing 1 vol% (Z1), 3 vol% (Z3), and 5 vol% (Z5) of hybrid fibres were produced for further densification.

The zirconia and nanocomposite powders were packed into 30 mm graphite dies and consolidated using a Dr. Sinter SPS-510 CE (Fuji Electronic Industrial Co., Kawasaki, Japan) spark plasma sintering furnace. A set of tests was performed to investigate the optimal sintering conditions taking into consideration the relative density of the sintered composites.

The optimal conditions of pressure of 40 MPa, dwell temperature of 1250 °C, and dwell time of 5 min were applied for sample processing that was conducted in N_2 atmosphere. For reference, a fully dense (>99%) monolithic PSZ specimen was prepared following the same sintering conditions.

2.3. Characterization

A JEOL 2100F transmission electron microscope (TEM/HRTEM) operating at 200 KV and equipped with a field emission electron gun providing a point resolution of 0.19 nm was used to examine the nanofillers and analyse the precursor powders.

A microscope coupled with an INCA x-sight energy dispersive X-ray spectrometer (EDXS), from Oxford Instruments, was used for chemical elemental analysis. A high resolution field emission scanning electron microscopy (Zeiss HR FESEM Ultra 55) equipped with a Bruker EDS system ESPRIT 1.8 was used to observe microstructures and analyse surfaces of the fractured composites.

Differential thermal and thermo-gravimetric analyses (DTA/TG) were carried out in order to determine the amount of graphene in the sintered samples. The thermal analyses were performed on a Netzsch STA 449 F3 Jupiter Simultaneous Thermal Analyzer (TG–DSC/DTA Apparatus) coupled with a Netzsch QMS 403D Aeolos (mass 1–300 amu). The samples were analysed in Pt/Rh crucibles with a lid and a removable liner composed of thin-walled Al_2O_3. Identification of phases in the sintered samples was carried out by X-ray diffraction using a Bruker diffractometer (D8) with CuKα radiation.

A Raman spectroscopy with a Horiba Jobin Yvon LabRAM 300 spectrometer equipped with a 633 nm laser wavelength excitation was used to determine the degree of structural perfection of sp2 carbon and the presence of the graphene in the sintered product.

The density of the sintered compacts was assessed using the Archimedes method using a distilled water as an immersion media. Relative densities were calculated by the rule of mixtures using the manufacturer's density specification for zirconia powder (6.05 g cm^{-3}), alumina fibres (3.96 g cm^{-3}) and the published density value for graphene (2.2 g cm^{-3}) and the target fillers volume percentage.

To study the effect of fillers on mechanical properties, the Vickers hardness and indentation fracture toughness (IFT) of the composites were determined with the help of the indentation method using Vickers tester Indentec 5030 SKV. The indentation toughness approach was chosen as the easiest and effective way to make ranking of materials. The sintered samples were initially mounted and ground using a 600 grit size SiC abrasive paper and then polished using progressively finer diamond slurries, with the final polishing step utilizing a slurry with 50 nm diamond particles. The indentation was performed on the polished surfaces with a standard Vickers tip and the load of 49 N with a 10 s hold. The load on the indenter resulted in well-developed cracks that mitigate any surface effects of the indentation. The indents generated were observed under an optical microscope. The IFT was determined by the measurement of the crack lengths produced by the indent following the procedure proposed by Niihara [17] for the Palmqvist cracks. The diagonals and indentation induced crack lengths were measured by an optical microscope Zeiss Axiovert 25 equipped with a camera Canon EOS 350D. Data reported from indentation procedures were taken from an average of at least 10 indents. All error bars correspond to one standard deviation. It should be noted that the single-edge V-notch beam (SEVNB) route provides more reliable values of the fracture toughness as compared to the indentation fracture toughness, which often gives the overestimated values. However, difficulties with the preparation of the specimen of required geometry limit SEVNB method adaptability.

The room temperature electrical conductivity was measured on prismatic bars (25 × 6 x 5 mm) machined from the original sintered disk using the 4-probe DC method with a potentiostat/galvanostat

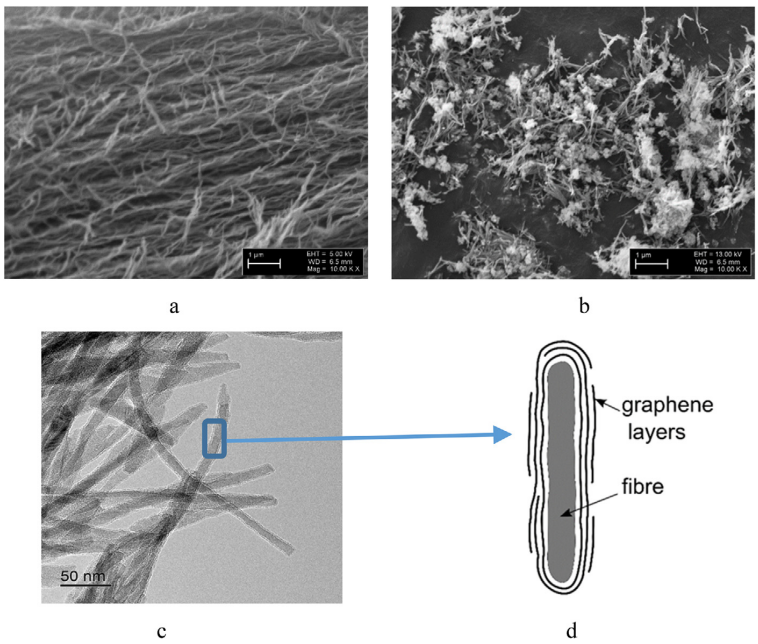

Fig. 1. SEM micrograph of the nanofibers network (a); SEM image of the mixture of zirconia nanoparticles and fibres (b); TEM image of alumina nanofibers after CVD treatment (c); and schematic representation of the single nanofiller.

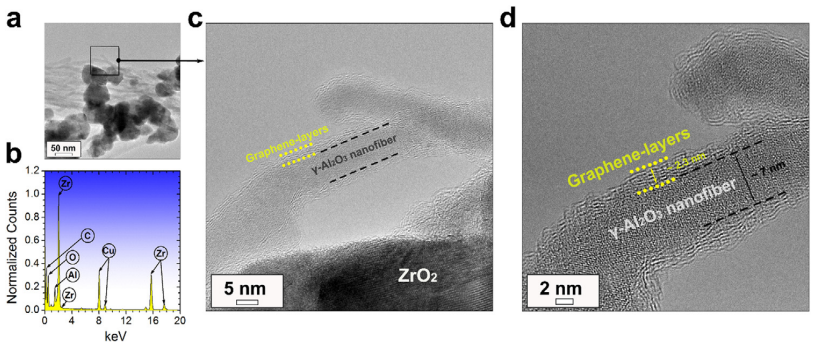

Fig. 2. HRTEM images of the processed PSZ-hybrid nanofibres green powder: the general micrograph of the powder (a); EDX spectra corresponding to the area shown in C (b); HRTEM image of the area specified in A at a higher magnification (c); HRTEM image of the single fibre in the mixture.

(Autolab PGSTAT 302N). Four platinum wires were attached to the specimen with silver paste (Electrolube ERSCP03B) and connected to the terminals of the potentiostat/galvanostat. The external electrodes were used to allow the electrical current to flow through the volume of the sample, whereas the inner electrodes were used to read the voltage difference associated to the volumetric resistance. The electrical resistance was calculated from the linear fit of the current – voltage data points obtained from the galvanostatic tests in the range 1–10 mA with a step of 1 mA.

3. Results and discussion

3.1. Microstructural characterization

The network of pristine γ-Al_2O_3 nanofibers, as described in [18], and SEM image of the zirconia – graphenated nanofibres mixture are shown in Fig. 1. The SEM image of the green mixture evidences a homogeneous distribution of the fibres within the mixture. Fig. 2 demonstrates HR-TEM images of the final powder confirming that ultrasound processing and/or attrition milling did not cause significant damage of the graphene. Unaffected 2–3 nm thick graphene layers can be well distinguished in Fig. 2c–d.

Fig. 3 shows the dilatometry of pure zirconia powder undergoing sintering. Shrinkage begins at 900 °C and ends at about 1400 °C. The total contraction of the sample is 27%. A relative maximum in the shrinkage rate curve corresponding to 1150 °C reflects the transformation of the remaining monoclinic phase of zirconia into tetragonal polymorph. The minimum of shrinkage derivative in the dilatometry curve corresponds to the temperature of the highest rate of densification reached at approximately 1250 °C and this temperature was chosen for the SPS processing.

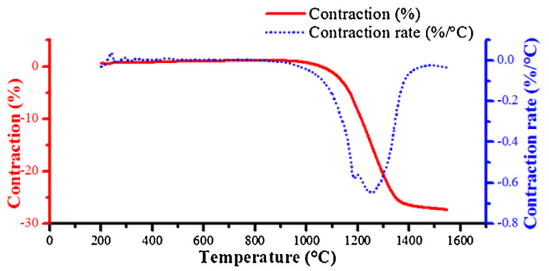

Fig. 3. Dilatometry of zirconia powder.

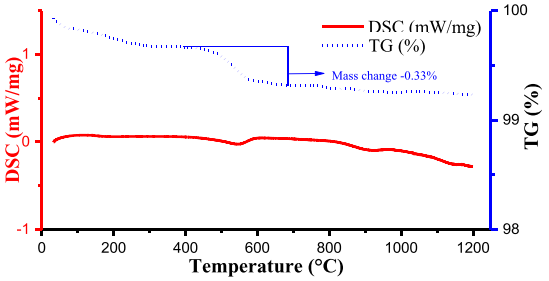

Fig. 4. DSC/TG curve for Z5.

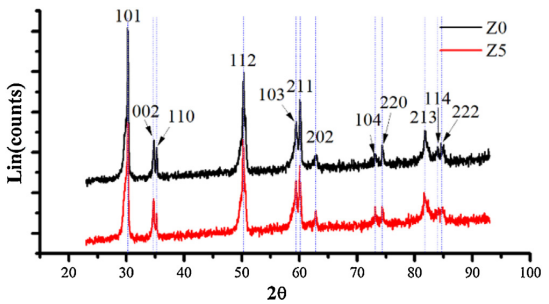

Fig. 5. XRD patterns of pure zirconia (Z0) and ZrO_2–5 vol.%hybrid nanofibres (Z5) composite.

To estimate the graphene amount in the sintered composites, DTA/TG analysis of the samples crushed into powders was performed. The TG curve of pure zirconia shows no mass change during heating up to 1200 °C. On the contrary, the TG curve of the composite with 5 vol.% fillers (Z5), depicted in Fig. 4, indicates a major mass loss in the temperature interval between 420 °C and 620 °C. The temperature interval is in a good agreement with the oxidation temperatures of multi-walled carbon nanotubes in air [19]. The mass loss for the composites Z5 and Z3 was calculated to be 0.33% and 0.20%, respectively, while for the material with the lowest content of graphenated hybrid nanofibres, Z1, the results obtained were in the range of an experimental error (0.02%).

The XRD pattern, presented in Fig. 5, depicts only ZrO_2 and Al_2O_3 phases and reveals no detectable third phase indicating that there has not been any significant reaction between graphene and zirconia or alumina.

Raman spectroscopy was used to confirm the structural integrity of the graphene in the zirconia matrix after sintering. The I_D/I_G ratio for the raw graphenated fibres is around 1.8.

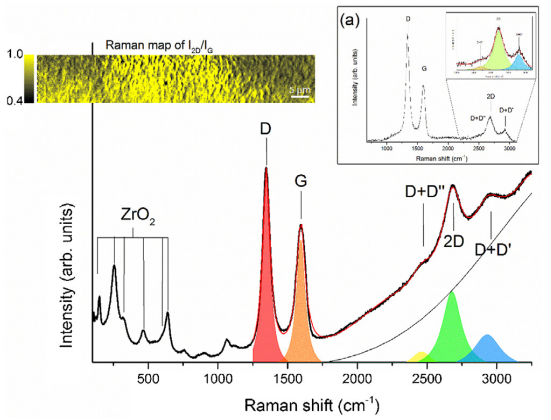

Fig. 6. Raman spectra of 5 vol.% ANFC added YSZ ceramics (Z5); insert – the RAMAN spectrum of nanofibres covered by graphene (a); and RAMAN map of I_{2D}/I_G ratio.

The Raman spectrum of the Z5 composite, Fig. 6, indicates strong peaks at 641, 465, 260 and 147 cm^{-1} with additional weaker feature at 606 cm^{-1}. These peaks are characteristic of tetragonal zirconia polycrystalline structures [20]. At higher shifts of Raman spectrum, three very strong peaks at around 1350 cm^{-1}, 1600 cm^{-1}, 2690 cm^{-1}, a strong peak at 2930 cm^{-1} along with a weak peak at 2480 cm^{-1} were detected. The Raman vibrational modes observed at 1350 cm^{-1} linked to the carbon lattice disorder, as well as the mode at 1597 cm^{-1}, associated with the sp^2 hybridization, represent the main features in the spectra of sp^2 carbon structures and correspond to the defect-derived D band and the structure-derived G band, respectively, identified in Fig. 6. In all probability, the graphene layers mostly remain undamaged after the SPS processing as the peak intensity ratio for the D band and the G band (I_D/I_G) is kept at the same level being of around 1.5. The presence of a few-layered graphene within the sintered bulks is confirmed by the Raman map showing the intensity ratio I_{2D}/I_G, insert in Fig. 6.

Fractured surfaces of the sintered composites were examined by FE-SEM as shown in Fig. 7. It can be noted that homogenous nearly pore-free zirconia microstructures with narrow grain size distribution were developed during sintering. PSZ grains show mixed intergranular and transgranular fracture modes. Fibres are evenly distributed throughout the composite matrix in the vicinity of grain boundaries (pointed out with arrows). However, an incorporation of nano-additives into the partially stabilized zirconia matrix up to 5 vol.% does not result in a noticeable change in grain size and/or morphology. Likewise, only insignificant decrease in the grain size was reported for reduced graphene oxide reinforced zirconia composites [11] in contrast to a widely reported grain growth inhibition by different types of graphenated structures when added to alumina [3,22] or silicon nitride matrix [7,23].

3.2. Mechanical properties

Table 1 collects mechanical properties and density of the materials tested at room temperature. The presence of hybrid fillers insignificantly reduces the composites sinterability, as relative densities above 98% are commonly achieved. The Vickers hardness and indentation fracture toughness of composites are presented in Table 1 as a function of fillers and graphene content. It is notable that changes in mechanical properties do not exceed ~7% as compared to the benchmark monolithic partially stabilized zirconia. The hardness of all composites shows a very slight gradual decrease with increase in graphene content. The hardness usu-

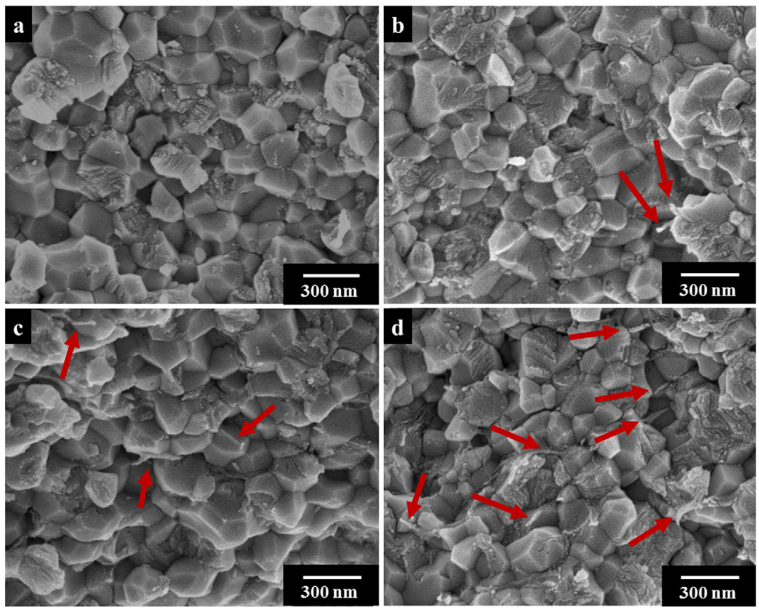

Fig. 7. FE-SEM images of the fractured surface of the sintered materials Z0 (a), Z1 (b), Z3 (c), and Z5 (d).

Table 1
Mechanical properties of the monolithic zirconia and composites added by the graphenated nanofibres.

Sample ID	Fillers, vol.%	Graphene, vol.%	Density	Theoretical Density, g cm^{-3}	Relative density, %	Hardness, GPa	ITF, MPa m$^{0.5}$
Z0	0	0	5.99	6.05	99	14.0 ± 0.3	5.73 ± 0.1
Z1	1	~0.2	5.90	6.03	>98	13.86 ± 0.3	6.25 ± 0.1
Z3	3	~0.6	5.85	5.98	>98	13.75 ± 0.2	6.91 ± 0.2
Z5	5	~1.0	5.82	5.94	~98	13.4 ± 0.4	5.77 ± 0.3

ally increases with substantial decrease in a grain size, which is not a case for zirconia-matrix composites. Similar behaviour was recorded for zirconia composites added by CNTs, graphene nanoplatelets or reduced graphene oxide [11,21,24,25] and commonly was attributed to an increased residual porosity in the materials with a relatively high carbon content. The measured indentation fracture toughness of the plain zirconia is rather low due to nano-sized grains. Modulus of elasticity (E) needed for calculation of the IFT was previously measured for a pure PSZ produced under the same conditions by the impulse excitation technique (IET) according to ASTM-E1876. Assuming insignificant effect of alumina nanofibers and porosity onto the modulus of elasticity of zirconia matrix composite, due to a low load of fillers and a low level of porosity, the obtained value of 210 GPa was used to determine toughness of all materials. An addition of graphenated nanofillers results in only modest toughness enhancement mostly within an experimental error. It worth mentioning that indentation is an indirect toughness-testing technique in shear mode, and a single edge V-notched beam (SEVNB) fracture toughness results may demonstrate a significant difference. Despite of this, IFT allows ranking materials tested at similar conditions. Several toughening mechanisms, such as pull out, bridging and crack deflection, were observed in the materials added by the graphenated nanofibres.

Fig. 8 shows the SEM micrographs of the indentation-induced cracks on the surface of monolithic, and the graphenated fibres added zirconia-based composites. The plain material exhibits a typical nearly smooth crack propagation (Fig. 8a), while the cracks initiated on the surface of the composites demonstrate bridging and pulled-out fibres along with crack deflections as shown in Fig. 8b–c.

3.3. Electrical conductivity

The electrical conductivity of the composites as a function of graphene load is depicted in Fig. 9. Pure zirconia has a dielectric constant ~30 and its conductivity is far below 10^{-10} S/m. Similarly, the addition of 1 vol.% of graphenated fillers or 0.07 wt.% graphene does not result in any detectable electro-conductivity. However, the remarkable enhancement in conductivity of nearly 11 orders of magnitude was measured for the composite with 3 vol.% fillers indicating a percolation threshold for intermediate nanofillers fraction. Therefore, the percolation for the PSZ-based composites with graphene encapsulated nanofibers is around or lower than 3 vol.% corresponding to 0.59 vol.% graphene. The relatively high electrical conductivity value of ~58 S/m was achieved for the composite added by 5 vol.% graphenated nanofibres (0.34 wt.% of graphene).

Noticing that the conductive phase content should be as high as 5.7 vol.% in carbon nanotube/Al_2O_3 composite to reach the same level of conductivity, this result shows the unparalleled advantage of graphene augmented inorganic nanofibers as reinforcing phase in composites compared with other carbon materials. The homogeneous distribution of the graphene-covered nanofibers throughout the matrix enables an interconnected network of the conductive fillers. This process is effective in the sample with a graphene content as low as 0.59 vol.% and is likely to be improved by the presence of the electroconductive additives, which produces an enlargement

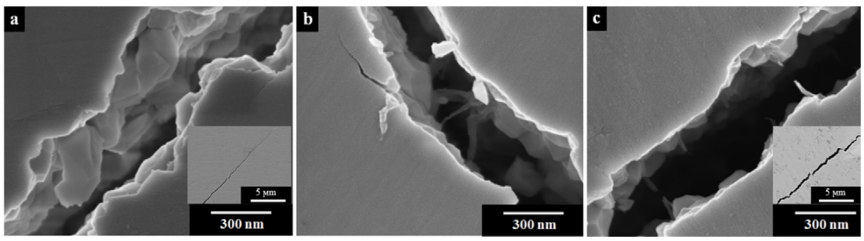

Fig. 8. FE-SEM images of the indentation-induced cracks in the materials Z0 (a), Z3 (b), and Z5 (c).

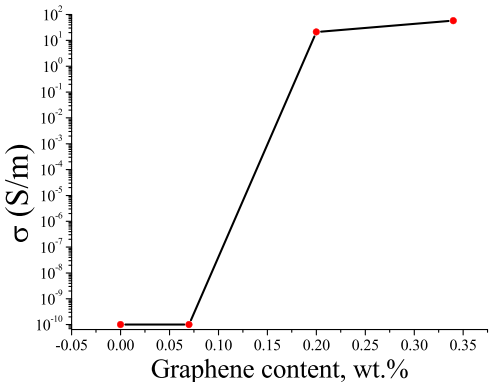

Fig. 9. Electrical conductivity of the composites as a function of graphene load.

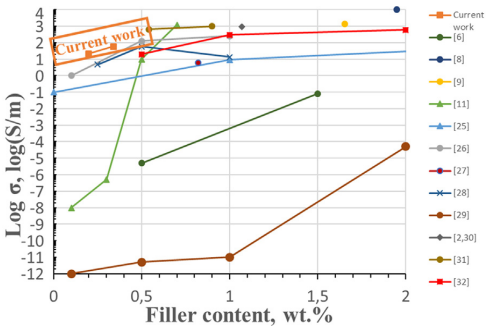

Fig. 10. Electrical conductivity of zirconia-based nanocomposites with carbon fillers measured in different studies.

of the effective electrical contact area of the conductive phase, thus enhancing electrical conductivity for a very low content of graphene in comparison to other carbon-based fillers. The results prove the success of our method in homogeneous dispersion of nanoadditives and their high electrical conductivity.

Fig. 10 includes data from various reports on electroconductive zirconia composites [6–8,26–32]. While there are reports on extremely high attained values of electrical conductivity up to 10,000 S m^{-1}, amount of graphene or CNT content needed to form composites with that value is comparatively high [2,8]. As a result, utilization of high graphene or CNT content can lead to considerable loss in mechanical properties of the composite, comparing to monolithic zirconia. Graphene augmented ceramic fibres used in this work contribute to building a percolation network, which permits decrease in required amount of graphene. Moreover, the incorporation of hybrid nanofibres renders maintenance of hardness at a high value.

4. Conclusions

In summary, highly electroconductive partially stabilized zirconia were developed through incorporation of the hybrid nanofillers, representing alumina nanofibres coated by multi-layer graphene, into the ceramic matrix. The fully dense (>98% of theoretical density) composites of PSZ and graphenated alumina nanofibers were produced by powder processing and densified using SPS technique at 1250 °C with 40 MPa pressure for 5 min. An increase in electroconductivity of 11 orders of magnitude as compared to the monolithic PSZ is achieved at as low load of carbon as only ~0.6 vol.%, which corresponds to 3 vol.% of the nanofillers. Moreover, an improvement in an indentation fracture toughness was ~20% for the composites containing 3 vol.% graphene coated nanofibres. An increase in conductivity does not result in deterioration of mechanical properties of these nanocomposites.

Acknowledgements

This research was supported by the Estonian Research Council under the personal research grant PUT1093 (I. Hussainova) and institutional research funding IUT19–29 of the Estonian Ministry of Education and Research as well as Baltic-American Freedom Foundation under research grant to I. Hussainova. The Raman spectroscopy was carried out in the Frederick Seitz Materials Research Laboratory Central Facilities, University of Illinois at Urbana-Champaign, USA.

References

[1] O. Malek, J. González-Julián, J. Vleugels, W. Vanderauwera, B. Lauwers, M. Belmonte, Carbon nanofillers for machining insulating ceramics, Mater. Today 14 (2011) 496–501, http://dx.doi.org/10.1016/S1369-7021(11)70214-0.
[2] A. Duszová, J. Dusza, K. Tomášek, J. Morgiel, G. Blugan, J. Kuebler, Zirconia/carbon nanofiber composite, Scr. Mater. 58 (2008) 520–523, http://dx.doi.org/10.1016/j.scriptamat.2007.11.002.
[3] M. Drozdova, I. Hussainova, D. Pérez-Coll, M. Aghayan, R. Ivanov, M.A. Rodríguez, et al., A novel approach to electroconductive ceramics filled by graphene covered nanofibers, Mater. Des. 90 (2016) 291–298, http://dx.doi.org/10.1016/j.matdes.2015.10.148.
[4] R.K. Chintapalli, F.G. Marro, B. Milsom, M. Reece, M. Anglada, Processing and characterization of high-density zirconia-carbon nanotube composites, Mater. Sci. Eng. A 549 (2012) 50–59, http://dx.doi.org/10.1016/j.msea.2012.03.115.
[5] B. Yazdani, Y. Xia, I. Ahmad, Y. Zhu, Graphene and carbon nanotube (GNT)-reinforced alumina nanocomposites, J. Eur. Ceram. Soc. 35 (2015) 179–186, http://dx.doi.org/10.1016/j.jeurceramsoc.2014.08.043.
[6] M. Mazaheri, D. Mari, Z.R. Hesabi, R. Schaller, G. Fantozzi, Multi-walled carbon nanotube/nanostructured zirconia composites: outstanding mechanical properties in a wide range of temperature, Compos. Sci. Technol. 71 (2011) 939–945, http://dx.doi.org/10.1016/j.compscitech.2011.01.017.
[7] M. Belmonte, A. Nistal, P. Boutbien, B. Román-Manso, M.I. Osendi, P. Miranzo, Toughened and strengthened silicon carbide ceramics by adding graphene-based fillers, Scr. Mater. 113 (2016) 127–130, http://dx.doi.org/10.1016/j.scriptamat.2015.10.023.
[8] A. Borrell, V.G. Rocha, R. Torrecillas, A. Fernández, Improvement of carbon nanofibers/ZrO 2 composites properties with a zirconia nanocoating on

carbon nanofibers by sol-gel method, J. Am. Ceram. Soc. 94 (2011) 2048–2052, http://dx.doi.org/10.1111/j.1551-2916.2010.04354.x.
[9] Y. Fan, L. Kang, W. Zhou, W. Jiang, L. Wang, A. Kawasaki, Control of doping by matrix in few-layer graphene/metal oxide composites with highly enhanced electrical conductivity, Carbon N. Y. 81 (2015) 83–90, http://dx.doi.org/10.1016/j.carbon.2014.09.027.
[10] B. Lee, M.Y. Koo, S.H. Jin, K.T. Kim, S.H. Hong, Simultaneous strengthening and toughening of reduced graphene oxide/alumina composites fabricated by molecular-level mixing process, Carbon N. Y. 78 (2014) 212–219, http://dx.doi.org/10.1016/j.carbon.2014.06.074.
[11] J. Shin, S. Hong, Fabrication and properties of reduced graphene oxide reinforced yttria-stabilized zirconia composite ceramics, J. Eur. Ceram. Soc. 34 (2013) 1297–1302, http://dx.doi.org/10.1016/j.jeurceramsoc.2013.11.034.
[12] F. Chen, D. Jin, K. Tyeb, B. Wang, Y.-H. Han, S. Kim, et al., Field assisted sintering of graphene reinforced zirconia ceramics, Ceram. Int. 41 (2015) 6113–6116, http://dx.doi.org/10.1016/j.ceramint.2014.12.147.
[13] M. Drozdova, D. Pérez-Coll, M. Aghayan, R. Ivanov, M.A. Rodríguez, I. Hussainova, Hybrid graphene/alumina nanofibers for electrodonductive zirconia, Key Eng. Mater. 674 (2016) 15–20, http://dx.doi.org/10.4028/www.scientific.net/KEM.674.15.
[14] I. Hussainova, J. Baronins, M. Antonov, Wear performance of hierarchically structured alumina reinforced by hybrid graphene encapsulated alumina nanofibers, Wear 368–369 (2016) 287–295 http://dx.doi.org/10.1016/j.wear.2016.09.028.
[15] R. Ivanov, I. Hussainova, M. Aghayan, M. Drozdova, D. Pérez-Coll, M.A. Rodríguez, et al., Graphene-encapsulated aluminium oxide nanofibers as a novel type of nanofillers for electroconductive ceramics, J. Eur. Ceram. Soc. 35 (2015) 4017–4021, http://dx.doi.org/10.1016/j.jeurceramsoc.2015.06.011.
[16] Roman Ivanov, Valdek Mikli, Jakob Kübarsepp, Irina Hussainova, Direct CVD growth of foliated graphene closed shells on alumina nanofibers, Key Eng. Mater. 674 (2016) 77–80, http://dx.doi.org/10.4028/www.scientific.net/KEM.674.77.
[17] K. Niihara, R. Morena, D.P. Hasselman, Evaluation of klc of brittle solids by the indentation method with low crack to indent ratios, J. Mater. Sci. Lett. 1 (1982) 13–16, http://dx.doi.org/10.1007/BF00724706.
[18] M. Aghayan, I. Hussainova, M. Gasik, M. Kutuzov, M. Friman, Coupled thermal analysis of novel alumina nanofibers with ultrahigh aspect ratio, Thermochim. Acta 574 (2013) 140–144, http://dx.doi.org/10.1016/j.tca.2013.10.010.
[19] S. Osswald, M. Havel, Y. Gogotsi, Recent Advances in linear and nonlinear Raman spectroscopy I, J. Raman Spectrosc. 38 (2007) 728–736, http://dx.doi.org/10.1002/jrs1686.
[20] J.C. Valmalette, M. Isa, Size effects on the stabilization of ultrafine zirconia nanoparticles, Chem. Mater. 14 (2002) 5098–5102, http://dx.doi.org/10.1021/cm021233n.
[21] A. Nieto, L. Huang, Y.H. Han, J.M. Schoenung, Sintering behavior of spark plasma sintered alumina with graphene nanoplatelet reinforcement, Ceram. Int. 41 (2015) 5926–5936, http://dx.doi.org/10.1016/j.ceramint.2015.01.027.
[22] M. Belmonte, J. Gonzalez-Julian, P. Miranzo, M.I. Osendi, Spark plasma sintering: a powerful tool to develop new silicon nitride-based materials, J. Eur. Ceram. Soc. 30 (2010) 2937–2946, http://dx.doi.org/10.1016/j.jeurceramsoc.2010.01.025.
[23] J. Sun, L. Gao, M. Iwasa, T. Nakayama, K. Niihara, Failure investigation of carbon nanotube/3Y-TZP nanocomposites, Ceram. Int. 31 (2005) 1131–1134, http://dx.doi.org/10.1016/j.ceramint.2004.11.010.
[24] J. Liu, H. Yan, M.J. Reece, K. Jiang, Toughening of zirconia/alumina composites by the addition of graphene platelets, J. Eur. Ceram. Soc. 32 (2012) 4185–4193, http://dx.doi.org/10.1016/j.jeurceramsoc.2012.07.007.
[25] S.-M. Kwon, S.-J. Lee, I.-J. Shon, Enhanced properties of nanostructured ZrO2–graphene composites rapidly sintered via high-frequency induction heating, Ceram. Int. 41 (2015) 835–842, http://dx.doi.org/10.1016/j.ceramint.2014.08.042.
[26] J.-H. Shin, S.-H. Hong, Microstructure and mechanical properties of single wall carbon nanotube reinforced yttria stabilized zircona ceramics, Mater. Sci. Eng. A 556 (2012) 382–387, http://dx.doi.org/10.1016/j.msea.2012.07.001.
[27] Y. Fukumura, D.K. Pattanayak, C. Wanghui, T. Shirai, M. Fuji, F. Wang, In situ zirconia/carbon network composite fabricated by gelcast following reduction-sintering, 2012, pp. 347–350, http://dx.doi.org/10.2109/jcersj2.120.347.
[28] T. Ukai, T. Sekino, A.T. Hirvonen, N. Tanaka, T. Kusunose, T. Nakayama, et al., Preparation and electrical properties of carbon nanotubes dispersed zirconia nanocomposites, Key Eng. Mater. (2006) 661–664, http://dx.doi.org/10.4028/www.scientific.net/KEM.317-318.661.317-318.661.
[29] S.L. Shi, J. Liang, Effect of multiwall carbon nanotubes on electrical and dielectric properties of yttria-stabilized zirconia ceramic, J. Am. Ceram. Soc. 89 (2006) 3533–3535, http://dx.doi.org/10.1111/j.1551-2916.2006.01232.
[30] A. Duszová, J. Dusza, K. Tomášek, G. Blugan, J. Kuebler, Microstructure and properties of carbon nanotube/zirconia composite, J. Eur. Ceram. Soc. 28 (2008) 1023–1027, http://dx.doi.org/10.1016/j.jeurceramsoc.2007.09.011.
[31] J. Dusza, G. Blugan, J. Morgiel, J. Kuebler, F. Inam, T. Peijs, et al., Hot pressed and spark plasma sintered zirconia/carbon nanofiber composites, J. Eur. Ceram. Soc. 29 (2009) 3177–3184, http://dx.doi.org/10.1016/j.jeurceramsoc.2009.05.030.
[32] L. Melk, M.-L. Antti, M. Anglada, Material removal mechanisms by EDM of zirconia reinforced MWCNT nanocomposites, Ceram. Int. (2016), http://dx.doi.org/10.1016/j.ceramint.2015.12.120.

DISSERTATIONS DEFENDED AT TALLINN UNIVERSITY OF TECHNOLOGY ON *MECHANICAL ENGINEERING*

1. **Jakob Kübarsepp**. Steel-Bonded Hardmetals. 1992.

2. **Jakub Kõo**. Determination of Residual Stresses in Coatings &Coated Parts. 1994.

3. **Mart Tamre**. Tribocharacteristics of Journal Bearings Unlocated Axis. 1995.

4. **Paul Kallas**. Abrasive Erosion of Powder Materials. 1996.

5. **Jüri Pirso**. Titanium and Chromium Carbide Based Cermets. 1996.

6. **Heinrich Reshetnyak**. Hard Metals Serviceability in Sheet Metal Forming Operations. 1996.

7. **Arvi Kruusing**. Magnetic Microdevices and Their Fabrication methods. 1997.

8. **Roberto Carmona Davila**. Some Contributions to the Quality Control in Motor Car Industry. 1999.

9. **Harri Annuka**. Characterization and Application of TiC-Based Iron Alloys Bonded Cermets. 1999.

10. **Irina Hussainova**. Investigation of Particle-Wall Collision and Erosion Prediction. 1999.

11. **Edi Kulderknup**. Reliability and Uncertainty of Quality Measurement. 2000.

12. **Vitali Podgurski**. Laser Ablation and Thermal Evaporation of Thin Films and Structures. 2001.

13. **Igor Penkov**. Strength Investigation of Threaded Joints Under Static and Dynamic Loading. 2001.

14. **Martin Eerme**. Structural Modelling of Engineering Products and Realisation of Computer-Based Environment for Product Development. 2001.

15. **Toivo Tähemaa**. Assurance of Synergy and Competitive Dependability at Non-Safety-Critical Mechatronics Systems design. 2002.

16. **Jüri Resev**. Virtual Differential as Torque Distribution Control Unit in Automotive Propulsion Systems. 2002.

17. **Toomas Pihl**. Powder Coatings for Abrasive Wear. 2002.

18. **Sergei Letunovitš**. Tribology of Fine-Grained Cermets. 2003.

19. **Tatyana Karaulova**. Development of the Modelling Tool for the Analysis of the Production Process and its Entities for the SME. 2004.

20. **Grigori Nekrassov**. Development of an Intelligent Integrated Environment for Computer. 2004.

21. **Sergei Zimakov**. Novel Wear Resistant WC-Based Thermal Sprayed Coatings. 2004.

22. **Irina Preis**. Fatigue Performance and Mechanical Reliability of Cemented Carbides. 2004.

23. **Medhat Hussainov**. Effect of Solid Particles on Turbulence of Gas in Two-Phase Flows. 2005.

24. **Frid Kaljas**. Synergy-Based Approach to Design of the Interdisciplinary Systems. 2005.

25. **Dmitri Neshumayev**. Experimental and Numerical Investigation of Combined Heat Transfer Enhancement Technique in Gas-Heated Channels. 2005.

26. **Renno Veinthal**. Characterization and Modelling of Erosion Wear of Powder Composite Materials and Coatings. 2005.

27. **Sergei Tisler**. Deposition of Solid Particles from Aerosol Flow in Laminar Flat-Plate Boundary Layer. 2006.

28. **Tauno Otto**. Models for Monitoring of Technological Processes and Production Systems. 2006.

29. **Maksim Antonov**. Assessment of Cermets Performance in Aggressive Media. 2006.

30. **Tatjana Barashkova**. Research of the Effect of Correlation at the Measurement of Alternating Voltage. 2006.

31. **Jaan Kers**. Recycling of Composite Plastics. 2006.

32. **Raivo Sell**. Model Based Mechatronic Systems Modeling Methodology in Conceptual Design Stage. 2007.

33. **Hans Rämmal**. Experimental Methods for Sound Propagation Studies in Automotive Duct Systems. 2007.

34. **Meelis Pohlak**. Rapid Prototyping of Sheet Metal Components with Incremental Sheet Forming Technology. 2007.

35. **Priidu Peetsalu**. Microstructural Aspects of Thermal Sprayed WC-Co Coatings and Ni-Cr Coated Steels. 2007.

36. **Lauri Kollo**. Sinter/HIP Technology of TiC-Based Cermets. 2007.

37. **Andrei Dedov**. Assessment of Metal Condition and Remaining Life of In-service Power Plant Components Operating at High Temperature. 2007.

38. **Fjodor Sergejev**. Investigation of the Fatigue Mechanics Aspects of PM Hardmetals and Cermets. 2007.

39. **Eduard Ševtšenko**. Intelligent Decision Support System for the Network of Collaborative SME-s. 2007.

40. **Rünno Lumiste**. Networks and Innovation in Machinery and Electronics Industry and Enterprises (Estonian Case Studies). 2008.

41. **Kristo Karjust**. Integrated Product Development and Production Technology of Large Composite Plastic Products. 2008.

42. **Mart Saarna**. Fatigue Characteristics of PM Steels. 2008.

43. **Eduard Kimmari**. Exothermically Synthesized B_4C-Al Composites for Dry Sliding. 2008.

44. **Indrek Abiline**. Calibration Methods of Coating Thickness Gauges. 2008.

45. **Tiit Hindreus**. Synergy-Based Approach to Quality Assurance. 2009.

46. **Karl Raba**. Uncertainty Focused Product Improvement Models. 2009.

47. **Riho Tarbe**. Abrasive Impact Wear: Tester, Wear and Grindability Studies. 2009.

48. **Kristjan Juhani**. Reactive Sintered Chromium and Titanium Carbide-Based Cermets. 2009.

49. **Nadežda Dementjeva**. Energy Planning Model Analysis and Their Adaptability for Estonian Energy Sector. 2009.

50. **Igor Krupenski**. Numerical Simulation of Two-Phase Turbulent Flows in Ash Circulating Fluidized Bed. 2010.

51. **Aleksandr Hlebnikov**. The Analysis of Efficiency and Optimization of District Heating Networks in Estonia. 2010.

52. **Andres Petritšenko**. Vibration of Ladder Frames. 2010.

53. **Renee Joost**. Novel Methods for Hardmetal Production and Recycling. 2010.

54. **Andre Gregor**. Hard PVD Coatings for Tooling. 2010.

55. **Tõnu Roosaar**. Wear Performance of WC- and TiC-Based Ceramic-Metallic Composites. 2010.

56. **Alina Sivitski**. Sliding Wear of PVD Hard Coatings: Fatigue and Measurement Aspects. 2010.

57. **Sergei Kramanenko**. Fractal Approach for Multiple Project Management in Manufacturing Enterprises. 2010.

58. **Eduard Latõsov**. Model for the Analysis of Combined Heat and Power Production. 2011.

59. **Jürgen Riim**. Calibration Methods of Coating Thickness Standards. 2011.

60. **Andrei Surzhenkov**. Duplex Treatment of Steel Surface. 2011.

61. **Steffen Dahms**. Diffusion Welding of Different Materials. 2011.

62. **Birthe Matsi**. Research of Innovation Capasity Monitoring Methodology for Engineering Industry. 2011.

63. **Peeter Ross**. Data Sharing and Shared Workflow in Medical Imaging. 2011.

64. **Siim Link**. Reactivity of Woody and Herbaceous Biomass Chars. 2011.

65. **Kristjan Plamus**. The Impact of Oil Shale Calorific Value on CFB Boiler Thermal Efficiency and Environment. 2012.

66. **Aleksei Tšinjan**. Performance of Tool Materials in Blanking. 2012.

67. **Martinš Sarkans**. Synergy Deployment at Early Evaluation of Modularity of the Multi-Agent Production Systems. 2012.

68. **Sven Seiler**. Laboratory as a Service – A Holistic Framework for Remote and Virtual Labs. 2012.

69. **Tarmo Velsker**. Design Optimization of Steel and Glass Structures. 2012.

70. **Madis Tiik**. Access Rights and Organizational Management in Implementation of Estonian Electronic Health Record System. 2012.

71. **Marina Kostina**. Reliability Management of Manufacturing Processes in Machinery Enterprises. 2012.

72. **Robert Hudjakov**. Long-Range Navigation for Unmanned Off-Road Ground Vehicle. 2012.

73. **Arkadi Zikin**. Advanced Multiphase Tribo-Functional PTA Hardfacings. 2013.

74. **Alar Konist**. Environmental Aspects of Oil Shale Power Production. 2013.

75. **Inge Roos**. Methodology for Calculating CO_2 Emissions from Estonian Shale Oil Industry. 2013.

76. **Dmitri Shvarts**. Global 3D Map Merging Methods for Robot Navigation. 2013.

77. **Kaia Lõun**. Company's Strategy Based Formation of e-Workplace Performance in the Engineering Industry. 2013.

78. **Maido Hiiemaa**. Motion Planner for Skid-Steer Unmanned Ground Vehicle. 2013.

79. **Dmitri Goljandin**. Disintegrator Milling System Development and Milling Technologies of Different Materials. 2013.

80. **Dmitri Aleksandrov**. Light-Weight Multicopter Structural Design for Energy Saving. 2013.

81. **Henrik Herranen**. Design Optimization of Smart Composite Structures with Embedded Devices. 2014.

82. **Heiki Tiikoja**. Experimental Acoustic Characterization of Automotive Inlet and Exhaust System. 2014.

83. **Jelena Priss**. High Temperature Corrosion and Abrasive Wear of Boiler Steels. 2014.

84. **Aare Aruniit**. Thermoreactive Polymer Composite with High Particulate Filler Content. 2014.

85. **Dmitri Gornostajev**. Development of the Calculation Method for Barge Hull. 2014.

86. **Liina Lind**. Wear of PVD Coatings on Fineblanking Punches. 2014.

87. **Nikolai Voltšihhin**. Design and Technology of Oxides-Containing Ceramic-Based Composites. 2014.

88. **Aleksander Šablinski**. RANS Numerical Modelling of Turbulent Polydispersed Flows in CFB Freeboard. 2015.

89. **Tanel Aruväli**. Wireless Real-time Monitoring of Machining Processes. 2015.

90. **Andrei Bogatov**. Morphological Changes on Diamond and DLC Films During Sliding Wear. 2015.

91. **Raimo Kabral**. Aero-Acoustic Studies and Innovative Noise Control with Application to Modern Automotive Gas Exchange System. 2015.

92. **Jevgeni Sahno**. Dynamic Management Framework for Continuous Improvement of Production Processes. 2015.

93. **Ott Pabut**. Optimal Design of Slotless Permanent Magnet Generators. 2015.

94. **Merili Kukuškin**. Value Centric Business Development for Estonian Manufacturing Small and Medium Sized Enterprises. 2015.

95. **Kaimo Sonk**. Development of Additive Manufacturing Based on Functional Requirements. 2015.

96. **Marina Aghayan**. Functionalization of Alumina Nanofibers with Metal Oxides. 2016.

97. **Marek Jõeleht**. Titanium Carbide Cermet as Ballistic Protection Material. 2016.

98. **Heikki Sarjas**. Novel Synthesized and Milled Carbide-based Composite Powders for HVOF Spray. 2016.

99. **Klodian Dhoska**. Measurement Methods with 3D Coordinate Measuring Machine and Improved Characterization Setup for Detector Performance. 2016.

100. **Aleksei Snatkin**. Development and Optimisation of Production Monitoring System. 2016.

101. **Igor Poljantšikov**. Partners Selection Tool for Virtual Enterprise in SMEs Network. 2016.

102. **Sergei Žigailov**. Experimental and Analytical Modelling of Pelvic Motion. 2016.

103. **Rommi Källo**. Synergy-Based Chaos Control in the Multi-Agent Hierarchical Systems. 2016.

104. **Der-Liang Yung**. ZrC-based and ZrC-doped Composites for High-Temperature and Wear Applications. 2016.

105. **Viive Pille**. Development of a Model for the Prevention of Work-Related Musculoskeletal Disorders in the Upper Extremities. 2016.

106. **Agus Pramono**. Investigation of Severe Plastic Deformation Processes for Aluminum Based Composites. 2016.

107. **Zorjana Mural**. Technology and Properties of Fine-grained Nd-Fe-B Magnets. 2017.

108. **Eero Väljaots**. Energy Efficiency Evaluation Method for Mobile Robot Platform Design. 2017.

109. **Viktoria Baškite**. Decision-Making Tool Development for Used Industrial Equipment Life Cycle Evaluation and Improvement. 2017.